# Supersymmetry, from Baryogenesis at the Electroweak Phase Transition to Low-energy Precision Experiments

Thesis by

Sean Tulin

In Partial Fulfillment of the Requirements

for the Degree of

Doctor of Philosophy


California Institute of Technology

Pasadena, California

2009

(Submitted June 10, 2009)

In memory of

Shirley and Norman Tulin, my grandparents,

Jane Tulin, my aunt,

Doug Michael, my first advisor at Caltech.

# Acknowledgements

Thank you to the three most supportive people without whom I would be much worse off: Sarah Payne, Nancy Tulin, Michael Ramsey-Musolf. In addition, thank you to all my awesome collaborators: Shin'ichiro Ando, Vincenzo Cirigliano, Daniel Chung, Bjorn Garbrecht, Christopher Lee, Stefano Profumo, and Shufang Su. Thank you to my committee members: Marc Kamionkowski, Bob McKeown, Mark Wise, and, previously, Brad Filippone. Thank you to all my friends and family, who have supported and encouraged me these past five years, especially Mark Rosow, Lynn and John Payne, and lastly Joel Wolpert, who helped get me to Caltech in the first place.

# Abstract

Electroweak-scale supersymmetry is one of the most popular extensions of the Standard Model and has many important implications for nuclear physics, particle physics, and cosmology. First, supersymmetric electroweak baryogenesis may explain the origin of the matter-antimatter asymmetry in the universe. In this scenario, electroweak symmetry is broken in the early universe by a first-order phase transition, when bubbles of broken phase nucleate and expand, eventually consuming the unbroken phase. Charge density is generated within the expanding bubble wall and diffuses into the unbroken phase. Through inelastic collisions in the plasma, this charge is partially converted into left-handed quark and lepton charge, which in turn leads to the production of baryon number through weak sphaleron transitions. In this work, we study these charge transport dynamics, from its generation within the bubble wall, to the final baryon asymmetry. We evaluate which collisions are important for baryogenesis, and what is their impact upon the final baryon asymmetry. Our main result is that bottom and tau Yukawa interactions, previously neglected, can play a crucial role, affecting the magnitude and sign of baryon asymmetry. We investigate how this works in detail in the Minimal Supersymmetric Standard Model (MSSM); we suggest that these interactions may be even more important in gauge-singlet extensions of the MSSM. Second, low-energy precision measurements of weak decays may provide interesting signals of supersymmetry. We study in detail the supersymmetric radiative corrections to (i) leptonic pion decay branching ratios, and (ii) muon and beta decay coefficients. A deviation from the Standard Model predictions would imply strong departures from the minimal, commonly-assumed, theoretical assumptions about supersymmetry breaking.

# Contents

# Chapter 1

# Introduction: Cosmology, Precision Tests, and the Electroweak Scale

The Standard Model (SM), despite its forty years of experimental success, falls completely flat in the cosmological arena. It fails to explain the nature of dark matter and dark energy that currently dominate the energy density of the Universe; it fails to explain why the Universe is so flat, and why acausally-separated regions on the surface of last scattering have the same temperature; and, lastly, it fails to explain the origin of the baryon asymmetry of the Universe (BAU). In the near future, experiments at the Large Hadron Collider (LHC) aim to discover the last missing piece of the SM, the Higgs boson, which is responsible for electroweak symmetry breaking and the generation of mass. However, the Higgs boson is still a wild card. Although the SM Higgs boson is the simplest incarnation of electroweak symmetry breaking, it may not be the correct one. Electroweak-scale supersymmetry (SUSY) is one theoretically attractive alternative. Its primary virtue lies in its resolution of the SM's hierarchy problem — that in the SM, the Higgs boson mass (which sets the scale of electroweak symmetry breaking) receives large radiative corrections, and therefore the observed electroweak scale is realized only at the expense of an extreme fine-tuning of the underlying parameters. SUSY may also explain some of these unanswered cosmological puzzles, potentially providing an exciting connection between the Universe and upcoming experimental exploration of the electroweak scale. In this work, we study two of its implications: (i) the generation of the BAU through the dynamics of supersymmetric particles during the electroweak phase transition in the early universe, and (ii)

signatures of supersymmetry in low-energy precision measurements of weak decays.

Characterized by the ratio of baryon number density to entropy density, the BAU has been measured through studies of Big Bang Nucleosynthesis (BBN) and the cosmic microwave background (CMB) to be in the following range

$$n_B/s = \begin{cases} (6.7 \ - \ 9.2) \times 10^{-11} & \text{BBN [1]} \\ (8.36 \ - \ 9.32) \times 10^{-11} & \text{CMB [1, 2]} \end{cases} \tag{1.1}$$

at 95% confidence level. This translates into about one baryon per cubic meter, averaged over the entire observable universe. Anti-baryons, in comparison, are rare. The only evidence for extraterrestrial anti-baryons is cosmic ray anti-protons, whose abundance is consistent with secondary production from collisions of primary cosmic rays with the interstellar medium [5].

Of course, the BAU might simply be an initial condition. However, this hypothesis is nearly (but not completely) inconsistent with the much-beloved inflationary paradigm. To explore this in more detail, let us compute the initial baryon asymmetry at the beginning of inflation (denoted by time $t_i$), required to explain the present abundance, assuming that inflation lasted for $\mathcal{N}_e$ e-foldings, after which radiation domination proceeds with reheating temperature $T_{RH}$. The required initial baryon number density is

$$\begin{aligned} n_B(t_i) &\sim n_B(t_0) \, \frac{g_{*S}(T_{RH})}{g_{*S}(T_0)} \left(\frac{T_{RH}}{T_0}\right)^3 e^{3\mathcal{N}_e} \\ &\sim 10^{90} \text{ cm}^{-3} \times \left(\frac{g_{*S}(T_{RH})}{10}\right) \left(\frac{T_{RH}}{10 \text{ MeV}}\right)^3 \left(10^{65}\right)^{\mathcal{N}_e/50} . \end{aligned} \tag{1.2}$$

where $t_0$ and $T_0$ are the present time and radiation temperature, and $g_{*S}$ counts the effective number of degrees of freedom. The success of BBN requires $T_{RH} \gtrsim 4$ MeV [4], while the inflationary solution to the horizon and flatness problems requires $\mathcal{N}_e \gtrsim 50$ (e.g., [3]). In the SM baryon number is carried by quarks; at $t_i$ they would be a highly degenerate Fermi gas, with Fermi energy given by the chemical potential

$$\mu \sim n_B^{1/3} \sim 10^{16} \text{ GeV} \times \left(\frac{g_{*S}(T_{RH})}{10}\right)^{1/3} \left(\frac{T_{RH}}{10 \text{ MeV}}\right) \left(10^{22}\right)^{\mathcal{N}_e/50} . \tag{1.3}$$

If we require that $\mu < M_{\rm pl}$, where $M_{\rm pl} \sim 10^{19}$ GeV is the Planck scale, so that the baryon energy density $\rho_B \sim \mu^4 < M_{\rm pl}^4$, then we must have $\mathcal{N}_e$ and $T_{RH}$ extremely close to the aforementioned bounds; it is expected that both quantities may be much greater. Therefore, let us abandon this possibility and focus on a baryon asymmetry that arises dynamically sometime between the end of inflation and the BBN era.

Successful baryogenesis requires three conditions, due to Sakharov [6]. First, there must exist interactions that violate baryon number (B), or else no baryon number can be generated. Second, there must exist interactions that violate both C and CP symmetries, where C is charge conjugation and P is parity; otherwise, it is not possible to bias the generation of baryons over anti-baryons. Third, there must exist an arrow of time, or else the rate for the production of baryons will be equal to the rate for the inverse process to destroy baryons. This arrow can stem from a violation of CPT symmetry (where T is time reversal), or a departure from equilibrium during the evolution of the universe.

In principle, the SM does contain these ingredients; early work suggested that baryogenesis could occur during the electroweak phase transition (EWPT) when the universe cooled to a temperature $T \sim 100$ GeV and the Higgs field acquired a vacuum expectation value (vev) [7, 8]. In this scenario, a departure from equilibrium is provided by a strong first-order EWPT, where bubbles of broken symmetry nucleate and expand in a background of unbroken symmetry, filling the universe to complete the phase transition. Second, CP-violation is present in the Cabibbo-Kobayashi-Maskawa (CKM) quark mixing matrix; this induces CP-violating interactions at the expanding bubble walls, where the Higgs vev is spacetime-dependent, that leads to the production of a CP-asymmetric charge density. (This is the so-called CP-violating source.) This CP-asymmetry, created for one species, diffuses ahead of the advancing bubble and is converted into other species through inelastic interactions in the plasma; in particular, some fraction is converted into left-handed fermion charge density, denoted $n_L$. Third, baryon number is violated by electroweak sphaleron transitions, which are active outside the bubbles, in regions of unbroken electroweak symmetry [10, 11, 12, 13, 14]. The presence of non-zero left-handed fermion charge $n_L$ biases the sphaleron processes, resulting in the production of a baryon asymmetry [16]. Electroweak sphalerons become quenched once electroweak symmetry is broken,

as long as the EWPT is strongly first-order; therefore, the baryon asymmetry becomes frozen in once it is captured inside the expanding bubbles.

Despite its promise, the electroweak baryogenesis (EWB) scenario is not viable in the SM: (i) the CKM-phase is insufficient to generate the observed BAU, and (ii) for a SM Higgs boson with mass $m_h > 114.4$ GeV [2], electroweak symmetry breaking occurs by a continuous crossover, rather than a phase transition [53]. However, all is not lost. Supersymmetric extensions of the SM can readily include all the ingredients for EWB to work. There are many new CP-violating phases that can drive the creation of $n_B$. In addition, there is an extended Higgs sector, reviving the possibility that the electroweak phase transition is first-order. In Chapter 2, we briefly describe supersymmetry and some of its key parameters relevant for EWB.

The baryogenesis computation is essentially a two step process. First, one studies the finite-temperature Higgs potential to determine the nature of the electroweak phase transition. It must be strongly enough first-order so that electroweak sphalerons are quenched within the bubble of broken symmetry. One computes the "bubble solutions" — the spacetime-dependent profiles of the vacuum expectation values (vevs) of all the Higgs fields from bubbles of broken electroweak symmetry expanding in a background of unbroken phase [39, 49].

Second, upon this stage of expanding bubbles, we let unfold the drama of charge transport dynamics in the hot electroweak plasma. This is the subject of our thesis. We study how charge densities, induced by the expanding bubble walls, diffuse, interact, and equilibrate in the plasma. Ultimately, some fraction of this charge density is converted into $n_L$, the left-handed quark and lepton charge. Our main result is that $n_L$ crucially depends upon which interactions are in chemical equilibrium during the electroweak phase transition. In particular, we show how the charge transport picture is dramatically impacted by bottom and tau Yukawa interactions, which until recently had not been included in EWB studies [24].

In Chapter 3, we formulate the charge transport problem as a system of coupled Boltzmann equations for the various charge densities during the EWPT. The conversion of charge from one species to another occurs via inelastic collisions. We compute these thermally-

averaged interaction rates in Chapters 3 and 4, showing under what conditions they lead to chemical equilibrium. The generation of charge density within the initially CP-symmetric plasma occurs within the bubble wall. In Chapter 5, we describe a novel interpretation for this physics, in analogy with neutrino oscillations.

Next, we solve the system of Boltzmann equations, both analytically (Chapter 6) and numerically (Chapter 7). Our analytic results, verified numerically, make it clear that bottom and tau Yukawa interactions can have a strong impact on $n_B$. In previous work, the sole contribution to $n_L$ was quarks of all three generations. We show that bottom Yukawa interactions, when active, strongly suppress left-handed quark charge when the scalar superpartners of right-handed top and bottom quarks have (i) masses greater than 500 GeV, or (ii) approximately equal masses. In addition, when tau Yukawa interactions are active, significant left-handed lepton charge is generated, which had not been included in previous studies. The question of whether quarks or leptons dominate $n_L$, thus driving baryon-number generation, is not purely academic. It can affect the overall sign and magnitude of $n_B$, thus is important for connecting EWB to experiments. In the Appendix, we provide a review for how the Boltzmann equation can be derived from the Closed-Time-Path formalism of finite-temperature field theory.

Of primary importance is the question of whether electroweak-scale SUSY is actually realized in nature. There are two complementary experimental approaches: (i) direct production of supersymmetric particles at high-energy colliders such as the LHC, and (ii) precision measurements of (comparatively) low-energy observables that can be sensitive to virtual supersymmetric particles in quantum loops. In Chapters 8 and 9, we study several precision measurements of weak decays that can provide interesting signitures of SUSY. First, in Chapter 8, we study leptonic pion decays. In the SM, the ratio $R_{e/\mu}$ has been computed very accurately [65, 66]:

$$R_{e/\mu} = \frac{\Gamma[\pi^+ \to e + \nu_e(\gamma)]}{\Gamma[\pi^+ \to \mu^+ \nu_\mu(\gamma)]} = 1.2352 \pm 0.0001 \; . \tag{1.4}$$

A discrepency between this prediction and upcoming measurements of this ratio may be a signal for SUSY. We find that a large supersymmetric deviation in $R_{e/\mu}$ implies either

R-parity violation[1], or a nondegeneracy between the scalar supersymmetric partners of the electron and muon.

Second, in Chapter 9, we study supersymmetric effects in muon and beta decays. For each fermion $f$ in the SM (except neutrinos), there are two scalar supersymmetric partners $\widetilde{f}_L$ and $\widetilde{f}_R$, corresponding to the left- and right-handed chiralities $f_L$ and $f_R$. We find that these decays are sensitive to large tri-scalar, SUSY-breaking parameters that lead to mixing between $\widetilde{f}_L$ and $\widetilde{f}_R$ for the superpartners of the electron, muon, and first generation quarks.

None of these tests of weak decays will give a deviation from the SM predictions in the most minimal supersymmetric scenarios [52] where R-parity is conserved, electron and muon superpartners are degenerate, and the tri-scalar mixing parameters are small for the first and second generations. Therefore, these probes are interesting in that they provide handles on regions of parameter space that defy our theoretical prejudice and may be difficult to identify with collider studies. Lastly, we summarize our conclusions in Chapter 10.

[1]R-parity is a discrete symmetry under which SM particles have parity $(+1)$, while supersymmetric particles have parity $(-1)$.

# Chapter 2

# Supersymmetry, from a Baryon's Perspective

Electroweak-scale supersymmetry (SUSY) is one of the most popular and well-motivated extensions of the Standard Model (SM) [52]. One of its many virtues is the possibility that it may explain the origin of the baryon asymmetry of the universe. In this chapter, we describe the Minimal Supersymmetric Standard Model (MSSM), at least those parts that are relevant for electroweak baryogenesis. We also briefly comment on the Next-to-Minimal Supersymmetric Standard Model (NMSSM).

In a supersymmetric extension of the SM, for every gauge boson or chiral fermion degree of freedom in the SM, there is an additional supersymmetric degree of freedom differing by half-integer spin. Gauginos are fermionic superparters of gauge bosons; squarks and sleptons are the scalar superpartners of quarks and leptons. In addition, the Higgs sector is enlarged beyond the SM. In the MSSM, there are two Higgs doublets, and their fermionic Higgsino superpartners; in the NMSSM, there is an additional gauge singlet, and its fermionic superpartner the singlino. In Table 2.1, we list all of these particles, and their respective gauge quantum numbers. For more information, we refer the reader to the excellent review given in Ref. [52].

Here we identify which pieces of the MSSM Lagrangian are most relevant for EWB charge transport dynamics. Recall, the key steps are (i) generation of charge density within the expanding bubble wall, (ii) diffusion of charge into the unbroken phase, and (iii) inelastic collisions that convert this charge into left-handed fermionic charge, which (iv) is then

| Chiral Supermultiplets | Spin-$1/2$ | Spin-0 | $SU(3)_C \times SU(2)_L \times U(1)_Y$ |
|---|---|---|---|
| quarks, squarks | $q_i \equiv (u_{iL},\, d_{iL})$ | $\widetilde{q}_i \equiv (\widetilde{u}_{iL},\, \widetilde{d}_{iL})$ | $(3,\, 2,\, 1/6)$ |
| | $u_i^\dagger \equiv u_{iR}^\dagger$ | $\widetilde{u}_i^* \equiv \widetilde{u}_{iR}^*$ | $(\bar{3},\, 1,\, -2/3)$ |
| | $d_i^\dagger \equiv d_{iR}^\dagger$ | $\widetilde{d}_i^* \equiv \widetilde{d}_{iR}^*$ | $(\bar{3},\, 1,\, 1/3)$ |
| leptons, sleptons | $\ell_i \equiv (\nu_{iL},\, e_{iL})$ | $\widetilde{\ell}_i \equiv (\widetilde{\nu}_{iL},\, \widetilde{e}_{iL})$ | $(1,\, 2,\, -1/2)$ |
| | $e_i^\dagger \equiv e_{iR}^\dagger$ | $\widetilde{e}_i^* \equiv \widetilde{e}_{iR}^*$ | $(1,\, 1,\, 1)$ |
| Higgs, Higgsinos | $H_u \equiv (H_u^+,\, H_u^0)$ | $\widetilde{H}_u \equiv (\widetilde{H}_u^+,\, \widetilde{H}_u^0)$ | $(1,\, 2,\, 1/2)$ |
| | $H_d \equiv (H_d^0,\, H_d^-)$ | $\widetilde{H}_d \equiv (\widetilde{H}_d^0,\, \widetilde{H}_d^-)$ | $(1,\, 2,\, -1/2)$ |
| Singlet, Singlino$^\dagger$ | $S$ | $\widetilde{S}$ | $(1, 1, 0)$ |
| **Gauge Supermultiplets** | **Spin-$1/2$** | **Spin-1** | **$SU(3)_C \times SU(2)_L \times U(1)_Y$** |
| $U(1)_Y$ | Bino $\widetilde{B}$ | $B^\mu$ | (1,1,0) |
| $SU(2)_L$ | Wino $\widetilde{W}_{1,2,3}$ | $W^\mu_{1,2,3}$ | (1,3,0) |
| $SU(3)_C$ | gluino $\widetilde{g}$ | $G^\mu$ | (8,1,0) |

Table 2.1: The particles, with gauge quantum numbers, of the Minimal Supersymmetric Standard Model. The Next-to-Minimal Supersymmetric Standard Model also includes an additional gauge singlet, denoted by †.

converted into baryon number by weak sphaleron transitions.

## 2.1 Electroweak phase transition

First and foremost, a strong, first-order phase transition is required for electroweak baryogenesis to work. When electroweak symmetry is broken at temperature $T$, the Higgs fields acquire their vacuum expectation values:

$$\langle H_u^0 \rangle = v_u(T)\ , \qquad \langle H_d^0 \rangle = v_d(T)\ . \tag{2.1}$$

Furthermore, electroweak sphaleron transitions are no longer unsuppressed; a barrier of height $E_{sph} = (\text{const}) \times v(T)$ rises between neighboring electroweak vacua, where

$$v(T) = \sqrt{|v_u(T)|^2 + |v_d(T)|^2}\ . \tag{2.2}$$

Baryon-number-changing transitions between vacua must surmount this barrier by thermal excitation; hence, the rate for electroweak sphaleron transitions is suppressed by a Boltz-

mann factor [14]:

$$\Gamma_{ws} \propto e^{-E_{sph}/T} . \tag{2.3}$$

This suppression is good news for EWB; electroweak sphalerons, if in equilibrium after the phase transition, would wash out any baryon number previously created by EWB. Thus, we require that $\Gamma_{ws}$ be less than the Hubble rate $H$; this is achieved if the electroweak phase transition is "strongly" first-order, such that $v(T)/T \gtrsim 1$ [15, 7, 9].

A first-order phase transition can occur in the MSSM [47]. The tree-level Higgs potential (including only neutral degrees of freedom) is

$$\begin{aligned} V_0 &= (M_{H_u}^2 + |\mu|^2)\,|H_u^0|^2 + (M_{H_d}^2 + |\mu|^2)\,|H_d^0|^2 \\ &\quad - (\,b\,H_u^0\,H_d^0 + \text{c.c.}\,) + \frac{g_1^2+g_2^2}{8}\left(|H_u^0|^2 - |H_d^0|^2\right)^2 , \end{aligned} \tag{2.4}$$

where $M_{H_{u,d}}^2$ and $b$ are SUSY-breaking parameters, and $\mu$ is the Higgsino mass parameter. We can eliminate these parameters using the minimization conditions for electroweak symmetry breaking at $T = 0$ [52]:

$$M_{H_u}^2 + |\mu|^2 = m_A^2 \cos^2\beta + \frac{1}{2} m_Z^2 \cos 2\beta \tag{2.5a}$$

$$M_{H_d}^2 + |\mu|^2 = m_A^2 \sin^2\beta - \frac{1}{2} m_Z^2 \cos 2\beta \tag{2.5b}$$

$$b = m_A^2 \sin\beta\cos\beta , \tag{2.5c}$$

where $m_Z$ and $m_A$ are the $Z$ and pseudoscalar Higgs boson masses at $T = 0$, and $\tan\beta \equiv v_u/v_d$. Furthermore, we assume that $\tan\beta$ is approximately constant during and after the electroweak phase transition. With this simplification, electroweak symmetry breaking occurs along a fixed direction in $H_u^0$-$H_d^0$ field space, defined by $H_u^0 = \varphi \sin\beta$ and $H_d^0 = \varphi \cos\beta$. The tree-level potential becomes

$$V_0 = -\frac{1}{2} m_Z^2 \cos^2 2\beta\, \varphi^2 + \frac{g_1^2+g_2^2}{8} \cos^2 2\beta\, \varphi^4 . \tag{2.6}$$

The origin at $\varphi = 0$ is unstable; the potential is minimized for $m_Z^2 = (g_1^2 + g_2^2)\,\varphi^2/2$, as expected.

To study the nature of the electroweak phase transition, one computes the one-loop, daisy-improved, finite-temperature potential. Following Ref. [9], this is given by

$$\begin{aligned} V = V_0 + & \sum_i \frac{n_i}{64\pi^2}\, m_i(\varphi)^4 \, \left[ \log\left(\frac{m_i(\varphi)^2}{Q^2}\right) - \frac{3}{2} \right] \\ & + \frac{T^4}{2\pi^2}\left( \sum_{i\in \text{bosons}} n_i\, J_B(m_i(\varphi)^2/T^2) + \sum_{i\in \text{fermions}} n_i\, J_F(m_i(\varphi)^2/T^2) \right) \\ & + \frac{T}{12\pi} \sum_{i\in \text{bosons}} n_i \, \left[ \mathcal{M}_i(\varphi,T)^3 - m_i(\varphi)^3 \right] \end{aligned} \tag{2.7}$$

where $m_i(\varphi)^2$ is the field-dependent mass-squared for particle $i$, and $\mathcal{M}_i(\varphi,T)^2 \equiv m_i(\varphi)^2 + \delta m_i^2$, where $\delta m_i^2$ is the finite-temperature plasma mass for particle $i$, given below in Table 2.2. The loop functions $J_{B,F}$ are

$$\begin{aligned} J_B(m^2/T^2) &\equiv \int_0^\infty dx\; x^2 \; \log\left[1 - \exp\left(-\sqrt{x^2 + m^2/T^2}\right)\right] \\ &= -\frac{\pi^4}{45} + \frac{\pi^2}{12}\frac{m^2}{T^2} - \frac{\pi}{6}\left(\frac{m^2}{T^2}\right)^{3/2} + \mathcal{O}\left(\frac{m^4}{T^4}\right) \end{aligned} \tag{2.8}$$

$$\begin{aligned} J_F(m^2/T^2) &\equiv \int_0^\infty dx\; x^2 \; \log\left[1 + \exp\left(-\sqrt{x^2 + m^2/T^2}\right)\right] \\ &= \frac{7\pi^4}{360} - \frac{\pi^2 m^2}{24 T^2} + \mathcal{O}\left(\frac{m^4}{T^4}\right) \; , \end{aligned} \tag{2.9}$$

with $n_i$ counting the number of on-shell degrees of freedom (with an additional (–) for fermions). Eqs. (2.8,2.9) follow from a high-temperature expansion.

Electroweak symmetry restoration occurs from the terms in $J_{B,F}$ proportional to $m_i^2/T^2$ in the high $T$ expansion. As an example, consider the top quark contribution, for which

$$m_t^2(\varphi) = y_t^2 \, \sin^2\beta\, \varphi^2 \qquad n_t = -12 \; . \tag{2.10}$$

The top quark contributes to the potential the following term quadratic in $\varphi$

$$V \;\supset\; \frac{y_t^2}{4}\, \sin^2\beta\, T^2\, \varphi^2 \; . \tag{2.11}$$

The complete set of terms of this type are

$$V \supset \left(\sin^2\beta\,\delta m_{H_u}^2 + \cos^2\beta\,\delta m_{H_d}^2\right)\,\varphi^2 \propto T^2\,\varphi^2\,, \tag{2.12}$$

where $\delta m_{H_{u,d}}^2$ denotes the plasma masses for $H_{u,d}$, listed in Table 2.2; they are proportional to $T^2$ and depend on which degrees of freedom are active in the plasma. These terms stabilize the origin and restore electroweak symmetry at sufficiently high $T$.

In order for buble nucleation to occur, there must be a critical temperature $T$ where the potential has two degenerate minima, one at $\varphi = 0$ and another at $\varphi \neq 0$, separated by a barrier. The symmetric minimum at $\varphi = 0$ is stabilized by positive quadratic terms given in Eq. (2.12); the potential is stabilized at large $\varphi$ by quartic terms. Therefore, in order to have another minimum at $\varphi \neq 0$, we need a negative cubic term. This is provided by the daisy term, the last term in Eq. (2.7), which receives contributions from bosons. To the extent that $\mathcal{M}_i^2 \propto \varphi^2$, these daisy terms will induce cubic terms in the potential. In the MSSM, the right-handed top squark ("stop") is the only phenomenologically viable candidate to generate a large enough cubic term consistent with a strong first-order phase transition [47]. If we neglect mixing with the left-handed stop, the field-dependent stop mass is

$$\mathcal{M}_{\widetilde{t}_R}^2(\varphi) = M_T^2 + \left(y_t^2\,\sin^2\beta - \frac{2}{3}\,\sin^2\theta_W\,\frac{g_1^2+g_2^2}{2}\,\cos 2\beta\right)\,\varphi^2 + \delta m_{\widetilde{t}_R}^2\,, \tag{2.13}$$

where $\theta_W$ is the weak mixing angle, $M_T^2$ is the SUSY-breaking right-handed stop mass parameter, and $\delta m_{\widetilde{t}_R}^2$ is the RH stop plasma mass. This term gives rise to a cubic term in $V$ only if there is a delicate cancellation between the SUSY-breaking and plasma masses, such that

$$M_T^2 \approx -\delta m_{\widetilde{t}_R}^2 < 0\,. \tag{2.14}$$

Only if the $\varphi^2$ term is exposed is a cubic term generated. It is required that $M_T^2 \lesssim 0$. However, this parameter cannot be made arbitrarily negative without destabilizing the MSSM scalar potential in the $\widetilde{t}_R$-direction, spontaneously breaking SU(3)$_C$. Indeed, the latest results indicate that a strong first-order phase transition in the MSSM is consistent with

experimental bounds only if (i) the zero-temperature right-handed stop mass is less than approximately 125 GeV, (ii) the left-handed stop has mass in excess of 6.5 TeV, and (iii) the zero-temperature electroweak vacuum is meta-stable (with lifetime to decay to the true, color-breaking vacuum longer than the age of the universe) [46].

One popular and simple extension of the MSSM is the addition of a gauge singlet super multiplet. This extension comes in several flavors, differing in which parameters in the singlet sector are allowed or forbidden. We use the moniker NMSSM to refer to all of them. As far as EWB is concerned, the NMSSM has a huge advantage over the MSSM in that it is much easier to generate a strong first-order phase transition [49, 50, 51]. It is not hard to see why. If we assume for simplicity that all three vevs $\langle H_u \rangle$, $\langle H_d \rangle$, $\langle S \rangle$ are real, then by gauge invariance, the most general tree-level potential has the form

$$V_0 = a\,\varphi^2 + b\,\varphi^4 + c\,\varphi_s + d\,\varphi_s^2 + e\,\varphi_s^3 + f\,\varphi_s^4 + g\,\varphi_s\,\varphi^2 + h\,\varphi_s^2\,\varphi^2 \;, \tag{2.15}$$

where $\varphi_s = \langle S \rangle$, $\varphi$ is defined as above, and other parameters are functions of the various Lagrangian parameters and $\beta$. Now, we can perform a shift $\varphi_s \to \varphi_s +$ constant, such that for $\varphi = 0$, $V_0$ is minimized at $\varphi_s = 0$. This eliminates the linear $c$-term. Absorbing this shift into a redefinition of the parameters, Eq. (2.15) becomes

$$V_0 = a\,\varphi^2 + b\,\varphi^4 + d\,\varphi_s^2 + e\,\varphi_s^3 + f\,\varphi_s^4 + g\,\varphi_s\,\varphi^2 + h\,\varphi_s^2\,\varphi^2 \;. \tag{2.16}$$

The fact that electroweak symmetry is broken implies $a < 0$. The leading field-dependent, finite-temperature corrections from the one-loop potential lead to contributions of the form $V_1 \propto \delta a\, T^2 \varphi^2$ in the high-$T$ limit, with dimensionless coefficient $\delta a$, restoring electroweak symmetry. Now, let us assume that electroweak symmetry breaking occurs along a fixed direction in the $\varphi$-$\varphi_s$ plane, defined by $\varphi = \rho\,\cos\theta$ and $\varphi_s = \rho\,\sin\theta$. We see that the potential has the form:

$$\begin{aligned} V \;\supset\; & \left[(\delta a T^2 - |a|)\cos^2\theta + d\,\sin^2\theta\right]\,\rho^2 \;+\; \left[e\,\sin^3\theta + g\,\cos^2\theta\,\sin\theta\right]\,\rho^3 \\ & +\; \left[b\,\cos^4\theta + f\,\sin^4\theta + h\,\sin^2\theta\,\cos^2\theta\right]\,\rho^4 \;. \end{aligned} \tag{2.17}$$

At tree-level, there is a cubic term that may give rise to a first-order EWPT, without a fine-tuned cancellation in the effective potential. This scenario does not require a light, right-handed stop. In this work, we do not study the NMSSM in any detail; rather we use it as motivation to consider a broader range of parameter space than may be viable in the MSSM.

## 2.2 Particle masses, outside and inside the bubble

During the electroweak phase transition, most of the collision and diffusion dynamics take place outside the bubble, where the charge densities are largest, in the phase of unbroken electroweak symmetry. Therefore, when computing inelastic collision rates, we take the degrees of freedom to be those listed in Table 2.1, with well-defined SU(3)$_C$×SU(2)$_L$× U(1)$_Y$ quantum numbers. The particle masses are given by $m_0^2 = M^2 + \delta m^2$, the sum of the renormalized mass parameters $m_0^2$ in the Lagrangian, and the finite temperature plasma masses $\delta m^2$ [43]; the latter are given in Table 2.2.

For Higgs bosons, the story is more potentially more complicated. In order to find the Higgs spectrum in the unbroken phase, one must compute the curvature of the one-loop finite temperature potential at $\langle H_u \rangle = \langle H_d \rangle = 0$. Here, we approximate that the quadratic terms in the potential are given by

$$V \supset \left(H_u^{+\dagger}, H_d^{-}\right) \begin{pmatrix} m_u^2 + |\mu|^2 + \delta m_{H_u} & b \\ b & m_d^2 + |\mu|^2 + \delta m_{H_d} \end{pmatrix} \begin{pmatrix} H_u^{+} \\ H_d^{-\dagger} \end{pmatrix} , \qquad (2.18)$$

and the same for $(H_u^0, H_d^{0\dagger})$ but with $b \to -b$. This is the tree-level potential, but we have included by hand the finite temperature corrections that restore electroweak symmetry, denoted by $\delta m^2_{H_{u,d}}$. These corrections, valid in the high $T$ limit, are given in Tab. 2.2. Again, we use the minimization conditions at $T = 0$ to eliminate the parameters in the

| Species | $\delta m^2_{\rm SM}/T^2 \quad (A)$ | $\delta m^2_{\rm SUSY}/T^2 \quad (B)$ | $\delta m^2_{\rm SUSY}/T^2 \quad (C)$ |
|---|---|---|---|
| $q_L$ | $\frac{1}{6}g_3^2 + \frac{3}{32}g_2^2 + \frac{1}{288}g_1^2 + \frac{1}{16}y_t^2 + \frac{1}{16}y_b^2$ | $+\frac{1}{16}y_t^2$ | $+\frac{1}{16}y_b^2$ |
| $t_R$ | $\frac{1}{6}g_3^2 + \frac{1}{18}g_1^2 + \frac{1}{8}y_t^2$ | $+\frac{1}{18}g_1^2$ | |
| $b_R$ | $\frac{1}{6}g_3^2 + \frac{1}{72}g_1^2 + \frac{1}{8}y_b^2$ | | $+\frac{1}{72}g_1^2$ |
| $\ell_L$ | $\frac{3}{32}g_2^2 + \frac{1}{32}g_1^2 + \frac{1}{16}y_\tau^2$ | | $+\frac{1}{16}y_\tau^2$ |
| $\tau_R$ | $\frac{1}{8}g_1^2 + \frac{1}{8}y_\tau^2$ | | $+\frac{1}{8}g_1^2$ |
| $\widetilde{H}_u$ | | $\frac{3}{16}g_2^2 + \frac{1}{16}g_1^2 + \frac{3}{16}y_t^2$ | |
| $\widetilde{H}_d$ | | $\frac{3}{16}g_2^2 + \frac{1}{16}g_1^2$ | $+\frac{3}{16}y_b^2 + \frac{1}{16}y_\tau^2$ |
| $\widetilde{W}$ | | $\frac{3}{8}g_2^2$ | |
| $\widetilde{B}$ | | $\frac{5}{12}g_2^2$ | $+\frac{2}{12}g_2^2$ |
| $\widetilde{t}_R$ | | $\frac{4}{9}g_3^2 + \frac{1}{3}g_1^2 + \frac{1}{3}y_t^2$ | $-\frac{1}{9}g_1^2$ |
| $\widetilde{b}_R$ | | | $\frac{4}{9}g_3^2 + \frac{1}{18}g_1^2 + \frac{1}{3}y_b^2$ |
| $\widetilde{\tau}_R$ | | | $\frac{1}{2}g_1^2 + \frac{1}{3}y_\tau^2$ |
| $H_u$ | $\frac{3}{16}g_2^2 + \frac{1}{16}g_1^2 + \frac{1}{4}y_t^2$ | $+\frac{3}{16}g_2^2 - \frac{1}{48}g_1^2 + \frac{1}{4}y_t^2$ | $+\frac{1}{12}g_1^2$ |
| $H_d$ | $\frac{3}{16}g_2^2 + \frac{1}{16}g_1^2 + \frac{1}{4}y_b^2 + \frac{1}{12}y_\tau^2$ | $+\frac{3}{16}g_2^2 + \frac{7}{48}g_1^2$ | $-\frac{1}{12}g_1^2 + \frac{1}{4}y_b^2 + \frac{1}{12}y_\tau^2$ |

Table 2.2: Thermal masses $\delta m^2$ for active particles in the plasma during the electroweak phase transition. The different contributions arise from thermal loops involving: (A) SM fermions and gauge bosons only; (B) Higgsinos, Winos, Binos, and RH stops; and (C) RH sbottoms and RH staus.

mass matrix,

$$m_u^2 + |\mu|^2 = m_A^2 \cos^2\beta + \frac{1}{2} m_Z^2 \cos 2\beta \simeq -\frac{1}{2}\, m_Z^2 \tag{2.19a}$$

$$m_d^2 + |\mu|^2 = m_A^2 \sin^2\beta - \frac{1}{2} m_Z^2 \cos 2\beta \simeq m_A^2 + \frac{1}{2}\, m_Z^2 \tag{2.19b}$$

$$b = m_A^2 \sin\beta_0 \cos\beta \simeq 0\ , \tag{2.19c}$$

where the approximations follow assuming $\tan\beta \gg 1$. Therefore, in this limit, the Higgs boson mass matrix (2.18) is diagonal, with eigenvalues

$$m_{H_u}^2 = -\frac{1}{2}\, m_Z^2 + \delta m_{H_u}^2 \tag{2.20a}$$

$$m_{H_d}^2 = m_A^2 + \frac{1}{2}\, m_Z^2 + \delta m_{H_d}^2\ . \tag{2.20b}$$

These are the Higgs boson masses during the electroweak phase transition. We note (i) if $m_A \sim \mathcal{O}(100\ \text{GeV})$, then $H_d$ is also light, and (ii) for sufficiently small $T$, we have $m_{H_u}^2 < 0$, corresponding to the destabilization of the symmetric minimum.

Inside the bubble, within the broken phase, the spacetime-dependent Higgs field leads to spacetime-dependent mass terms that mix supersymmetric particles with different $\mathrm{SU}(2)_L \times \mathrm{U}(1)_Y$ quantum numbers. This effect is what is responsible for charge generation within the bubble wall: the so-called "CP-violating sources." For example, the mass term for charged Higgsinos and Winos is

$$\mathcal{L} \supset - \left(\widetilde{W}^-,\, \widetilde{H}_d^-\right) \begin{pmatrix} M_2 & g_2\, v_u(x) \\ g_2\, v_d(x) & \mu \end{pmatrix} \begin{pmatrix} \widetilde{W}^+ \\ \widetilde{H}_u^+ \end{pmatrix} + \text{h.c.} \tag{2.21}$$

where $\widetilde{W}^\pm$, $\widetilde{H}^\pm_{u,d}$ are two component spinors. In addition, the spacetime-dependent Higgs vevs are $v_{u,d}(x) \equiv \langle H^0_{u,d} \rangle$, and the gauge couplings are $g_i$, for $i = 1, 2, 3$. The coefficients $M_2$ and $\mu$ are the Wino and Higgsino mass parameters, which in general are complex-valued. Now, we perform the phase redefinitions: $\widetilde{W}^- \to e^{-i \arg(M_2)}\, \widetilde{W}^-$ and $\widetilde{H}_d^- \to e^{-i \arg(\mu)}\, \widetilde{H}_d^-$. After this redefinition, we can express this mass term as

$$\begin{aligned} \mathcal{L} \;\supset\; & - |M_2|\, \bar{\Psi}_{\widetilde{W}^+} \Psi_{\widetilde{W}^+} - |\mu|\, \bar{\Psi}_{\widetilde{H}^+} \Psi_{\widetilde{H}^+} \\ & - g_2\, \bar{\Psi}_{\widetilde{H}^+} \left(v_u(x)\, P_L + e^{i\phi_2}\, v_d(x)\, P_R\right) \Psi_{\widetilde{W}^+} + \text{h.c.}\,, \end{aligned} \tag{2.22}$$

where we have defined the four-component Dirac fermions

$$\Psi_{\widetilde{W}^+} = \begin{pmatrix} \widetilde{W}^+ \\ \widetilde{W}^{-\dagger} \end{pmatrix} \qquad \Psi_{\widetilde{H}^+} = \begin{pmatrix} \widetilde{H}_u^+ \\ \widetilde{H}_d^{-\dagger} \end{pmatrix}, \tag{2.23}$$

and CP-violating phase $\phi_2 \equiv \arg(\mu\, M_2\, b^*)$. (Note: the phase of $b$ is implicitly hiding in Eq. (2.22); we have chosen it to vanish though our convention that the vevs $v_{u,d}$ are real.) Similar results apply for the neutral Higgsino, Bino, and Wino; the total spacetime-dependent mass terms are

$$\begin{aligned} \mathcal{L}_M \;=\; & - g_2\, \bar{\Psi}_{\widetilde{H}^+} \left(v_u(x)\, P_L + e^{i\phi_2}\, v_d(x)\, P_R\right) \Psi_{\widetilde{W}^+} \\ & - \frac{g_2}{\sqrt{2}}\, \bar{\Psi}_{\widetilde{H}^0} \left(v_u(x)\, P_L + e^{i\phi_2}\, v_d(x)\, P_R\right) \Psi_{\widetilde{W}^0} \\ & - \frac{g_1}{\sqrt{2}}\, \bar{\Psi}_{\widetilde{H}^0} \left(v_u(x)\, P_L + e^{i\phi_1}\, v_d(x)\, P_R\right) \Psi_{\widetilde{B}^0} \;+\; \text{h.c.} \end{aligned} \tag{2.24}$$

with Bino CP-violating phase $\phi_1 \equiv \arg(\mu\, M_1\, b^*)$, with $M_1$ the Bino mass parameter. defining the four-component spinors

$$\Psi_{\widetilde{B}^0} = \begin{pmatrix} \widetilde{B}^0 \\ \widetilde{B}^{0\dagger} \end{pmatrix}, \qquad \Psi_{\widetilde{W}^0} = \begin{pmatrix} \widetilde{W}^0 \\ \widetilde{W}^{0\dagger} \end{pmatrix}, \qquad \Psi_{\widetilde{H}^0} = \begin{pmatrix} -\widetilde{H}_u^0 \\ \widetilde{H}_d^{0\dagger} \end{pmatrix}. \tag{2.25}$$

In Eq. (2.24), we see how the CP-violating phases and Higgs vevs couple together. Clearly, within the bubble it is no longer appropriate to regard $\Psi_{\widetilde{W}^+}$ and $\Psi_{\widetilde{H}^+}$ as the true degrees of freedom in the plasma; they mix. In this work, we avoid this difficulty by treating the vev-dependent terms in Eq. (2.22) perturbatively, following Refs. [31, 22]; this approximation is valid sufficiently close to the bubble wall, where the vevs are small. More sophisticated treatments, involving a spacetime-dependent diagonalization of the full vev-dependent mass matrix, have been pursued in Refs. [32, 33, 34].

## 2.3 MSSM Interactions

Inelastic interactions are of utmost importance for electroweak baryogenesis. Charge density, initially created for a supersymmetric species, must be converted into left-handed quark or lepton charge density in order to bias baryon number generation via electroweak sphalerons. How effective this conversion is depends crucially upon which interactions are in chemical equilibrium during the phase transition.

Two classes of interactions are relevant: gaugino interactions and Yukawa interactions. Gaugino interactions, the supersymmetric variant of SM gauge interactions, are processes that convert SM particles into their supersymmetric partners via the absorption or decay of gluinos, Winos, and Binos. They lead to interaction coefficients, generically denoted $\Gamma_{\widetilde{V}}$, which tend to equilibrate the chemical potentials for particles and their superpartners. All previous studies have assumed the limit $\Gamma_{\tilde{V}} \to \infty$, which leads to superequilibrium. In Chapter 4, we examine under what conditions this assumption is true or false.

We list the gaugino interaction terms: for Higgs bosons and Higgsinos, we have

$$\begin{aligned}\mathcal{L}_{\widetilde{V}} \supset & -\frac{g_1}{\sqrt{2}}\left[\bar{\Psi}_{\widetilde{H}^+}(H_d^{-*}\,P_L + e^{i\phi_\mu}H_u^+\,P_R)\Psi_{\widetilde{B}} + \bar{\Psi}_{\widetilde{H}^0}(H_d^{0*}\,P_L - e^{i\phi_\mu}H_u^0\,P_R)\Psi_{\widetilde{B}}\right] \\ & -\frac{g_2}{\sqrt{2}}\left[\bar{\Psi}_{\widetilde{H}^+}(-H_d^{-*}\,P_L + e^{i\phi_\mu}H_u^+\,P_R)\Psi_{\widetilde{W}^0} + \bar{\Psi}_{\widetilde{H}^0}(H_d^{0*}\,P_L + e^{i\phi_\mu}H_u^0\,P_R)\Psi_{\widetilde{W}^0}\right] \\ & -g_2\left[\bar{\Psi}_{\widetilde{H}^+}(H_d^{0*}\,P_L + e^{i\phi_\mu}H_u^0\,P_R)\Psi_{\widetilde{W}^+} + \bar{\Psi}_{\widetilde{W}^+}(H_d^{-*}\,P_L - e^{i\phi_\mu}H_u^+\,P_R)\Psi^C_{\widetilde{H}^0}\right] \\ & +\text{ h.c. ;}\end{aligned} \tag{2.26a}$$

for quarks and quarks, we have

$$\begin{aligned}\mathcal{L}_{\widetilde{V}} \supset & -\frac{g_2}{\sqrt{2}}\left[\widetilde{u}_L^{i*}\,\bar{\Psi}_{\widetilde{W}^0}\,P_L\,u_L^i - \widetilde{d}_L^{i*}\,\bar{\Psi}_{\widetilde{W}^0}\,P_L\,d_L^i\right] \\ & -\frac{g_1}{3\sqrt{2}}\left[\widetilde{u}_L^{i*}\,\bar{\Psi}_{\widetilde{B}}\,P_L\,u_L^i + \widetilde{d}_L^{i*}\,\bar{\Psi}_{\widetilde{B}}\,P_L\,d_L^i\right] \\ & -g_3\sqrt{2}\left[\widetilde{u}_L^{i*}\,\lambda^a\bar{\Psi}^a_{\widetilde{G}}\,P_L\,u_L^i + \widetilde{d}_L^{i*}\,\lambda^a\,\bar{\Psi}^a_{\widetilde{G}}\,P_L\,d_L^i\right] \\ & -g_2\,\widetilde{d}_L^{i*}\,\bar{\Psi}_{\widetilde{W}^+}\,P_L\,u_L^i - g_2\,\widetilde{u}_L^{i*}\,\bar{\Psi}^C_{\widetilde{W}^+}\,P_L\,d_L^i \\ & -g_3\sqrt{2}\left[\widetilde{u}_R^i\,\bar{\lambda}^a\bar{u}_R^i P_L\Psi^a_{\widetilde{G}} + \widetilde{d}_R^i\,\bar{\lambda}^a\bar{d}_R^i P_L\Psi^a_{\widetilde{G}}\right] \\ & +\frac{2\sqrt{2}}{3}\,g_1\left[\widetilde{u}_R^i\,\bar{u}_R^i\,P_L\,\Psi_{\widetilde{B}}\right] - \frac{\sqrt{2}}{3}\,g_1\left[\widetilde{d}_R^i\,\bar{d}_R^i\,P_L\,\Psi_{\widetilde{B}}\right] + \text{ h.c. ;}\end{aligned} \tag{2.26b}$$

and for leptons and sleptons, we have

$$\begin{aligned}\mathcal{L}_{\widetilde{V}} \supset & -\frac{g_2}{\sqrt{2}}\left[\widetilde{\nu}_L^{i*}\,\bar{\Psi}_{\widetilde{W}^0}\,P_L\,\nu_L^i - \widetilde{e}_L^{i*}\,\bar{\Psi}_{\widetilde{W}^0}\,P_L\,e_L^i\right] \\ & +\frac{g_1}{\sqrt{2}}\left[\widetilde{\nu}_L^{i*}\,\bar{\Psi}_{\widetilde{B}}\,P_L\,\nu_L^i + \widetilde{e}_L^{i*}\,\bar{\Psi}_{\widetilde{B}}\,P_L\,e_L^i\right] \\ & -g_2\,\widetilde{e}_L^{j*}\,\bar{\Psi}_{\widetilde{W}^+}\,P_L\,\nu_L^i - g_2\,\widetilde{\nu}_L^{i*}\,\bar{\Psi}^C_{\widetilde{W}^+}\,P_L\,e_L^j \\ & -\sqrt{2}\,g_1\left[\widetilde{e}_R^i\,\bar{e}_R^i\,P_L\,\Psi_{\widetilde{B}}\right] + \text{ h.c. .}\end{aligned} \tag{2.26c}$$

Here, the index $i = 1, 2, 3$ labels generation. Color indeces have been suppressed; the matrices $\lambda^a$ ($\bar{\lambda}^a$) are the SU(3)$_C$ generators in the 3 ($\bar{3}$) representation, normalized such that $Tr[\lambda^a\lambda^b] = \delta_{ab}/2$. Furthermore, we have neglected flavor-violation altogether. Assuming that the CKM matrix is the only source of flavor-mixing, we can neglect Cabibbo-

suppressed interactions; they will be too slow compared to the dynamical time scales of EWB.

Next, we consider Yukawa interactions, here defined as all interactions mediated by third generation Yukawa couplings $y_{t,b,\tau}$. Until recently, it had been assumed that only top Yukawa interactions are relevant for EWB dynamics. This assumption is false; both bottom and tau Yukawa interactions can also be important, drastically affecting the conversion of charge density into left-handed quarks and leptons [24]. The third generation Yukawa interactions are

$$\begin{aligned}
\mathcal{L}_y \;=\; & y_t \left(\mu^* H_d^{-\dagger} - A_t H_u^+\right) \widetilde{b}_L \widetilde{t}_R^\dagger + y_t \left(\mu^* H_d^{0\dagger} + A_t H_u^0\right) \widetilde{b}_L \widetilde{t}_R^\dagger \\
& + y_b \left(\mu^* H_u^{+\dagger} + A_b H_d^-\right) \widetilde{t}_L \widetilde{b}_R^\dagger + y_b \left(\mu^* H_u^{+\dagger} - A_b H_d^0\right) \widetilde{b}_L \widetilde{b}_R^\dagger \\
& + y_\tau \left(\mu^* H_u^{+\dagger} + A_\tau H_d^-\right) \widetilde{\nu}_L^\tau \widetilde{\tau}_R^\dagger + y_\tau \left(\mu^* H_u^{+\dagger} - A_b H_d^0\right) \widetilde{\tau}_L \widetilde{\tau}_R^\dagger \\
& + y_t H_u^+ \bar{t}_R P_L b_L - y_t H_u^0 \bar{t}_R P_L t_L \\
& + y_b H_d^- \bar{b}_R P_L t_L - y_b H_d^0 \bar{b}_R P_L b_L \\
& + y_\tau H_d^+ \bar{\tau}_R P_L \nu_L^\tau - y_\tau H_d^0 \bar{\tau}_R P_L \tau_L \\
& + y_t \widetilde{t}_R^\dagger \bar{\Psi}^C_{\widetilde{H}^0} P_L t_L + y_t \widetilde{t}_R^\dagger \bar{\Psi}^C_{\widetilde{H}^+} P_L b_L \\
& + y_b \widetilde{b}_R^\dagger \bar{\Psi}_{\widetilde{H}^+} P_L t_L - y_b \widetilde{b}_R^\dagger \bar{\Psi}_{\widetilde{H}^0} P_L b_L \\
& + y_\tau \widetilde{\tau}_R^\dagger \bar{\Psi}_{\widetilde{H}^+} P_L \nu_L^\tau + y_\tau \widetilde{\tau}_R^\dagger \bar{\Psi}_{\widetilde{H}^0} P_L \tau_L \\
& + y_t \widetilde{t}_L \bar{t}_R P_L \Psi_{\widetilde{H}^0} + y_t \widetilde{b}_L \bar{t}_R P_L \Psi_{\widetilde{H}^+} \\
& + y_b \widetilde{t}_L \bar{b}_R P_L \Psi^C_{\widetilde{H}^+} - y_b \widetilde{b}_L \bar{b}_R P_L \Psi^C_{\widetilde{H}^0} \\
& + y_\tau \widetilde{\nu}_L^\tau \bar{\tau}_R P_L \Psi^C_{\widetilde{H}^+} - y_\tau \widetilde{\tau}_L \bar{\tau}_R P_L \Psi^C_{\widetilde{H}^0} \;+\; \text{h.c.}
\end{aligned} \tag{2.27}$$

with SUSY-breaking parameters $A_{t,b,\tau}$. These interactions lead to top, bottom, and tau Yukawa interaction rates, generically denoted $\Gamma_{yt}$, $\Gamma_{yb}$, and $\Gamma_{y\tau}$, respectively. In Chapter 4, we will compute these gaugino and Yukawa rates explicitly.

# Chapter 3

# Charge Transport Dynamics

The dynamics of the plasma during the electroweak phase transition are governed by a system of Boltzmann equations. These equations describe how charge density of a given species (i) is generated through CP-violating scattering with the expanding bubble wall, (ii) diffuses into the phase of unbroken electroweak symmetry, and (iii) reaches chemical equilibrium through interactions with other species in the plasma. Some fraction of the charge density generated by the wall is converted into left-handed fermion density $n_L$, which in turn biases the creation of baryon number via electroweak sphaleron processes. In this section, we will identify these Boltzmann equations and compute the collision terms therein.

## 3.1 Preliminaries

The Boltzman equations leading to EWB have been derived using the closed-time-path (CTP) formulation of non-equilibrium quantum field theory [25]. This formalism is summarized in the Appendix. We note that for the pupose of computing thermally-averaged collision rates, the CTP approach offers little over the usual semi-classical treatment (e.g., [36]); however, it is essential in computing scattering rates of particles with the background Higgs field of the expanding bubble. Ultimately, we arrive at a system of equations of the form

$$\partial_\mu \, j_i^\mu = -\frac{T^2}{6} \sum_X \Gamma_X \left( \mu_i + \mu_j + ... - \mu_k - \mu_\ell - ... \right) + S_i^{\not{CP}} \tag{3.1}$$

where $j_i^\mu$ is the charge current density of the species $i$. The density $j_i^\mu$, induced by CP-violating source $S_i^{\not CP}$, is coupled to other species via coefficients $\Gamma_X$ that describe the rate for a process $i + j + ... \leftrightarrow k + \ell + ...$ to occur. (We have explicitly factored $T^2/6$ out of $\Gamma_X$, for reasons that will become clear below.) The chemical potentials are denoted by $\mu_i$. Chemical equilibrium, when

$$\mu_i + \mu_j + ... - \mu_k - \mu_\ell - ... = 0 \ , \tag{3.2}$$

is maintained when when the interaction rate $\Gamma_X$ is sufficiently large.

Let us first consider the LHS of Eq. (3.1). First, we assume a planar bubble wall profile, so that all charge densities are functions only of $z \equiv v_w X^0 + X^3$, the displacement from the moving bubble wall in its rest frame (where $v_w$ is the velocity of the bubble wall, and $X^\mu$ is the plasma-frame coordinate). Second, we apply Fick's law [26, 27, 28, 16, 29], which allows us to replace $\mathbf{j}_i \to -D_i \nabla n_i$ on the LHS of Eq. (3.1), with charge density $n_i \equiv j_i^0$. The diffusion constant $D_i$ is the mean free path of particle $i$ in the plasma. In all, the LHS of Eq. (3.1) becomes

$$\partial_\mu \, j_i^\mu = v_w \, n_i' - D_i \, n_i'' \ . \tag{3.3}$$

We have neglected Hubble expansion in our Boltzmann equations; the Hubble time scale $H^{-1} \sim M_{\rm pl}/T^2$ is much much longer than all dynamical time scales relevant for EWB.

Next, we turn to the RHS of Eq. (3.1). The chemical potentials are related to their corresponding charge densities by

$$n_i = \frac{T^2}{6} \, k_i \, \mu_i + \mathcal{O}\left(\frac{\mu_i}{T}\right)^3 \ , \tag{3.4}$$

where we have performed an expansion assuming $\mu_i/T \ll 1$. The statistical weight $k_i$ is defined by

$$k_i = g_i \, \frac{6}{\pi^2} \int_{m_i/T}^\infty dx \, x \, \frac{e^x}{(e^x \pm 1)^2} \sqrt{x^2 - m_i^2/T^2} \ , \tag{3.5}$$

in which $g_i$ counts the number of internal degrees of freedom, the $+$ $(-)$ sign is taken for fermions (bosons), and the mass of the $i$th particle $m_i$ is taken to be the effective mass at

temperature $T$. For reference, chiral fermions have $k_i(0) = 1$, while Dirac fermions and complex scalars have $k_i(0) = 2$. In our analysis to follow, these $k$-factors are ubiquitous. They essentially count the effective number of degrees of freedom for a given species in the plasma, i.e., the true number of degrees of freedom, weighted by a Boltzmann factor.

While in principle there is an interaction coefficient $\Gamma_X$ for every interaction in the supersymmetric Lagrangian, we can determine which ones need to be taken into account for the EWB computation by considering the relevant time scales. After a time $t$, charge densities created at the bubble wall will have diffused on average by a distance $d_{\rm diff} = \sqrt{\bar{D}\,t}$ (with the effective diffusion constant $\bar{D}$ to be defined below). At the same time, the moving bubble wall advances a distance $d_{\rm wall} = v_w\,t$. The diffusion time scale, defined by $d_{\rm diff} = d_{\rm wall}$, gives the time that it takes for charge, having been created at the bubble wall and having diffused into the unbroken phase, to be recaptured by the advancing bubble wall and be quenched through CP-conserving scattering within the phase of broken electroweak symmetry. This time scale is

$$\tau_{\rm diff} \equiv \bar{D}/v_w^2 \ . \tag{3.6}$$

Numerically, we have $\tau_{\rm diff} \sim 10^4/T$ (shown later). To this, we compare $\tau_X \equiv \Gamma_X^{-1}$, the interaction time scale. If $\tau_X \gg \tau_{\rm diff}$, then the process $i + j + ... \leftrightarrow k + \ell + ...$ is slow and $\Gamma_X$ may be neglected from the Boltzmann equations. Physically speaking, charge density is recaptured by the advancing bubble wall before conversion processes can occur. On the other hand, if $\tau_X \ll \tau_{\rm diff}$, then these interactions are rapidly occuring as the charge density is diffusing ahead of the advancing wall, leading to chemical equilibrium (3.2). Expressed in terms of charge densities, the chemical equilibrium condition is

$$\frac{n_i}{k_i} + \frac{n_j}{k_j} + \ ... \ - \frac{n_k}{k_k} - \frac{n_\ell}{k_\ell} \ - ... \ = 0 \ . \tag{3.7}$$

In this case, the interaction $\Gamma_X$ must be included in the Boltzmann equations.

A similar argument tells us how we expect deviations from Eq. (3.7) to arise. Suppose that species $i$ is produced from the expanding bubble wall at $z = 0$. On distance scales $|z| \lesssim \sqrt{\bar{D}\,\tau_X}$, close to the bubble wall, Eq. (3.7) will break down: particles $i$ have not had enough time to interact via $\Gamma_X$.

Finally, we see that the Boltzmann equations are a system of coupled, second order, ordinary differential equations for the set of charge densities $n_i(z)$. Ultimately, it is the total left-handed fermionic charge density

$$n_L \equiv \sum_{i=1}^{3} \left( n_{u_L^i} + n_{d_L^i} + n_{\nu_L^i} + n_{\ell_L^i} \right) \tag{3.8}$$

that biases weak sphaleron transitions, thereby determining $n_B/s$.

## 3.2 Boltzmann equations in the MSSM

Hypercharge $Y$ and the third component of weak isospin $T^3$ are conserved in the phase of unbroken electroweak symmetry, but not in the broken phase. Both charges, generated in the broken phase within the bubble wall, diffuse into the unbroken phase where they are conserved. (Of course, no electromagnetic charge is generated, since it is conserved in both phases.)

We now show that it is the hypercharge densities, carried by various species in the plasma, rather than the $T^3$ charge densities, which are relevant for the EWB computation. To see how this works, let us consider how this works for a subset of the Boltzmann equations. The hypercharge density carried by third generation LH quarks $t_L$ and $b_L$ is proportional to the isoscalar density $(t_L + b_L)$; the $T^3$ charge density is given by the isovector density $(t_L - b_L)$. (We adopt the notation, e.g., $t_L^\mu \equiv j_{t_L}^\mu$ and $t_L \equiv n_{t_L}$.) The Boltzmann equations for these species are

$$\partial_\mu t_L^\mu = -\Gamma\left[t_L, b_L, W^+\right] \left( \frac{t_L}{k_{t_L}} - \frac{b_L}{k_{b_L}} - \frac{W^+}{k_{W^+}} \right) + \ldots \tag{3.9a}$$

$$\partial_\mu b_L^\mu = \Gamma\left[t_L, b_L, W^+\right] \left( \frac{t_L}{k_{t_L}} - \frac{b_L}{k_{b_L}} - \frac{W^+}{k_{W^+}} \right) + \ldots \tag{3.9b}$$

where on the RHS we have isolated only the collision term for the scattering process $t_L\, g \leftrightarrow b_L\, W^+$ ($g$ is a gluon), with interaction rate $\Gamma\left[t_L, b_L, W^+\right]$ that is presumably fast

compared to $\tau_{\rm diff}$. Now, we take the sum and difference of Eqs. (3.9):

$$\partial_\mu \left(t_L + b_L\right)^\mu \;=\; 0 \;+\; ... \tag{3.10a}$$

$$\partial_\mu \left(t_L - b_L\right)^\mu \;=\; -\,2\,\Gamma\left[t_L, b_L, W^+\right]\left(\frac{t_L - b_L}{k_{q_L}} - \frac{W^+}{k_{W^+}}\right) \;+\; ... \tag{3.10b}$$

where $k_{q_L} \equiv k_{t_L} = k_{b_L}$ (valid in the unbroken phase since $m_{t_L} = m_{b_L}$). Therefore, we have shown that the isoscalar density $(t_L + b_L)$ decouples from the isovector densities $(t_L - b_L)$ and $W^+$, modulo weak isospin violation within the bubble wall. Although this is just one simple example, this idea is true in general: isoscalar and isovector densities decouple [35]. Since baryon number generation through weak sphalerons is biased by $n_L$, an isoscalar density, we only need to consider isoscalar densities. In other words, we only need to keep track of the hypercharge carried in various species in the plasma, not the $T^3$ charge density.

Hypercharge is carried by the following isoscalar densities: left-handed quarks $q_i \equiv (u_{iL} + d_{iL})$, right-handed quarks $u_i \equiv u_{iR}$ and $d_i \equiv d_{iR}$, left-handed leptons $\ell_i \equiv (\nu_{iL} + e_{iL})$, and right-handed leptons $e_i \equiv e_{iR}$, where $i = 1, 2, 3$ labels generation. In addition, hypercharge can be carried by Higgs boson and Higgsino charge densities, respectively: $H_i \equiv (H_i^+ + H_i^0)$ and $\widetilde{H} \equiv (\widetilde{H}^+ + \widetilde{H}^0)$. This last point may seem confusing, since it is known that neutral Higgs bosons $H_i^0$ and Higgsinos $\widetilde{H}^0$ decompose into real scalars and Majorana fermions, which can carry no charge. This is statement is only true after electroweak symmetry breaking has occured. In the unbroken phase, the neutral Higgs boson is a complex scalar, while the neutral Higgsino is a Dirac fermion. Both species can carry charge — which makes sense since both are charged under hypercharge, an unbroken symmetry in the unbroken phase.

We now present the full of set of Boltzmann equations in all their glory for the weak isoscalar charge densities relevant for EWB. First, we give the equations; then we discuss

their ingredients. The Boltzmann equations for left-handed quarks are

$$\begin{aligned}
\partial_\mu q_3^\mu &= -\Gamma_M[u_3,q_3]\left(\frac{q_3}{k_{q_3}}-\frac{u_3}{k_{u_3}}\right)-\Gamma_M[d_3,q_3]\left(\frac{q_3}{k_{q_3}}-\frac{d_3}{k_{d_3}}\right) \qquad (3.11a)\\
&\quad -\Gamma_{\widetilde{V}}[q_3,\widetilde{q}_3]\left(\frac{q_3}{k_{q_3}}-\frac{\widetilde{q}_3}{k_{\widetilde{q}_3}}\right)-2\,\Gamma_{\rm ss}\,N_5\\
&\quad -\Gamma_{yt}[u_3,q_3,H_u]\left(\frac{q_3}{k_{q_3}}-\frac{u_3}{k_{u_3}}+\frac{H_u}{k_{H_u}}\right)-\Gamma_{yb}[d_3,q_3,H_2]\left(\frac{q_3}{k_{q_3}}-\frac{d_3}{k_{d_3}}-\frac{H_2}{k_{H_2}}\right)\\
&\quad -\Gamma_{yt}[\widetilde{u}_3,q_3,\widetilde{H}]\left(\frac{q_3}{k_{q_3}}-\frac{\widetilde{u}_3}{k_{\widetilde{u}_3}}+\frac{\widetilde{H}}{k_{\widetilde{H}}}\right)-\Gamma_{yb}[\widetilde{d}_3,q_3,\widetilde{H}]\left(\frac{q_3}{k_{q_3}}-\frac{\widetilde{d}_3}{k_{\widetilde{d}_3}}-\frac{\widetilde{H}}{k_{\widetilde{H}}}\right)\\
\partial_\mu \widetilde{q}_3^\mu &= -\Gamma_M[\widetilde{u}_3,\widetilde{q}_3]\left(\frac{\widetilde{q}_3}{k_{\widetilde{q}_3}}-\frac{\widetilde{u}_3}{k_{\widetilde{u}_3}}\right)-\Gamma_M[\widetilde{d}_3,\widetilde{q}_3]\left(\frac{\widetilde{q}_3}{k_{\widetilde{q}_3}}-\frac{\widetilde{d}_3}{k_{\widetilde{d}_3}}\right) \qquad (3.11b)\\
&\quad -\Gamma_{yt}[\widetilde{u}_3,\widetilde{q}_3,H_u]\left(\frac{\widetilde{q}_3}{k_{\widetilde{q}_3}}-\frac{\widetilde{u}_3}{k_{\widetilde{u}_3}}+\frac{H_u}{k_{H_u}}\right)-\Gamma_{yb}[\widetilde{d}_3,\widetilde{q}_3,H_d]\left(\frac{\widetilde{q}_3}{k_{\widetilde{q}_3}}-\frac{\widetilde{d}_3}{k_{\widetilde{d}_3}}-\frac{H_d}{k_{H_d}}\right)\\
&\quad -\Gamma_{yt}[u_3,\widetilde{q}_3,\widetilde{H}]\left(\frac{\widetilde{q}_3}{k_{\widetilde{q}_3}}-\frac{u_3}{k_{u_3}}+\frac{\widetilde{H}}{k_{\widetilde{H}}}\right)-\Gamma_{yb}[d_3,\widetilde{q}_3,\widetilde{H}]\left(\frac{\widetilde{q}_3}{k_{\widetilde{q}_3}}-\frac{d_3}{k_{d_3}}-\frac{\widetilde{H}}{k_{\widetilde{H}}}\right)\\
&\quad +\Gamma_{\widetilde{V}}[q_3,\widetilde{q}_3]\left(\frac{q_3}{k_{q_3}}-\frac{\widetilde{q}_3}{k_{\widetilde{q}_3}}\right)-S_{\widetilde{t}}^{\not{C}\not{P}}+S_{\widetilde{b}}^{\not{C}\not{P}}\\
\partial_\mu q_i^\mu &= -\Gamma_{\widetilde{V}}[q_3,\widetilde{q}_3]\left(\frac{q_3}{k_{q_3}}-\frac{\widetilde{q}_3}{k_{\widetilde{q}_3}}\right)-2\,\Gamma_{\rm ss}\,N_5 \qquad (3.11c)\\
\partial_\mu \widetilde{q}_i^\mu &= \Gamma_{\widetilde{V}}[q_3,\widetilde{q}_3]\left(\frac{q_3}{k_{q_3}}-\frac{\widetilde{q}_3}{k_{\widetilde{q}_3}}\right)\,. \qquad (3.11d)
\end{aligned}$$

For right-handed up-type quarks, we have

$$\begin{aligned}
\partial_\mu u_3^\mu &= \Gamma_M[u_3,q_3]\left(\frac{q_3}{k_{q_3}}-\frac{u_3}{k_{u_3}}\right)-\Gamma_{\widetilde{V}}[u_3,\widetilde{u}_3]\left(\frac{u_3}{k_{u_3}}-\frac{\widetilde{u}_3}{k_{\widetilde{u}_3}}\right) && \text{(3.12a)}\\
&\quad+\Gamma_{yt}[u_3,q_3,H_u]\left(\frac{q_3}{k_{q_3}}-\frac{u_3}{k_{u_3}}+\frac{H_u}{k_{H_u}}\right)\\
&\quad+\Gamma_{yt}[u_3,\widetilde{q}_3,\widetilde{H}]\left(\frac{\widetilde{q}_3}{k_{\widetilde{q}_3}}-\frac{u_3}{k_{u_3}}+\frac{\widetilde{H}}{k_{\widetilde{H}}}\right)+\Gamma_{\rm ss}\,N_5\\
\partial_\mu \widetilde{u}_3^\mu &= \Gamma_M[\widetilde{u}_3,\widetilde{q}_3]\left(\frac{\widetilde{q}_3}{k_{\widetilde{q}_3}}-\frac{\widetilde{u}_3}{k_{\widetilde{u}_3}}\right)+\Gamma_{\widetilde{V}}[u_3,\widetilde{u}_3]\left(\frac{u_3}{k_{u_3}}-\frac{\widetilde{u}_3}{k_{\widetilde{u}_3}}\right) && \text{(3.12b)}\\
&\quad\Gamma_{yt}[\widetilde{u}_3,\widetilde{q}_3,H_u]\left(\frac{\widetilde{q}_3}{k_{\widetilde{q}_3}}-\frac{\widetilde{u}_3}{k_{\widetilde{u}_3}}+\frac{H_u}{k_{H_u}}\right) && \text{(3.12c)}\\
&\quad+\Gamma_{yt}[\widetilde{u}_3,q_3,\widetilde{H}]\left(\frac{q_3}{k_{q_3}}-\frac{\widetilde{u}_3}{k_{\widetilde{u}_3}}+\frac{\widetilde{H}}{k_{\widetilde{H}}}\right)+S_{\widetilde{t}}^{\not{\rm CP}}
\end{aligned}$$

For right-handed down-type quarks, we have

$$\begin{aligned}
\partial_\mu d_3^\mu &= \Gamma_M[d_3,q_3]\left(\frac{q_3}{k_{q_3}}-\frac{d_3}{k_{d_3}}\right)-\Gamma_{\widetilde{V}}[d_3,\widetilde{d}_3]\left(\frac{d_3}{k_{d_3}}-\frac{\widetilde{d}_3}{k_{\widetilde{d}_3}}\right) && \text{(3.13a)}\\
&\quad+\Gamma_{yb}[d_3,q_3,H_d]\left(\frac{q_3}{k_{q_3}}-\frac{d_3}{k_{d_3}}+\frac{H_d}{k_{H_d}}\right)\\
&\quad+\Gamma_{yb}[d_3,\widetilde{q}_3,\widetilde{H}]\left(\frac{\widetilde{q}_3}{k_{\widetilde{q}_3}}-\frac{d_3}{k_{d_3}}-\frac{\widetilde{H}}{k_{\widetilde{H}}}\right)+\Gamma_{\rm ss}\,N_5\\
\partial_\mu \widetilde{d}_3^\mu &= \Gamma_M[\widetilde{d}_3,\widetilde{q}_3]\left(\frac{\widetilde{q}_3}{k_{\widetilde{q}_3}}-\frac{\widetilde{d}_3}{k_{\widetilde{d}_3}}\right)+\Gamma_{\widetilde{V}}[d_3,\widetilde{d}_3]\left(\frac{d_3}{k_{d_3}}-\frac{\widetilde{d}_3}{k_{\widetilde{d}_3}}\right) && \text{(3.13b)}\\
&\quad+\Gamma_{yb}[\widetilde{d}_3,\widetilde{q}_3,H_d]\left(\frac{\widetilde{q}_3}{k_{\widetilde{q}_3}}-\frac{\widetilde{d}_3}{k_{\widetilde{d}_3}}+\frac{H_d}{k_{H_d}}\right)\\
&\quad+\Gamma_{yb}[\widetilde{d}_3,q_3,\widetilde{H}]\left(\frac{q_3}{k_{q_3}}-\frac{\widetilde{d}_3}{k_{\widetilde{d}_3}}-\frac{\widetilde{H}}{k_{\widetilde{H}}}\right)-S_{\widetilde{b}}^{\not{\rm CP}}
\end{aligned}$$

Next, the Boltzmann equations for left-handed leptons are

$$\begin{aligned}
\partial_\mu \ell_3^\mu &= -\Gamma_M[e_3,\ell_3]\left(\frac{\ell_3}{k_{\ell_3}}-\frac{e_3}{k_{e_3}}\right)-\Gamma_{\widetilde{V}}[\ell_3,\widetilde{\ell}_3]\left(\frac{\ell_3}{k_{\ell_3}}-\frac{\widetilde{\ell}_3}{k_{\widetilde{\ell}_3}}\right) \\
&\quad -\Gamma_{y\tau}[e_3,\ell_3,H_d]\left(\frac{\ell_3}{k_{\ell_3}}-\frac{e_3}{k_{e_3}}+\frac{H_d}{k_{H_d}}\right) \\
&\quad -\Gamma_{y\tau}[\widetilde{e}_3,\ell_3,\widetilde{H}]\left(\frac{\ell_3}{k_{\ell_3}}-\frac{\widetilde{e}_3}{k_{\widetilde{e}_3}}-\frac{\widetilde{H}}{k_{\widetilde{H}}}\right)
\end{aligned} \tag{3.14a}$$

$$\begin{aligned}
\partial_\mu \widetilde{\ell}_3^\mu &= -\Gamma_M[\widetilde{e}_3,\widetilde{\ell}_3]\left(\frac{\widetilde{\ell}_3}{k_{\widetilde{\ell}_3}}-\frac{\widetilde{e}_3}{k_{\widetilde{e}_3}}\right)+\Gamma_{\widetilde{V}}[\ell_3,\widetilde{\ell}_3]\left(\frac{\ell_3}{k_{\ell_3}}-\frac{\widetilde{\ell}_3}{k_{\widetilde{\ell}_3}}\right) \\
&\quad -\Gamma_{y\tau}[\widetilde{e}_3,\widetilde{\ell}_3,H_d]\left(\frac{\widetilde{\ell}_3}{k_{\widetilde{\ell}_3}}-\frac{\widetilde{e}_3}{k_{\widetilde{e}_3}}+\frac{H_d}{k_{H_d}}\right) \\
&\quad -\Gamma_{y\tau}[\widetilde{e}_3,\ell_3,\widetilde{H}]\left(\frac{\widetilde{\ell}_3}{k_{\widetilde{\ell}_3}}-\frac{e_3}{k_{e_3}}-\frac{\widetilde{H}}{k_{\widetilde{H}}}\right)+S_{\widetilde{\tau}}^{\not{C}\not{P}}
\end{aligned} \tag{3.14b}$$

$$\begin{aligned}
\partial_\mu \ell_i^\mu &= 0\,, \qquad i=1,2 \\
\partial_\mu \widetilde{\ell}_i^\mu &= 0\,, \qquad i=1,2
\end{aligned} \tag{3.14c}$$

For right-handed leptons we have

$$\begin{aligned}
\partial_\mu e_3^\mu &= \Gamma_M[e_3,\ell_3]\left(\frac{\ell_3}{k_{\ell_3}}-\frac{e_3}{k_{e_3}}\right)-\Gamma_{\widetilde{V}}[e_3,\widetilde{e}_3]\left(\frac{e_3}{k_{e_3}}-\frac{\widetilde{e}_3}{k_{\widetilde{e}_3}}\right) \qquad (3.15a)\\
&\quad +\Gamma_{y\tau}[e_3,\ell_3,H_d]\left(\frac{\ell_3}{k_{\ell_3}}-\frac{e_3}{k_{e_3}}+\frac{H_d}{k_{H_d}}\right)\\
&\quad +\Gamma_{y\tau}[\widetilde{e}_3,\ell_3,\widetilde{H}]\left(\frac{\ell_3}{k_{\ell_3}}-\frac{\widetilde{e}_3}{k_{\widetilde{e}_3}}-\frac{\widetilde{H}}{k_{\widetilde{H}}}\right)\\
\partial_\mu \widetilde{e}_3^\mu &= \Gamma_M[\widetilde{e}_3,\widetilde{\ell}_3]\left(\frac{\widetilde{\ell}_3}{k_{\widetilde{\ell}_3}}-\frac{\widetilde{e}_3}{k_{\widetilde{e}_3}}\right)+\Gamma_{\widetilde{V}}[e_3,\widetilde{e}_3]\left(\frac{e_3}{k_{e_3}}-\frac{\widetilde{e}_3}{k_{\widetilde{e}_3}}\right) \qquad (3.15b)\\
&\quad +\Gamma_{y\tau}[\widetilde{e}_3,\widetilde{\ell}_3,H_d]\left(\frac{\widetilde{\ell}_3}{k_{\widetilde{\ell}_3}}-\frac{\widetilde{e}_3}{k_{\widetilde{e}_3}}+\frac{H_d}{k_{H_d}}\right)\\
&\quad +\Gamma_{y\tau}[\widetilde{e}_3,\ell_3,\widetilde{H}]\left(\frac{\widetilde{\ell}_3}{k_{\widetilde{\ell}_3}}-\frac{e_3}{k_{e_3}}-\frac{\widetilde{H}}{k_{\widetilde{H}}}\right)-S_{\widetilde{\tau}}^{\not{C}\not{P}}\\
\partial_\mu e_i^\mu &= 0\,, \qquad i=1,2 \qquad (3.15c)\\
\partial_\mu \widetilde{e}_i^\mu &= 0\,, \qquad i=1,2 \qquad (3.15d)
\end{aligned}$$

Lastly, the Boltzmann equations for Higgs and Higgsino densities are

$$\begin{aligned}
\partial_\mu H_i^\mu &= -\Gamma_{yt}[u_3,q_3,H_i]\left(\frac{q_3}{k_{q_3}}-\frac{u_3}{k_{u_3}}+\frac{H_i}{k_{H_i}}\right)-\Gamma_{yt}[\widetilde{u}_3,\widetilde{q}_3,H_i]\left(\frac{\widetilde{q}_3}{k_{\widetilde{q}_3}}-\frac{\widetilde{u}_3}{k_{\widetilde{u}_3}}+\frac{H_i}{k_{H_i}}\right)\\
&\quad+\Gamma_{yb}[d_3,q_3,H_i]\left(\frac{q_3}{k_{q_3}}-\frac{d_3}{k_{d_3}}-\frac{H_i}{k_{H_i}}\right)+\Gamma_{yb}[\widetilde{d}_3,\widetilde{q}_3,H_i]\left(\frac{\widetilde{q}_3}{k_{\widetilde{q}_3}}-\frac{\widetilde{d}_3}{k_{\widetilde{d}_3}}-\frac{H_i}{k_{H_i}}\right)\\
&\quad+\Gamma_{y\tau}[e_3,\ell_3,H_i]\left(\frac{\ell_3}{k_{\ell_3}}-\frac{e_3}{k_{e_3}}-\frac{H_i}{k_{H_i}}\right)+\Gamma_{y\tau}[\widetilde{e}_3,\widetilde{\ell}_3,H_i]\left(\frac{\widetilde{\ell}_3}{k_{\widetilde{\ell}_3}}-\frac{\widetilde{e}_3}{k_{\widetilde{e}_3}}-\frac{H_i}{k_{H_i}}\right)\\
&\quad-\Gamma_{\widetilde{V}}[H_i,\widetilde{H}]\left(\frac{H_i}{k_{H_i}}-\frac{\widetilde{H}}{k_{\widetilde{H}}}\right)-\Gamma_M[H_i]\left(\frac{H_i}{k_{H_i}}\right)\pm S_{H_i}^{\not{C}\not{P}}\ , \qquad i=u,d
\end{aligned} \tag{3.16a}$$

$$\begin{aligned}
\partial_\mu \widetilde{H}^\mu &= -\Gamma_{yt}[\widetilde{u}_3,q_3,\widetilde{H}]\left(\frac{q_3}{k_{q_3}}-\frac{\widetilde{u}_3}{k_{\widetilde{u}_3}}+\frac{\widetilde{H}}{k_{\widetilde{H}}}\right)-\Gamma_{yt}[u_3,\widetilde{q}_3,\widetilde{H}]\left(\frac{\widetilde{q}_3}{k_{\widetilde{q}_3}}-\frac{u_3}{k_{u_3}}+\frac{\widetilde{H}}{k_{\widetilde{H}}}\right)\\
&\quad+\Gamma_{yb}[\widetilde{d}_3,q_3,\widetilde{H}]\left(\frac{q_3}{k_{q_3}}-\frac{\widetilde{d}_3}{k_{\widetilde{d}_3}}-\frac{\widetilde{H}}{k_{\widetilde{H}}}\right)+\Gamma_{yb}[d_3,\widetilde{q}_3,\widetilde{H}]\left(\frac{\widetilde{q}_3}{k_{\widetilde{q}_3}}-\frac{d_3}{k_{d_3}}-\frac{\widetilde{H}}{k_{\widetilde{H}}}\right)\\
&\quad+\Gamma_{y\tau}[\widetilde{e}_3,\ell_3,\widetilde{H}]\left(\frac{\ell_3}{k_{\ell_3}}-\frac{\widetilde{e}_3}{k_{e_3}}-\frac{\widetilde{H}}{k_{\widetilde{H}}}\right)+\Gamma_{y\tau}[e_3,\widetilde{\ell}_3,\widetilde{H}]\left(\frac{\widetilde{\ell}_3}{k_{\widetilde{\ell}_3}}-\frac{e_3}{k_{e_3}}-\frac{\widetilde{H}}{k_{\widetilde{H}}}\right)\\
&\quad+\sum_{i=1,2}\Gamma_{\widetilde{V}}[H_i,\widetilde{H}]\left(\frac{H_i}{k_{H_i}}-\frac{\widetilde{H}}{k_{\widetilde{H}}}\right)-\Gamma_M[\widetilde{H}]\left(\frac{\widetilde{H}}{k_{\widetilde{H}}}\right)+S_{\widetilde{H}}^{\not{C}\not{P}}
\end{aligned} \tag{3.16b}$$

In order to facilitate a comparison with results appearing previously in the literature, we give the values for the statistical weight factors in the massless limit: $k_q = k_{\widetilde{q}}/2 = 12$, $k_{u_R} = k_{d_R} = k_{\widetilde{u}_R}/2 = k_{\widetilde{d}_R}/2 = 6$, $k_{H_u} = k_{H_d} = 4$, and $k_{\widetilde{H}} = 8$.

The general notation is that interaction rates are given by $\Gamma_X[...]$, where $X$ denotes the type of interaction, while the $[...]$ denotes the participating particles, the masses of which determine the interaction rate. The quantities in parentheses, which multiply each interaction rate, are the linear combination chemical potentials (3.7) that vanish when chemical equilibrium is reached.

There are several different types of collision terms that appear on the RHS of these Boltzmann equations (we have included only those that are fast compared to $\tau_{\rm diff}$). First,

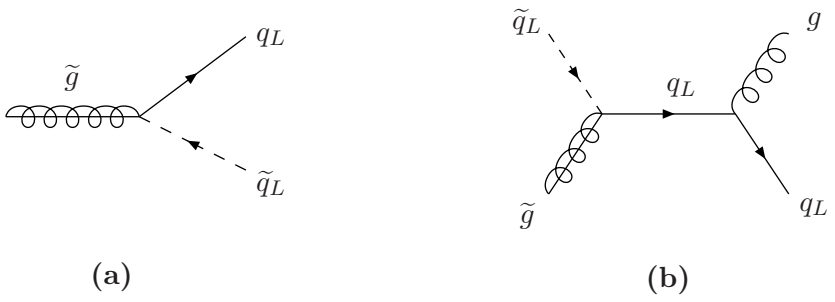


Figure 3.1: Examples of gaugino interactions that lead to superequilibrium: (a) absorption/decay, (b) and scattering, via an additional gluon.

there are the interactions of particles with the background Higgs field of the expanding bubble. These interactions come in two classes: (1) the CP-violating sources $S_i^{\not CP}$ responsible for the generation of hypercharge, and (2) CP-conserving wash-out processes (denoted by $\Gamma_M$) that quenches hypercharge density within the broken phase [22].

Second, there are strong sphaleron processes [19]. These are non-perturbative chirality-flipping processes $\sum_i u_{iL} d_{iL} \leftrightarrow \sum_i u_{iR} d_{iR}$ that tend to wash out a asymmetry between left- and right-handed quarks. In other words, this interaction causes the combination of chemical potentials

$$\sum_{i=1}^{3} \Big( \mu_{u_{iL}} + \mu_{d_{iL}} - \mu_{u_{iR}} - \mu_{d_{iR}} \Big) \tag{3.17}$$

to relax to zero (thus reaching chemical equilibrium). This interaction has been included in the quark Boltzmann equations above through the term

$$\Gamma_{\rm ss}\, N_5 \ , \tag{3.18}$$

where

$$N_5 \equiv \sum_{i=1}^{3} \left( \frac{2\, q_i}{k_{q_i}} - \frac{u_i}{k_{u_i}} - \frac{d_i}{k_{d_i}} \right) \ . \tag{3.19}$$

The rate for strong sphaleron transitions is given by

$$\Gamma_{\rm ss} = 16\, \kappa_s\, \alpha_s^4\, T \tag{3.20}$$

with $\kappa_s \simeq 1$ [42].

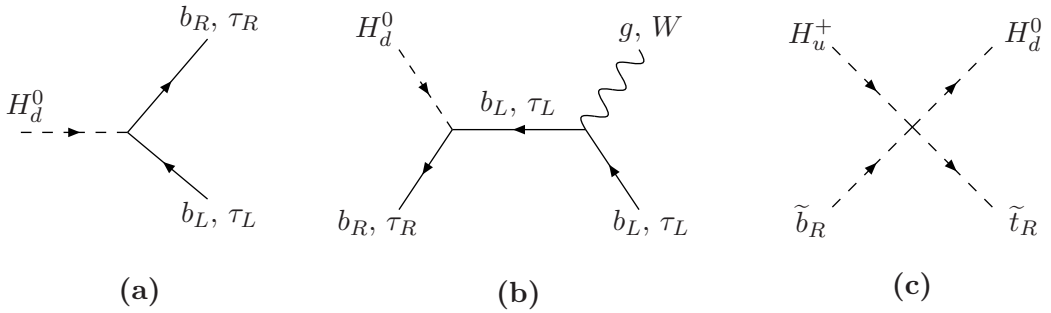


Figure 3.2: Examples of bottom and tau interactions: (a) absorption/decay, (b) and scattering, via an additional gauge boson, and (c) $F$-term-induced four-scalar scattering.

Third, there are gaugino interactions, denoted $\Gamma_{\widetilde{V}}$, that lead to chemical equilibrium between particles and their superpartners — a condition we call *superequilibrium*. In Fig. 3.1, we show examples of gaugino interactions that lead to superequilibrium for left-handed quarks and squarks. The dominant process involves decay and inverse-decay of the gluino $\widetilde{g}$ (a); however, if the masses of the squark, quark, gluino are such that decay is kinematically forbidden, scattering processes (b) can still lead to chemical equilibration. Other gauginos (the Bino $\widetilde{B}$ and Wino $\widetilde{W}$) contribute similarly. Gaugino interactions only lead to superequilibrium if the gauginos are sufficiently light.

Lastly, and most importantly for this thesis, we have the Yukawa interactions. We include third generation Yukawa couplings only. These interaction rates are generically denoted by $\Gamma_{yi}$, where $i = t, b, \tau$ denotes the corresponding Yukawa coupling ($y_t,\ y_b,\ y_\tau$) that enters into the rate. In Fig. 3.2, we show examples of interactions mediated by third generation Yukawa couplings. The dominant processes are absorption and decay (a); however, scattering processes (b), through an additional gauge boson, can be the leading contribution when decay is kinematically forbidden. There are many supersymmetric permutations of the Yukawa interaction, each one leading to a different chemical equilibration. For example, we list all six supersymmetric variants of the top Yukawa interaction, along with the

corresponding chemical equilibrium condition if that rate is fast:

$$\begin{aligned} u_3 &\leftrightarrow q_3\ H_{u,d} & \mu_{q_3} \pm \mu_{H_{u,d}} - \mu_{u_3} &= 0 \\ \widetilde{u}_3 &\leftrightarrow q_3\ \widetilde{H} & \mu_{q_3} + \mu_{\widetilde{H}} - \mu_{\widetilde{u}_3} &= 0 \\ \widetilde{u}_3 &\leftrightarrow \widetilde{q}_3\ H_{u,d} & \mu_{\widetilde{q}_3} \pm \mu_{H_{u,d}} - \mu_{\widetilde{u}_3} &= 0 \\ u_3 &\leftrightarrow \widetilde{q}_3\ \widetilde{H} & \mu_{\widetilde{q}_3} + \mu_{\widetilde{H}} - \mu_{u_3} &= 0 \end{aligned} \tag{3.21}$$

Similar expressions apply for bottom and tau Yukawa interactions.

To conclude, let us make two important points. First, the standard lore [20] was, until recently [24], that only top Yukawa interactions were fast compared to $\tau_{\rm diff}$; this is not necessarily true. As we discuss later, bottom and tau Yukawa interactions are also fast in large, reasonable regions of parameter space, and their inclusion has a dramatic impact upon the final computation of the baryon asymmetry.

Second, although it appears that we have specialized our Boltzmann equations to the MSSM, these equations apply to the NMSSM as well. Recall, we argued that only hypercharge densities are relevant for the computation of the BAU. Additional degrees of freedom that do not carry hypercharge, such as the singlet in the NMSSM, do not lead to additional Boltzmann equations. Their effect is entirely contained in the various interaction rates and CP-violating sources that enter therein.

# Chapter 4

# Collisions in the Plasma

Inelastic collisions in the plasma are an essential, but often underappreciated, ingredient in the story of electroweak baryogenesis. Since the CP-violation that drives EWB is contained SUSY sector, it is the job of collisions to convert this CP-asymmetry into the left-handed fermion charge density $n_L$ that biases electroweak sphalerons into generating the baryon asymmetry. With so many different collision rates entering into the Boltzmann equations, one might expect that $n_L$ depends very sensitively upon the detailed competition between these various interactions. This is not the case. To a good approximation, a given interaction rate is either on or off, depending on whether it is fast or slow compared to $\tau_{\rm diff}$. If interactions are fast, the resulting densities are determined solely by the corresponding chemical equilibrium conditions, not by how fast each interaction is in comparison to one another.

In this chapter, we will compute the Yukawa and gaugino interaction rates that enter into system of Boltzmann equations (3.11a-3.16b). We will compare them to the diffusion time scale to see under what conditions they lead to chemical equilibration.

## 4.1 Thermally-averaged absorption/decay rates

The leading contribution to Yukawa and gaugino interactions comes from absorption and decay of particles in the plasma. In this section, we will develop the building blocks so that we may compute these interaction rates. The Yukawa and gaugino interactions, given in Eqs. (2.26-2.27), fall into two general classes: (i) tri-scalar interactions and (ii) scalar-

fermion-fermion interactions. (Common usage of "Yukawa" refers to all interactions of the latter type; here, we use "Yukawa" to refer to interactions proportional to the Yukawa couplings.)

First, we consider the following tri-scalar interaction with three complex scalars

$$\mathcal{L}_{\rm int} = a\,\phi_1\,\phi_2^\dagger\,\phi_3^\dagger \;+\; \text{h.c.} \tag{4.1}$$

Our computation of the corresponding thermally-averaged decay rate follows from the Closed-Time-Path formalism described in the Appendix. From Eq. (A.37), the Boltzmann equation for $j_1^\mu(X)$, the current density for $\phi_1$, is

$$\begin{aligned}\partial_\mu\, j_1^\mu(X) = \int d^3z \int_{-\infty}^{X^0} dz^0 \;\Big[\, &\Sigma^>(X,z)\,G_1^<(z,X) - G_1^>(X,z)\,\Sigma^<(z,X) \\ &+ \Sigma^<(X,z)\,G_1^>(z,X) - G_1^<(X,z)\,\Sigma^>(z,X)\Big]\;,\end{aligned} \tag{4.2}$$

where $G_1^{>,<}(x,y)$ are CTP Green's functions for $\phi_1$, and the self-energy for this tri-scalar interaction is

$$\Sigma^\lambda(x,y) = -\;|a|^2\;G_2^\lambda(x,y)\,G_3^\lambda(x,y)\;, \tag{4.3}$$

for $\lambda = <, >$. The form for the CTP Green's functions, which follows by assuming that the plasma is nearly in kinetic equilibrium, is

$$G_a^<(x,y) \;=\; \int\frac{d^4p}{(2\pi)^4}\;\rho_a(p)\;n_B(p^0-\mu_a)\;e^{-i\,p\cdot(x-y)} \tag{4.4a}$$

$$G_a^>(x,y) \;=\; \int\frac{d^4p}{(2\pi)^4}\;\rho_a(p)\;(1+n_B(p^0-\mu_a))\;e^{-i\,p\cdot(x-y)}\;, \tag{4.4b}$$

where $a = 1,2,3$ denotes each of the three scalars. The spectral function is $\rho_a(p)$, and the distribution function is a Bose-Einstein distribution function $n_B(p^0-\mu_a) = [\exp(p^0-\mu_a)/T-1]^{-1}$ (with chemical potential $\mu_a$). The collision term induced by $\mathcal{L}_{\rm int}$ in Eq. (4.1) is obtained by evaluating the RHS of Eq. (4.2) explicitly, expanding to linear order in the

chemical potentials $\mu_a$. The end result is [23]

$$\begin{aligned} \partial_\mu j_1^\mu(X) &= -|a|^2 \frac{T^2}{6} \mathcal{I}_B(m_1,m_2,m_3)\ (\mu_1-\mu_2-\mu_3) \\ &= -|a|^2 \mathcal{I}_B(m_1,m_2,m_3)\ \left(\frac{n_1}{k_1}-\frac{n_2}{k_2}-\frac{n_3}{k_3}\right)\ , \end{aligned} \tag{4.5}$$

where the second line follows from Eq. (3.4). The function $\mathcal{I}_B$ is given by

$$\begin{aligned} \mathcal{I}_B(m_1,m_2,m_3) = -\frac{3}{8\pi^3 T^2}\int_{m_1}^\infty d\omega_1\ \frac{e^{\omega_1/T}}{(e^{\omega_1/T}-1)^2} \\ \times\ \left\{ \log\left(\frac{e^{\omega_1/T}-e^{\omega_2^+/T}}{e^{\omega_1/T}-e^{\omega_2^-/T}}\frac{e^{\omega_2^-/T}-1}{e^{\omega_2^+/T}-1}\right)\ [\theta(m_1-m_2-m_3)-\theta(m_2-m_1-m_3)] \right. \\ \left. +\ \log\left(\frac{e^{-\omega_1/T}-e^{\omega_2^+/T}}{e^{-\omega_1/T}-e^{\omega_2^-/T}}\frac{e^{\omega_2^-/T}-1}{e^{\omega_2^+/T}-1}\right)\ \theta(m_3-m_1-m_2)\right\} \end{aligned} \tag{4.6}$$

with

$$\begin{aligned} \omega_2^\pm = \frac{1}{2m_1^2}\Big\{ \omega_1\ \left|m_1^2+m_2^2-m_3^2\right| \\ \pm\sqrt{(\omega_1^2-m_1^2)(m_1^2-(m_2+m_3)^2)(m_1^2-(m_2-m_3)^2)}\ \Big\}\ . \end{aligned} \tag{4.7}$$

The thermally-averaged decay rate is

$$\Gamma[\phi_1,\phi_2,\phi_3] = |a|^2\,\mathcal{I}_B(m_1,m_2,m_3)\ ; \tag{4.8}$$

however, exactly what interaction is occuring depends on the masses. Here we list the possibilities — corresponding to the three $\theta$-functions in $\mathcal{I}_B$ — along with the corresponding decay process:

$$\begin{aligned} m_1 > m_2+m_3 \qquad & \phi_1 \leftrightarrow \phi_2\,\phi_3 \\ m_2 > m_1+m_3 \qquad & \phi_2 \leftrightarrow \phi_1\,\phi_3^* \\ m_3 > m_1+m_2 \qquad & \phi_3 \leftrightarrow \phi_1\,\phi_2^*\ . \end{aligned}$$

If none of the preceding inequalities are satisfied, the decay rate vanishes; all decay pro-

cesses are kinematically forbidden. Lastly, note that $\mathcal{I}_B$ is symmetric under permutation of any of its arguments, although this is far from apparent from Eq. (4.6).

Next, we move to the second type of interaction: scalar-fermion-fermion. Consider the interaction

$$\mathcal{L}_{\rm int} = \phi_1 \, \bar{\psi}_2 \, (g_L \, P_L + g_R \, P_R) \, \psi_3 \; + \; \text{h.c.} \, , \tag{4.9}$$

where $\phi_1$ is a complex scalar, and $\psi_{2,3}$ are fermions. Again, we consider the Boltzmann equation (4.2), but with this interaction the self-energy is

$$\Sigma^{>,<}(x,y) = \; - \, \text{Tr} \left[ \, (g_L P_L + g_R P_R) \, S_3^{>,<}(x,y) \, (g_L^* P_R + g_R^* P_L) \, S_2^{<,>}(y,x) \, \right] \; . \tag{4.10}$$

The fermion propagators are

$$S_a^<(x,y) \;\; = \;\; - \int \frac{d^4p}{(2\pi)^4} \, \rho_a(p) \, (\not{p} + m) \, n_F(p^0 - \mu_a) \, e^{-i\,p\cdot(x-y)} \tag{4.11a}$$

$$S_a^>(x,y) \;\; = \;\; \int \frac{d^4p}{(2\pi)^4} \, \rho_a(p) \, (\not{p} + m) \, (1 - n_F(p^0 - \mu_a)) \, e^{-i\,p\cdot(x-y)} \, , \tag{4.11b}$$

for fermion $a = 2, 3$; the Fermi-Dirac distribution function is $n_F(p^0 - \mu_a) = [\exp(p^0 - \mu_a)/T + 1]^{-1}$ (with chemical potential $\mu_a$). Evaluating the collision term on the RHS of Eq. (4.2) explicitly, and expanding to leading order in chemical potentials, we get

$$\partial_\mu \, j_1^\mu(X) = \; - \, \Gamma[\phi_1, \psi_2, \psi_3] \, \left( \frac{n_1}{k_1} - \frac{n_2}{k_2} + \frac{n_3}{k_3} \right) \; . \tag{4.12}$$

The thermally-averaged decay rate is

$$\Gamma[\phi_1, \psi_2, \psi_3] = \left( |g_L|^2 + |g_R|^2 \right) \, \mathcal{I}_F(m_2, m_1, m_3) + 2 \, \text{Re}[g_L^* g_R] \, \mathcal{I}_{F'}(m_2, m_1, m_3) \, , \tag{4.13}$$

where

$$\mathcal{I}_F(m_2,m_1,m_3) = -\frac{3}{8\pi^3\,T^2}\left(m_1^2-m_2^2-m_3^2\right)\int_{m_2}^{\infty} d\omega_2\;\frac{e^{\omega_2/T}}{(e^{\omega_2/T}+1)^2} \tag{4.14}$$
$$\times\;\left\{\log\left(\frac{e^{\omega_1^-/T}+e^{\omega_2/T}}{e^{\omega_1^+/T}+e^{\omega_2/T}}\,\frac{e^{\omega_1^+/T}-1}{e^{\omega_1^-/T}-1}\right)\;[\theta(m_2-m_1-m_3)-\theta(m_1-m_2-m_3)]\right.$$
$$\left.+\;\log\left(\frac{e^{\omega_1^-/T}+e^{-\omega_2/T}}{e^{\omega_1^+/T}+e^{-\omega_2/T}}\,\frac{e^{\omega_1^+/T}-1}{e^{\omega_1^-/T}-1}\right)\;\theta(m_3-m_1-m_2)\right\}$$
$$\mathcal{I}_{F'}(m_2,m_1,m_3) = \frac{2\,m_2\,m_3}{m_2^2+m_3^2-m_1^2}\;\mathcal{I}_F(m_1,m_2,m_3)\;, \tag{4.15}$$

with

$$\omega_1^{\pm} = \frac{1}{2m_2^2}\left\{\omega_2\;\left|m_1^2+m_2^2-m_3^2\right|\right. \tag{4.16}$$
$$\left.\pm\sqrt{(\omega_2^2-m_2^2)(m_2^2-(m_1+m_3)^2)(m_2^2-(m_1-m_3)^2)}\;\right\}\;.$$

In this work, only $\mathcal{I}_F$ will come into play. (A word of caution: when writing $\Gamma[\phi_1,\psi_2,\psi_3]$ we will not worry about the ordering of the fields; however, in evaluating the function $\mathcal{I}_F$, the scalar mass must always be in the middle slot, as per the convention in Ref. [23]. These functions are symmetric only under the exchange of the two fermion masses.) Once again, the $\theta$-functions permit only those decays that are allowed kinematically:

$$\begin{aligned} m_1 &> m_2+m_3 & \phi_1 &\leftrightarrow \psi_2\,\bar{\psi}_3 \\ m_2 &> m_1+m_3 & \psi_2 &\leftrightarrow \phi_1\,\psi_3 \\ m_3 &> m_1+m_2 & \psi_3 &\leftrightarrow \phi_1^*\,\bar{\psi}_2\;. \end{aligned}$$

To conclude, we present a useful analytic form of $\mathcal{I}_F$. For the case of a scalar decaying into two fermions, $\phi \leftrightarrow \psi_1\,\bar{\psi}_2$, this function is approximately given by

$$\mathcal{I}_F(m_1,\,m_\phi,\,m_2) \simeq \frac{T^3}{4}\;\left(\frac{m_\phi}{2\pi T}\right)^{5/2}\;\left[1-\left(\frac{m_1+m_2}{m_\phi}\right)^2\right]\;e^{-m_\phi/T}\;. \tag{4.17}$$

This simplied form for $\mathcal{I}_F$ is obtained by assuming $m_\phi > m_1+m_2 \gg |m_1-m_2|$, and taking

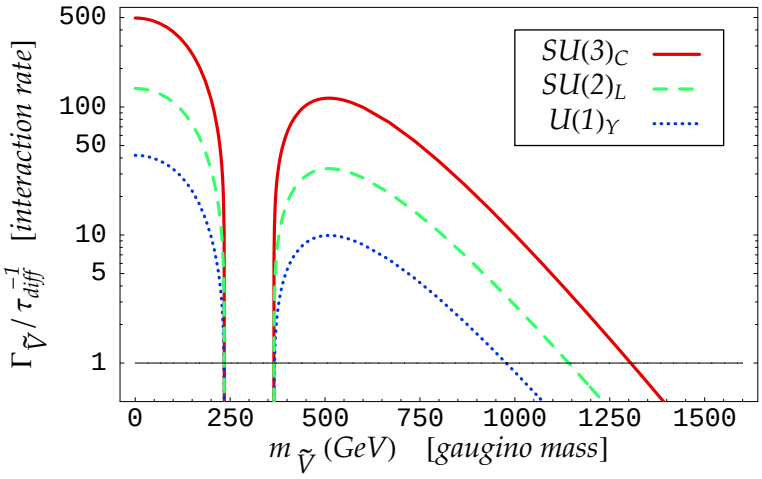


Figure 4.1: Gaugino absorption/decay rates $\Gamma_{\widetilde{V}}$ as a function of gaugino mass $m_{\widetilde{V}}$ for SU(3)$_C$ (red/solid), SU(2)$_L$ (green/dashed), and U(1)$_Y$ (blue/dotted), normalized to $\tau_{\rm diff}^{-1}$. Where $\Gamma_{\widetilde{V}}/\tau_{\rm diff}^{-1} \gg 1$, superequilibrium is maintained; here, this is when the curves exceed the horizontal line.

Maxwell-Boltzmann statistics for these particles; it is valid at the $\mathcal{O}(25\%)$ level for $m_\phi \gtrsim 2(m_1+m_2)$. This form clearly illustrates that $\mathcal{I}_F \to 0$ when (i) $\phi$ is Boltzmann suppressed in the plasma ($m_\phi \gg T$), or (ii) the allowed phase space for the decay approaches zero ($m_\phi - m_1 - m_2 \to 0$).

## 4.2 Gaugino interactions

Gaugino interactions, denoted $\Gamma_{\widetilde{V}}$, lead to superequilibrium, i.e., chemical equilibrium between particles and their supersymmetric partners. The most important parameters governing these interaction rates are the gaugino masses. Consider a fermion $f$ and its superpartner $\widetilde{f}$; superequilibrium is maintained through the decay $\widetilde{V} \leftrightarrow \widetilde{f}^*\, f$, or through gaugino absorption $f\, \widetilde{V} \leftrightarrow \widetilde{f}$, depending on which process is kinematically allowed. In Fig. 4.1, we plot the gaugino absorption/decay rates

$$\Gamma_{\widetilde{V}}[f,\widetilde{f}] = \begin{cases} g_1^2\, \mathcal{I}_F(m_f, m_{\widetilde{f}}, m_{\widetilde{B}}) \\ g_2^2\, \mathcal{I}_F(m_f, m_{\widetilde{f}}, m_{\widetilde{W}}) \\ g_3^2\, \mathcal{I}_F(m_f, m_{\widetilde{f}}, m_{\widetilde{g}}) \end{cases} \quad ; \tag{4.18}$$

the total gaugino interaction rate will be a linear combination of these three rates, depending on the quantum numbers of $f$. In the figure, we have set $m_{\tilde{f}} = 300$ GeV and $m_f = 60$ GeV (approximately equal to a quark thermal mass). Furthermore, the rates have been normalized with respect to the inverse diffusion time, given by $\tau_{\rm diff} \simeq 5 \times 10^{-3}$ GeV (shown below). The condition for superequilibrium is realized when the gaugino interaction time scale $\tau_{\widetilde{V}} \equiv \Gamma_{\widetilde{V}}^{-1}$ satisfies $\tau_{\widetilde{V}} \ll \tau_{\rm diff}$; in Fig 4.1 this is when the curves exceed the horizonal line.

The general conclusion from Fig. 4.1 is that the gaugino interaction rates can indeed be large enough to enforce superequilibrium. However, there are two exceptions. First, in the region near $m_{\widetilde{V}} \sim 300$ GeV, the interaction rate vanishes; here absorption/decay is kinematically forbidden, since $|m_{\widetilde{V}} - m_{\tilde{f}}| < m_f$. In this region, scattering processes (Fig. 3.1b), suppressed by $\mathcal{O}(\alpha_{1,2,3})$ over absorption/decay, may still be sufficient for superequilibrium. Second, the interaction rate is suppressed for $m_{\widetilde{V}} \to \infty$, since gauginos become Boltzmann suppressed in the plasma; here departures from superequilibrium may occur. From Fig. 4.1, this occurs for $m_{\widetilde{V}} \gtrsim 1$ TeV.

Now, we list all the gaugino interaction rates that enter the Boltzmann equations (3.11a-3.16b):

$$\Gamma_{\widetilde{V}}[H_u, \widetilde{H}] = g_1^2 \mathcal{I}_F(m_{\widetilde{H}}, m_{H_u}, m_{\widetilde{B}}) + 3 g_2^2 \mathcal{I}_F(m_{\widetilde{H}}, m_{H_1}, m_{\widetilde{W}}) \tag{4.19a}$$

$$\Gamma_{\widetilde{V}}[H_d, \widetilde{H}] = g_1^2 \mathcal{I}_F(m_{\widetilde{H}}, m_{H_d}, m_{\widetilde{B}}) + 3 g_2^2 \mathcal{I}_F(m_{\widetilde{H}}, m_{H_d}, m_{\widetilde{W}}) \tag{4.19b}$$

$$\Gamma_{\widetilde{V}}[q, \widetilde{q}] = \frac{N_C g_1^2}{9} \mathcal{I}_F(m_q, m_{\tilde{q}}, m_{\widetilde{B}}) + 3 N_C g_2^2 \mathcal{I}_F\left(m_q, m_{\tilde{q}}, m_{\widetilde{W}}\right) + 2(N_C^2 - 1) g_3^2 \mathcal{I}_F\left(m_q, m_{\tilde{q}}, m_{\widetilde{G}}\right) \tag{4.19c}$$

$$\Gamma_{\widetilde{V}}[u, \widetilde{u}] = \frac{8 N_C g_1^2}{9} \mathcal{I}_F\left(m_u, m_{\tilde{u}}, m_{\widetilde{B}}\right) + (N_C^2 - 1) g_3^2 \mathcal{I}_F\left(m_u, m_{\tilde{u}}, m_{\widetilde{G}}\right) \tag{4.19d}$$

$$\Gamma_{\widetilde{V}}[d, \widetilde{d}] = \frac{2 N_C g_1^2}{3} \mathcal{I}_F\left(m_d, m_{\tilde{d}}, m_{\widetilde{B}}\right) + (N_C^2 - 1) g_3^2 \mathcal{I}_F\left(m_d, m_{\tilde{d}}, m_{\widetilde{G}}\right) \tag{4.19e}$$

$$\Gamma_{\widetilde{V}}[\ell, \widetilde{\ell}] = g_1^2 \mathcal{I}_F(m_\ell, m_{\tilde{\ell}}, m_{\widetilde{B}}) + 3 g_2^2 \mathcal{I}_F\left(m_\ell, m_{\tilde{\ell}}, m_{\widetilde{W}}\right) \tag{4.19f}$$

$$\Gamma_{\widetilde{V}}[e, \widetilde{e}] = 4 g_1^2 \mathcal{I}_F\left(m_e, m_{\tilde{e}}, m_{\widetilde{B}}\right) \ . \tag{4.19g}$$

In Eqs. (4.19c-g), we have omitted a generational index since these expressions are identical for all generations.

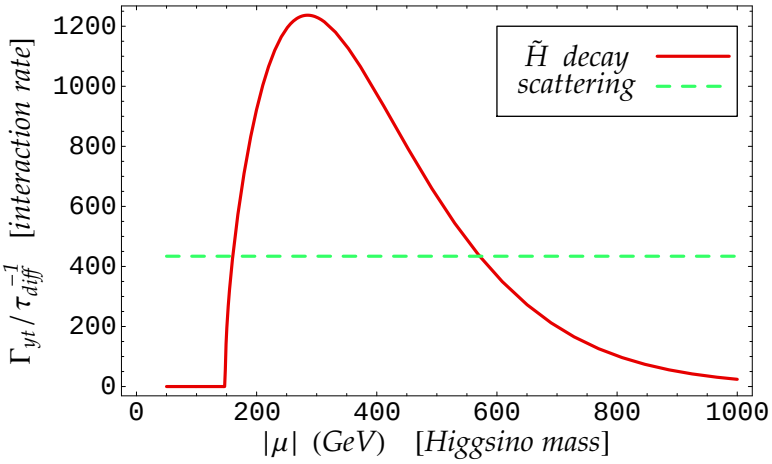


Figure 4.2: Leading top Yukawa interactions from the decay $\widetilde{H} \leftrightarrow \bar{q}_3\,\widetilde{t}_R$ (solid) and scattering $H_u\,q_3 \leftrightarrow u_3\,g$ (dashed), compared to $\tau_{\rm diff}^{-1}$, the inverse diffusion time scale. When $\Gamma_{yt}/\tau_{\rm diff}^{-1} \gg 1$, top Yukawa chemical equilibrium is satisfied.

## 4.3 Yukawa interactions

Yukawa interactions are of the utmost importance for the dynamics of EWB. Before we explore the phenomenology of these interaction rates, we first list all the Yukawa rates that enter into the Boltzmann equations (3.11a-3.16b). The top Yukawa interaction rates are [23]

$$\Gamma_{yt}[\widetilde{u}_3, \widetilde{q}_3, H_u] = 2\,N_C\,y_t^2\,|A_t|^2\,\mathcal{I}_B\,(m_{\widetilde{u}_3}, m_{\widetilde{q}_3}, m_{H_u}) \tag{4.20a}$$

$$\Gamma_{yt}[\widetilde{u}_3, \widetilde{q}_3, H_d] = 2\,N_C\,y_t^2\,|\mu|^2\,\mathcal{I}_B\,(m_{\widetilde{u}_3}, m_{\widetilde{q}_3}, m_{H_d}) \tag{4.20b}$$

$$\Gamma_{yt}[\widetilde{u}_3, q_3, \widetilde{H}] = 2\,N_C\,y_t^2\,\mathcal{I}_F\left(m_{\widetilde{H}}, m_{\widetilde{u}_3}, m_{q_3}\right) \tag{4.20c}$$

$$\Gamma_{yt}[u_3, q_3, H_u] = 2\,N_C\,y_t^2\,\mathcal{I}_F\,(m_{u_3}, m_{H_u}, m_{q_3}) \tag{4.20d}$$

$$\Gamma_{yt}[u_3, \widetilde{q}_3, \widetilde{H}] = 2\,N_C\,y_t^2\,\mathcal{I}_F\left(m_{u_3}, m_{\widetilde{q}_3}, m_{\widetilde{H}}\right) \tag{4.20e}$$

For EWB in the MSSM, only a subset of these rates are relevant. First, the left-handed third generation squarks must be very heavy, with masses in excess of 6.5 TeV, as required by precision electroweak constraints and having a viable electroweak phase transition [46]. Therefore, all Yukawa interactions involving decays of $\widetilde{q}_3$ will be Boltzmann suppressed, shown in Eq. (4.17). Second, decay processes involving $H_u$, $q_3$, $u_3$ are kinematically for-

bidden. However, scattering processes ($H_u\, q_3 \leftrightarrow u_3\, g$, and permutations) also contribute to $\Gamma_{yt}[q_3, u_3, H_u]$ and are very active; their total rate was estimated in Refs. [20, 29] to be

$$\Gamma_{yt}[u_3, H_u, q_3] \;\simeq\; 0.2\,\alpha_s\, y_t^2\, T\ . \tag{4.21}$$

Lastly, the rate for decays $\widetilde{H} \leftrightarrow \bar{q}_3\, \widetilde{t}_R$ can be largest top Yukawa rate of all. In particular, viable EWB requires both a light right-handed top squark (for a strong first-order phase transition) and a light Higgsino (to have a sufficiently large CP-violating source to generate the observed BAU). In Fig. 4.2, we show the ratio $\Gamma_{yt}[\widetilde{u}_3, q_3, \widetilde{H}]/\tau_{\rm diff}^{-1}$, as a function of the Higgsino mass parameter $\mu$ (red, solid curve), for $m_{\widetilde{t}_R} = 80$ GeV. When this ratio is much greater than unity, chemical equilibrium is reached; the combination of chemical potentials $(\mu_{q_3} - \mu_{\widetilde{u}_3} - \mu_{\widetilde{H}})$ vanishes. In addition, we also plot $\Gamma_{yt}[u_3, H_u, q_3]/\tau_{\rm diff}^{-1}$ (dashed green), for the scattering contribution in Eq. (4.21).

The bottom Yukawa interaction rates are

$$\begin{aligned}
\Gamma_{yb}[\widetilde{d}_3, \widetilde{q}_3, H_u] &= 2\, N_C\, y_b^2\, |\mu|^2\, \mathcal{I}_B\left(m_{\widetilde{d}_3}, m_{\widetilde{q}_3}, m_{H_u}\right) && \text{(4.22a)}\\
\Gamma_{yb}[\widetilde{d}_3, \widetilde{q}_3, H_d] &= 2\, N_C\, y_b^2\, |A_b|^2\, \mathcal{I}_B\left(m_{\widetilde{d}_3}, m_{\widetilde{q}_3}, m_{H_d}\right) && \text{(4.22b)}\\
\Gamma_{yb}[\widetilde{d}_3, q_3, \widetilde{H}] &= 2\, N_C\, y_b^2\, \mathcal{I}_F\left(m_{\widetilde{H}}, m_{\widetilde{d}_3}, m_{q_3}\right) && \text{(4.22c)}\\
\Gamma_{yb}[d_3, q_3, H_d] &= 2\, N_C\, y_b^2\, \mathcal{I}_F\left(m_{d_3}, m_{H_d}, m_{q_3}\right) && \text{(4.22d)}\\
\Gamma_{yb}[d_3, \widetilde{q}_3, \widetilde{H}] &= 2\, N_C\, y_b^2\, \mathcal{I}_F\left(m_{d_3}, m_{\widetilde{q}_3}, m_{\widetilde{H}}\right) && \text{(4.22e)}
\end{aligned}$$

The tau Yukawa interaction rates are

$$\begin{aligned}
\Gamma_{y\tau}[\widetilde{e}_3, \widetilde{\ell}_3, H_u] &= 2\, y_\tau^2\, |\mu|^2\, \mathcal{I}_B\left(m_{\widetilde{e}_3}, m_{\widetilde{\ell}_3}, m_{H_u}\right) && \text{(4.23a)}\\
\Gamma_{y\tau}[\widetilde{e}_3, \widetilde{\ell}_3, H_2] &= 2\, y_\tau^2\, |A_t|^2\, \mathcal{I}_B\left(m_{\widetilde{e}_3}, m_{\widetilde{\ell}_3}, m_{H_d}\right) && \text{(4.23b)}\\
\Gamma_{y\tau}[\ell_3, \widetilde{e}_3, \widetilde{H}] &= 2\, y_\tau^2\, \mathcal{I}_F\left(m_{\widetilde{H}}, m_{\widetilde{e}_3}, m_{\ell_3}\right) && \text{(4.23c)}\\
\Gamma_{y\tau}[e_3, \ell_3, H_d] &= 2\, y_\tau^2\, \mathcal{I}_F\left(m_{e_3}, m_{H_d}, m_{\ell_3}\right) && \text{(4.23d)}\\
\Gamma_{y\tau}[e_3, \widetilde{\ell}_3, \widetilde{H}] &= 2\, y_\tau^2\, \mathcal{I}_F\left(m_{e_3}, m_{\widetilde{\ell}_3}, m_{\widetilde{H}}\right) && \text{(4.23e)}
\end{aligned}$$

The determination of the bottom and tau Yukawa couplings themselves is the subject of

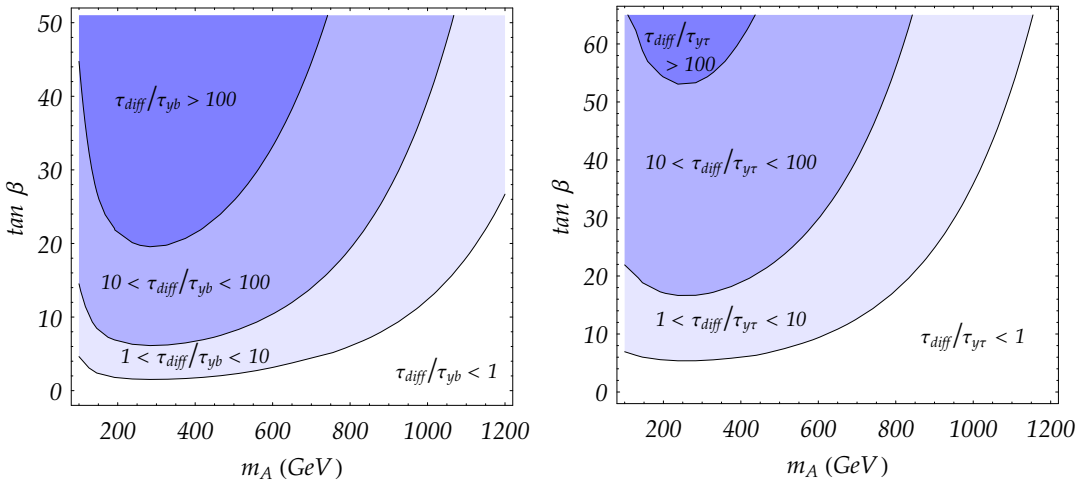


Figure 4.3: Contour plot of $\tau_{\rm diff}/\tau_{yb}$ (left) and $\tau_{\rm diff}/\tau_{y\tau}$ (right) in $\tan\beta$-$m_A$ parameter space. Values of $\tau_{yb}$ and $\tau_{y\tau}$ include contributions from $H_d \leftrightarrow q_L b_R$ and $H_d \leftrightarrow \ell_L \tau_R$ only. Tau Yukawa chemical equilibrium is maintained for $\tau_{\rm diff}/\tau_{y\tau} \gtrsim 10$; similarly for the bottom Yukawa.

some care. At tree-level, these couplings are determined by

$$y_\tau = \frac{m_\tau}{v\,\cos\beta}\,, \qquad y_b = \frac{m_b}{v\,\cos\beta}\,, \qquad y_t = \frac{m_t}{v\,\sin\beta}\,, \tag{4.24}$$

where $v \simeq 174$ GeV is the Higgs vev at $T = 0$. Both couplings are enhanced over their SM values for $\tan\beta \gg 1$. Quantum corrections lead to two complications. First, we include the QCD (QED) running of $y_b$ ($y_\tau$) from the scale where the mass $m_b$ ($m_\tau$) is measured to the electroweak scale $Q = M_Z$; this reduces $y_b$ by a factor $\eta_b \simeq 1.4$ and has negligible impact on $y_\tau$ [37]. Second, we allow for the possibility that $y_{b,\tau}$ is smaller than expected at tree-level, due to $m_{b,\tau}$ receiving large one-loop corrections enhanced by $\tan\beta$, denoted as $\delta_b$ and $\delta_\tau$, for which we include only the dominant contributions [37, 38]. Including both of these effects, we have

$$y_\tau(Q) = \frac{m_\tau}{v\,\cos\beta\,(1+\delta_\tau\tan\beta)}\,, \quad y_b(Q) = \frac{m_b/\eta_b}{v\,\cos\beta\,(1+\delta_b\tan\beta)}\,. \tag{4.25}$$

One important class of bottom and tau Yukawa interactions comes from the decays

$$H_d \longleftrightarrow \bar{q}_3\, d_3\,,\ \bar{\ell}_3\, e_3, \tag{4.26}$$

shown in Fig. 3.2a. The rate for these decays is largest when (i) the Yukawa couplings are enhanced by $\tan\beta \gg 1$, and (ii) the zero-temperature pseudoscalar Higgs mass $m_A$ sufficiently light, so that $H_d$ is not Boltzmann suppressed in the plasma; *cf.* Eq. (2.20). In Fig. 4.3 (left panel), we show a contour plot of ratio $\Gamma_{yb}[q_3, H_d, u_3]/\tau_{\rm diff}^{-1} \equiv \tau_{\rm diff}/\tau_{yb}$ in the $m_A$-$\tan\beta$ plane. Where the ratio is large, indicated by the darker regions, this bottom Yukawa interaction is in chemical equilibrium; we have $(\mu_{q_3} - \mu_{H_d} - \mu_{u_3}) \to 0$. This occurs for $\tan\beta \gtrsim 5$ and $m_A \lesssim 800$ GeV. Similarly, In Fig. 4.3 (right panel), we show the same plot for $\Gamma_{y\tau}[\ell_3, H_d, e_3]/\tau_{\rm diff}^{-1} \equiv \tau_{\rm diff}/\tau_{y\tau}$. Tau Yukawa chemical equilibrium occurs for $\tan\beta \gtrsim 15$ and $m_A \lesssim 600$ GeV. (The reason that the Yukawa interaction is weaker for tau than for bottom is because the latter is enhanced over the former by $N_C m_b^2/m_\tau^2 \eta_b^2 \sim 8$.)

Not only are bottom and tau Yukawa interactions enhanced when $m_A$ is light, CP-violating sources in the MSSM are enhanced as well. The leading, resonantly-enhanced contributions are proportional to the parameter $\Delta\beta$, the change in $\beta \equiv \tan^{-1}(v_u/v_d)$ as one moves from the symmetric to the broken phase. (We show how this arises in a toy model in Chapter. 5.) It has been shown numerically that $\Delta\beta \to 0$ for $m_A \to \infty$ [39]. However, even in this limit, there still survive contributions to the Higgsino CP-violating source that, though smaller, are sufficient to generate the BAU [41, 33].

Scattering contributions, shown in Fig. 3.2b, also contribute to bottom and tau Yukawa rates. They are suppressed in comparison by $\alpha_s$ or $\alpha_w$, but become the dominant contribution when absorption and decay are kinematically forbidden. In addition, F-term-induced four-scalar interactions, shown in Fig. 3.2c, also induce transport coefficients proportional to top, bottom, and tau Yukawa couplings; however, one can show that if all $\Gamma_{yi}$ (for $i = t, b, \tau$) interactions are in chemical equilibrium, then chemical equilibrium is satisfied for these four-scalar interactions as well.

Additional bottom and tau Yukawa interactions (4.22, 4.23) may also be significant, depending on the supersymmetric spectrum. In our results to follow, we work within the approximation that gaugino interactions successfully lead to superequilibrium. In this case,

it is the *total* Yukawa rates that enter into the transport equations:

$$\begin{aligned}\Gamma_{yt} \;\equiv\; & \Gamma_{yt}[\widetilde{u}_3, \widetilde{q}_3, H_u] + \Gamma_{yt}[\widetilde{u}_3, \widetilde{q}_3, H_d] \\ & + \Gamma_{yt}[\widetilde{u}_3, q_3, \widetilde{H}] + \Gamma_{yt}[u_3, q_3, H_u] + \Gamma_{yt}[u_3, \widetilde{q}_3, \widetilde{H}]\end{aligned} \tag{4.27a}$$

$$\begin{aligned}\Gamma_{yb} \;\equiv\; & \Gamma_{yb}[\widetilde{d}_3, \widetilde{q}_3, H_u] + \Gamma_{yb}[\widetilde{d}_3, \widetilde{q}_3, H_d] \\ & + \Gamma_{yb}[\widetilde{d}_3, q_3, \widetilde{H}] + \Gamma_{yb}[d_3, q_3, H_d] + \Gamma_{yb}[d_3, \widetilde{q}_3, \widetilde{H}]\end{aligned} \tag{4.27b}$$

$$\begin{aligned}\Gamma_{y\tau} \;\equiv\; & \Gamma_{y\tau}[\widetilde{e}_3, \widetilde{\ell}_3, H_u] + \Gamma_{y\tau}[\widetilde{e}_3, \widetilde{\ell}_3, H_2] \\ & + \Gamma_{y\tau}[\ell_3, \widetilde{e}_3, \widetilde{H}] + \Gamma_{y\tau}[e_3, \ell_3, H_d] + \Gamma_{y\tau}[e_3, \widetilde{\ell}_3, \widetilde{H}]\ .\end{aligned} \tag{4.27c}$$

We will evaluate these rates numerically in Chapter 7.

# Chapter 5

# Intermission: a Novel Interpretation of the CP-violating Source

So far, we have formulated the problem of charge transport during the electroweak phase transition. We derived a system of Boltzmann equations; we described which interactions are relevant and how to compute their rates. In subsequent chapters, we will solve these equations and investigate their phenomenology. However, we pause here for a brief, but somewhat tangential, intermission: the nature of the physics that gives rise to the CP-violating source. Our results here are not meant to be quantitative, but only a heuristic guide; for numerical evaluation, we rely upon Refs. [31, 22]. In the literature, the computation of the CP-violating source has been the subject of on-going scrutiny and significant theoretical machinery involving the Closed-Time-Path formalism [31, 32, 33, 34]. Here, we attempt to strip the CP-violating source down to its barest essence, and to answer: how does a spacetime-dependent Higgs field give rise to a CP-asymmetric charge from an initially CP-symmetric plasma?

We present a very simplified toy model that shows how a CP-violating source arises from two-flavor oscillations, similar to neutrino oscillations, with a spacetime-dependent mass matrix. This statement may seem peculiar; it is well-known that there can be no CP-violation in two-flavor neutrino oscillations in vacuum. Here, however, CP-violation is physical; the spacetime-dependence of the mixing matrix plays a key role.

Consider a system with two states $\{|L\rangle, |R\rangle\}$ ("flavor basis" states). The spacetime-dependent Higgs field induces spacetime-dependent masses for these states. For simplicity,

we neglect the spatial-dependence of the Higgs field and consider a time-dependent Hamiltonian $H(t)$. We diagonalize $H(t)$ using the time-dependent mixing matrix $V(t)$, such that

$$V(t)^T\, H(t)\, V(t)^* = \omega(t) \equiv \begin{pmatrix} \omega_1(t) & 0 \\ 0 & \omega_2(t) \end{pmatrix} \ , \tag{5.1}$$

where $\omega_{1,2}$ are the energy eigenvalues and $V(t)$ is given in Eq. (2.7). Let us define a new basis $\{|1\rangle,\, |2\rangle\}$ ("mass basis" states), by

$$|\alpha\rangle = V^*_{\alpha i}(t)\, |i(t)\rangle \ , \tag{5.2}$$

where $\alpha = L, R$ and $i = 1, 2$. The Schrodinger equation for the mass basis states is

$$i\, \frac{d}{dt}\ |i(t)\rangle = \big(\, \omega(t) + \Sigma^T(t)\, \big)_{ij}\ |j(t)\rangle \ , \tag{5.3}$$

where $\Sigma = i\, V^\dagger\, \dot{V}$. The solution to this equation is

$$\begin{aligned} |i(t)\rangle &= \exp\left[ -i \int_0^t dt'\ \big(\, \omega(t') + \Sigma^T(t')\, \big) \right]_{ij} |j(0)\rangle \\ &= \exp\left[ -i \left( \omega(t)\, t + \Sigma^T(t')\, t + \dot{\omega}(t)\, \frac{t^2}{2} \right) \right]_{ij} |j(0)\rangle \end{aligned} \tag{5.4}$$

where the second line follows by expanding to linear order in derivatives of $H(t)$ (i.e. linear order in $\dot{\omega}$ and $\Sigma$).

The initial condition for our states is one of thermal equilibrium. In equilibrium, the density matrix is diagonal in the mass basis. Therefore, we assume that for $t \leq 0$, we have $H(t) =$ constant; our initial condition at $t = 0$ is an ensemble of mass basis states $|1(0)\rangle$ and $|2(0)\rangle$, with weights $\mathsf{w}_{1,2}$. The weights are the thermal abundances of the mass states in the plasma, given by

$$\mathsf{w}_i \ = \ \frac{1}{e^{\omega_i/T} - 1} \ . \tag{5.5}$$

Note that $\mathsf{w}_1 \neq \mathsf{w}_2$ since in general $\omega_1 \neq \omega_2$.

Now suppose that for $t > 0$, we have $\dot{H} \neq 0$. We ask: what is the probability that $|L\rangle$

states will be produced after time $t$? Consider the following amplitude:

$$A_{\alpha j}(t) \equiv V^*_{\alpha i}(t)\, \exp\left[-i \int_0^t dt'\ \left(\omega(t') + \Sigma^T(t')\right)\right]_{ij} , \tag{5.6}$$

This is the amplitude for a mass state $|j(0)\rangle$ to be converted into a flavor state state $|\alpha\rangle$ after time $t$. Let us evaluate explicitly the probabilities for states $|1(0)\rangle$ and $|2(0)\rangle$ to be converted into state $|L\rangle$. We have

$$|A_{L1}(t)|^2 = \cos^2\theta - 2\,\frac{\sin 2\theta}{\Delta\omega}\,\sin\left(\frac{\Delta\omega\, t}{2}\right)\,\left[\dot\theta\,\cos\left(\frac{\Delta\omega\, t}{2}\right) - \sin\theta\,\cos\theta\,\dot\sigma\,\sin\left(\frac{\Delta\omega\, t}{2}\right)\right] \tag{5.7a}$$

$$|A_{L2}(t)|^2 = \sin^2\theta + 2\,\frac{\sin 2\theta}{\Delta\omega}\,\sin\left(\frac{\Delta\omega\, t}{2}\right)\,\left[\dot\theta\,\cos\left(\frac{\Delta\omega\, t}{2}\right) - \sin\theta\,\cos\theta\,\dot\sigma\,\sin\left(\frac{\Delta\omega\, t}{2}\right)\right] , \tag{5.7b}$$

where $\Delta\omega = \omega_1 - \omega_2$. These amplitudes have been evaluated to linear order in the derivatives $\dot\omega_i$, $\dot\theta$, and $\dot\sigma$ — collectively denoted as $\mathcal{O}(\partial_X)$. The probability of finding a state $L$ after time $t$ is

$$P_L(t) = \mathsf{w}_1\ |A_{L1}(t)|^2 + \mathsf{w}_2\ |A_{L2}(t)|^2\ . \tag{5.8}$$

This probability does not equal unity, as long as $\mathsf{w}_1 \neq \mathsf{w}_2$.

Now, consider an analogous two-state system corresponding to antiparticles, with flavor states $|\bar L\rangle$, $|\bar R\rangle$. It is helpful to regard these states as related to their particle counterparts by the time-reversal operator $\Theta$: $\Theta\,|\alpha\rangle = \langle\bar\alpha|$. (By CPT-symmetry, this is equilivalent to CP-conjugation.) Using the fact that $\langle i|\alpha\rangle = V^*_{i\alpha}$, we have

$$\langle\bar i|\bar\alpha\rangle = \langle\alpha|i\rangle = V_{i\alpha}\ , \tag{5.9}$$

with mass basis antiparticle states $|\bar 1\rangle$, $|\bar 2\rangle$. The antiparticle states transform differently from the particle states, according to

$$|\bar\alpha\rangle = V_{\alpha i}(t)\,|\bar i(t)\rangle\ . \tag{5.10}$$

The mass-basis Schrodinger equation is

$$i\,\frac{d}{dt}\;|\bar{i}(t)\rangle = (\;\omega(t) - \Sigma(t)\;)_{ij}\;|\bar{j}(t)\rangle\;\;. \tag{5.11}$$

We wish to consider the amplitudes

$$\bar{A}_{\alpha j}(t) \equiv V_{\alpha i}(t)\;\exp\left[-i\int_0^t dt'\;\;(\;\omega(t') - \Sigma(t')\;)\right]_{ij} \tag{5.12}$$

for producing an $|\bar{\alpha}\rangle$ state after time $t$ from state $|\bar{j}(0)\rangle$. In particular, the formulae are identical to the particle amplitudes (5.7) with the replacement $\sigma \to -\sigma$. We assume that the thermal bath is initially CP-symmetric; therefore, the antiparticle mass states $|\bar{i}(0)\rangle$ have the same weights $\mathsf{w}_i$ as the particle states $|i(0)\rangle$. The probability of finding state $\bar{L}$ after time $t$ is

$$P_{\bar{L}}(t) = \mathsf{w}_1\;\left|\bar{A}_{L1}(t)\right|^2 + \mathsf{w}_2\;\left|\bar{A}_{L2}(t)\right|^2\;\;. \tag{5.13}$$

Given this analysis, is a CP-asymmetry created? The CP-violating source

$$S_L^{\not{C}\not{P}}(t) \equiv \frac{d}{dt}\;(P_L(t) - P_{\bar{L}}(t)) \tag{5.14}$$

is the rate of production of an asymmetry between $L$ and $\bar{L}$ states, given a CP-symmetric, equilibrium initial state. Using Eq. (5.7), it is

$$S_L^{\not{C}\not{P}}(t) = (\mathsf{w}_1 - \mathsf{w}_2)\,\dot{\sigma}\;\sin^2 2\theta\;\sin\left(\Delta\omega\,t\right)\;\;, \tag{5.15}$$

to linear order in derivatives of $H(t)$, with $\Delta\omega = (\omega_1 - \omega_2)$. The spacetime-dependent phase $\sigma(t)$ leads to a CP-violating source that generates more $L$ than $\bar{L}$. If we apply this toy model to the case of Higgsino/Wino mixing (2.21), we find

$$\sigma = \arg\left[M_2\,v_u + \mu^*\,v_d\right]\;\;, \tag{5.16}$$

so that

$$\dot{\sigma} = \sin\phi_2\,\dot{\beta}\;. \tag{5.17}$$

We note that $\dot{\beta} \neq 0$ when the vevs $v_{u,d}$ are spacetime-dependent; therefore, the CP-violating source is non-zero only within the bubble walls themselves.

# Chapter 6

# Computing the Baryon Asymmetry, Part I: Analytic Results

We now embark upon a long road of solving the full system of Boltzmann equations. Ultimately, we are interested in

$$n_L \equiv \sum_{i=1}^{3} \left( n_{u_L^i} + n_{d_L^i} + n_{\nu_L^i} + n_{\ell_L^i} \right) \ , \tag{6.1}$$

the total left-handed quark and lepton charge density that biases electroweak sphalerons.

The Boltzmann equations, given in Eqs. (6.16-6.18), may seem like a dark and impenetrable jungle. Charge density, created in one species, is converted into other species through a web of Yukawa, gaugino, and supergauge interactions. We can illumimate the situation greatly by considering the Boltzmann equation, not for a single species, but for the total hypercharge in the plasma

$$\begin{aligned} Y \equiv \sum_{i=1}^{3} \left( \frac{1}{6} \left( q_i + \widetilde{q}_i \right) + \frac{2}{3} \left( u_i + \widetilde{u}_i \right) - \frac{1}{3} \left( d_i + \widetilde{d}_i \right) - \frac{1}{2} \left( \ell_i + \widetilde{\ell}_i \right) - \left( e_i + \widetilde{e}_i \right) \right) \\ + \frac{1}{2} \left( H_u - H_d + \widetilde{H} \right) \ . \end{aligned} \tag{6.2}$$

The Boltzmann equation for $Y$ is

$$\begin{aligned}\partial_\mu j^\mu_Y(X) = -\frac{1}{2}\Bigg[ & \Gamma_M[u_3,q_3]\left(\frac{u_3}{k_{u_3}}-\frac{q_3}{q_3}\right)+\Gamma_M[d_3,q_3]\left(\frac{q_3}{q_3}-\frac{d_3}{k_{d_3}}\right) \\ & +\ \Gamma_M[\widetilde{u}_3,\widetilde{q}_3]\left(\frac{\widetilde{u}_3}{k_{\widetilde{u}_3}}-\frac{\widetilde{q}_3}{\widetilde{q}_3}\right)+\Gamma_M[\widetilde{d}_3,\widetilde{q}_3]\left(\frac{\widetilde{q}_3}{\widetilde{q}_3}-\frac{\widetilde{d}_3}{k_{\widetilde{d}_3}}\right) \\ & +\ \Gamma_M[e_3,\ell_3]\left(\frac{\ell_3}{k_{\ell_3}}-\frac{e_3}{e_3}\right)+\Gamma_M[\widetilde{e}_3,\widetilde{\ell}_3]\left(\frac{\widetilde{\ell}_3}{k_{\widetilde{\ell}_3}}-\frac{\widetilde{e}_3}{\widetilde{e}_3}\right) \\ & +\Gamma_M[H_u]\,\frac{H_u}{k_{H_u}}-\Gamma_M[H_d]\,\frac{H_d}{k_{H_d}}+\Gamma_M[\widetilde{H}]\,\frac{\widetilde{H}}{k_{\widetilde{H}}}\Bigg] \\ & +\frac{1}{2}\left(S^{\not{C}\not{P}}_{\widetilde{t}}+S^{\not{C}\not{P}}_{\widetilde{b}}+S^{\not{C}\not{P}}_{\widetilde{\tau}}+S^{\not{C}\not{P}}_{\widetilde{H}}+S^{\not{C}\not{P}}_{H_u}+S^{\not{C}\not{P}}_{H_d}\right)\,.\end{aligned} \tag{6.3}$$

If all charge densities on the RHS are proportional to $Y$, as we show below, then this equation takes the form

$$\partial_\mu j^\mu_Y(X) \;=\; -\,\bar{\Gamma}_M\,Y + S^{\not{C}\not{P}}_Y\,. \tag{6.4}$$

All Yukawa, gaugino, and strong sphaleron rates cancel from the hypercharge Boltzmann equation; the only terms that remain are the total CP-violating source

$$S^{\not{C}\not{P}}_Y \equiv \frac{1}{2}\left(S^{\not{C}\not{P}}_{\widetilde{t}}+S^{\not{C}\not{P}}_{\widetilde{b}}+S^{\not{C}\not{P}}_{\widetilde{\tau}}+S^{\not{C}\not{P}}_{\widetilde{H}}+S^{\not{C}\not{P}}_{H_u}+S^{\not{C}\not{P}}_{H_d}\right) \tag{6.5}$$

that generates hypercharge, and rate $\Gamma^{(Y)}_M$, a linear combination of various $\Gamma_M$ rates in Eq. (6.3), that washes out hypercharge within the broken phase.

In writing Eq. (6.4), we have decoupled the full system of coupled Boltzmann equations into two separate, much simpler questions. First, how is hypercharge generated, diffused into the unbroken phase, and ultimately washed out? The answer is provided by the single Boltzmann equation for $Y$. Second, how much hypercharge is converted into the left-handed quark and lepton charge density that drives weak sphaleron processes? By assuming certain interactions are in chemical equilibrium, we find a series of algebraic relations between various charge densities, using which we find

$$n_L = \kappa_Y\,Y\,, \tag{6.6}$$

where $\kappa_Y$ is a constant of proportionality that depends on various statistical $k$-factors. The hypercharge $Y$ depends on interactions with the expanding bubble wall; the conversion factor $\kappa_Y$ depends on which inelastic interactions are chemical equilibrium in the plasma. In this section, we pursue these arguments in more detail.

## 6.1 Superequilibrium

If we assume that gauginos are sufficiently light ($m_{\widetilde{V}} \lesssim 1$ TeV), so that $\tau_{\widetilde{V}} \ll \tau_{\text{diff}}$, then superequilibrium is satisfied. This assumption is extremely useful; it allows us to consider supermultiplet charge densities, e.g., $Q_i \equiv q_i + \widetilde{q}_i$, rather than $q_i$ and $\widetilde{q}_i$ separately.

Let us see how this works in more detail. For example, consider left-handed quarks and squarks; their Boltzmann equations are

$$\partial_\mu \, q_i^\mu = -\Gamma_{\widetilde{V}}[q_i, \widetilde{q}_i] \left( \frac{q_i}{k_{q_i}} - \frac{\widetilde{q}_i}{k_{\widetilde{q}_i}} \right) + \ ... \tag{6.7a}$$

$$\partial_\mu \, \widetilde{q}_i^\mu = \Gamma_{\widetilde{V}}[q_i, \widetilde{q}_i] \left( \frac{q_i}{k_{q_i}} - \frac{\widetilde{q}_i}{k_{\widetilde{q}_i}} \right) + \ ... \tag{6.7b}$$

where we have isolated only the gaugino interaction terms. By taking a linear combination of these equations, we can write a Boltzmann equation for the difference of chemical potentials $(\mu_{q_i} - \mu_{\widetilde{q}_i})$:

$$\begin{aligned} &\frac{6}{T^2} \left( \frac{1}{k_{q_i}} \, \partial_\mu \, q_i^\mu - \frac{1}{k_{\widetilde{q}_i}} \, \partial_\mu \, \widetilde{q}_i^\mu \right) \\ &\quad = \frac{d}{dt} \left( \mu_{q_i} - \mu_{\widetilde{q}_i} \right) - D_{q_i} \nabla^2 \mu_{q_i} + D_{\widetilde{q}_i} \nabla^2 \mu_{\widetilde{q}_i} \\ &\quad = -2 \left( \frac{1}{k_{q_i}} + \frac{1}{k_{\widetilde{q}_i}} \right) \Gamma_{\widetilde{V}}[q_i, \widetilde{q}_i] \left( \mu_{q_i} - \mu_{\widetilde{q}_i} \right) + ... \end{aligned} \tag{6.8}$$

It is clear that in the limit that $\Gamma_{\widetilde{V}} \to \infty$, the plasma is rapidly driven to chemical equilibrium, where $(\mu_{q_i} - \mu_{\widetilde{q}_i}) \to 0$. In other words, on time scales longer than $\tau_{\widetilde{V}}$, superequilibrium is approximately satisfied; we have

$$\frac{q_i}{k_{q_i}} - \frac{\widetilde{q}_i}{k_{\widetilde{q}_i}} = \mathcal{O}\left( \frac{1}{\Gamma_{\widetilde{V}}} \right) \ , \tag{6.9}$$

where the RHS vanishes in the limit of $\Gamma_{\widetilde{V}} \to \infty$. (In practice, we will neglect these and other $\mathcal{O}\left(\frac{1}{\Gamma}\right)$ corrections; their impact upon the analytic solution to the Boltzmann equations was studied to some extent in Ref. [23].) Expressing this relation in terms of charge densities, we have

$$\frac{q_i}{k_{q_i}} = \frac{\widetilde{q}_i}{k_{\widetilde{q}_i}} = \frac{Q_i}{k_{Q_i}} \,, \tag{6.10}$$

where $k_{Q_i} \equiv k_{q_i} + k_{\widetilde{q}_i}$. Furthermore, if we take the sum of Eqs. (6.7), the resulting Boltzmann equation for $Q_i$ is independent of $\Gamma_{\widetilde{V}}$.

Similar arguments can be repeated for all species. Ultimately, the complete set of supermultiplet isoscalar charge densities is

$$\begin{aligned}
U_i &\equiv n_{u_R^i} + n_{\widetilde{u}_R^i} \,, & Q_i &\equiv n_{u_L^i} + n_{d_L^i} + n_{\widetilde{u}_L^i} + n_{\widetilde{d}_L^i} \,, \\
D_i &\equiv n_{d_R^i} + n_{\widetilde{d}_R^i} \,, & H &\equiv n_{H_u^+} + n_{H_u^0} - n_{H_d^-} - n_{H_d^0} + n_{\widetilde{H}^\pm} + n_{\widetilde{H}^0} \,, \\
R_i &\equiv n_{e_R^i} + n_{\widetilde{e}_R^i} \,, & L_i &\equiv n_{\nu_L^i} + n_{e_L^i} + n_{\widetilde{\nu}_L^i} + n_{\widetilde{e}_L^i} \,,
\end{aligned} \tag{6.11}$$

where $i \in \{1, 2, 3\}$ labels the generations. Furthermore, we define the following additional notation: $Q \equiv Q_3$, $T \equiv U_3$, $B \equiv D_3$, $L \equiv L_3$, and $R \equiv R_3$.

However, not all of these supermultiplet densities are independent, or relevant for EWB. Because we have neglected both flavor mixing and first and second generation Yukawa couplings, first and second generation lepton charge is not produced. We have $L_{1,2} = 0$, which follows directly from Eqs. (3.15). Similarly, first and second generation quark charge is produced solely through strong sphaleron processes, e.g., $t_L\, \bar{t}_R\, b_L\, \bar{b}_R \xrightarrow{\text{ss}} \sum_{i=1,2} \bar{u}_L^i\, u_R^i\, \bar{d}_L^i\, d_R^i$. Clearly, first and second generation left- and right-handed quarks are produced in equal numbers; therefore, we have

$$Q_1 = Q_2 = -2\, U_1 = -2\, U_2 = -2\, D_1 = -2\, D_2 \,. \tag{6.12}$$

Next, we have decoupled weak sphalerons from the system of Boltzmann eqns, since $\Gamma_{ws}^{-1} \sim$

$10^5/T \gg \tau_{\rm diff}$ [44]; therefore, lepton and baryon number are individually conserved:

$$\int_{-\infty}^{\infty} dz \sum_{i=1}^{3}(Q_i + U_i + D_i) = \int_{-\infty}^{\infty} dz \, (L + R) = 0 \, . \tag{6.13}$$

Because the left- and right-handed (s)lepton have different gauge quantum numbers, they have different diffusion constants in the plasma. Even though lepton number is *globally conserved*, regions of net lepton number can develop since $R$ diffuses more easily than $L$. For quarks and squarks, this does not occur since the left- and right-handed (s)quark diffusion constants, dominated by strong interactions, are approximately equal [29]. Therefore, baryon number is *locally* conserved:

$$\sum_{i=1}^{3} (Q_i + U_i + D_i) = 0 \, . \tag{6.14}$$

Combining Eqs. (6.12,6.14), we have

$$B = -(T + Q) \, . \tag{6.15}$$

Therefore, we may consider a reduced set of Boltzmann equations involving only the densities $Q$, $T$, $Q_1$, $L$ , $R$, $H$; the remaining densities are then determined by Eqs. (6.12,6.15).

We now present the Boltzmann equations that result under the present assumptions: (i) superequilibrium, (ii) no first and second generation Yukawa couplings, and (iii) no flavor

mixing. For the quarks and squarks, we obtain

$$\begin{aligned} v_w\,Q' - D_Q\,Q'' &= -\,\Gamma_{yt}\left(\frac{Q}{k_Q} - \frac{T}{k_T} + \frac{H}{k_H}\right) - \,\Gamma_{yb}\left(\frac{Q}{k_Q} + \frac{T+Q}{k_B} - \frac{H}{k_H}\right) \\ &\quad - \Gamma_{mt}\left(\frac{Q}{k_Q} - \frac{T}{k_T}\right) - \Gamma_{mb}\left(\frac{Q}{k_Q} + \frac{T+Q}{k_B}\right) - S_{\widetilde{t}}^{\not{CP}} - S_{\widetilde{b}}^{\not{CP}} \\ &\quad -2\,\Gamma_{ss}\left(2\,\frac{Q}{k_Q} - \frac{T}{k_T} + \frac{Q+T}{k_B} + \frac{1}{2}\sum_{i=1}^{2}\left[4\,\frac{1}{k_{Q_i}} + \frac{1}{k_{U_i}} + \frac{1}{k_{D_i}}\right] Q_1\right) \end{aligned} \tag{6.16a}$$

$$\begin{aligned} v_w\,T' - D_Q\,T'' &= \Gamma_{yt}\left(\frac{Q}{k_Q} - \frac{T}{k_T} + \frac{H}{k_H}\right) + \Gamma_{mt}\left(\frac{Q}{k_Q} - \frac{T}{k_T}\right) + S_{\widetilde{t}}^{\not{CP}} \\ &\quad + \Gamma_{ss}\left(2\,\frac{Q}{k_Q} - \frac{T}{k_T} + \frac{Q+T}{k_B} + \frac{1}{2}\sum_{i=1}^{2}\left[4\,\frac{1}{k_{Q_i}} + \frac{1}{k_{U_i}} + \frac{1}{k_{D_i}}\right] Q_1\right) \end{aligned} \tag{6.16b}$$

$$v_w\,Q_1' - D_Q\,Q_1'' = -2\,\Gamma_{ss}\left(2\,\frac{Q}{k_Q} - \frac{T}{k_T} + \frac{T+Q}{k_B} + \frac{1}{2}\sum_{i=1}^{2}\left[4\,\frac{1}{k_{Q_i}} + \frac{1}{k_{U_i}} + \frac{1}{k_{D_i}}\right] Q_1\right)\,; \tag{6.16c}$$

and for Higgs bosons and Higgsinos we have

$$\begin{aligned} v_w\,H' - D_H\,H'' &= -\,\Gamma_{yt}\left(\frac{Q}{k_Q} - \frac{T}{k_T} + \frac{H}{k_H}\right) - \Gamma_h\,\frac{H}{k_H} + S_{\widetilde{H}}^{\not{CP}} \\ &\quad + \Gamma_{yb}\left(\frac{Q}{k_Q} + \frac{Q+T}{k_B} - \frac{H}{k_H}\right) + \Gamma_{y\tau}\left(\frac{L}{k_L} - \frac{R}{k_R} - \frac{H}{k_H}\right)\,; \end{aligned} \tag{6.17}$$

and lastly for leptons and sleptons we have

$$v_w\,L' - D_L\,L'' = -\,\Gamma_{y\tau}\left(\frac{L}{k_L} - \frac{R}{k_R} - \frac{H}{k_H}\right) - \Gamma_{m\tau}\left(\frac{L}{k_L} - \frac{R}{k_R}\right) - S_{\widetilde{\tau}}^{\not{CP}} \tag{6.18a}$$

$$v_w\,R' - D_R\,R'' = \Gamma_{y\tau}\left(\frac{L}{k_L} - \frac{R}{k_R} - \frac{H}{k_H}\right) + \Gamma_{m\tau}\left(\frac{L}{k_L} - \frac{R}{k_R}\right) + S_{\widetilde{\tau}}^{\not{CP}}\,. \tag{6.18b}$$

The relevant interaction coefficients in Eqs. (6.16-6.18) are as follows:

- The coefficients $\Gamma_{yi}$, where $i \in \{t, b, \tau\}$, denote the total interaction rates arising from third generation Yukawa couplings $y_i$, as defined in Eq. (4.27). (The top Yukawa interaction rate has been denoted $\Gamma_y$ in previous work.)

- The strong sphaleron rate is $\Gamma_{\rm ss} = 16\,\kappa'\,\alpha_s^4\,T$, where $\alpha_s$ is the strong coupling and

$\kappa' \sim \mathcal{O}(1)$ [42].

- The coefficients $\Gamma_h$ and $\Gamma_{mi}$, where $i \in \{t, b, \tau\}$, denote the CP-conserving scattering rates of particles with the background of broken electroweak symmetry within the bubble [22].

We also allow for new CP-violating sources $S^{\not{CP}}_{\widetilde{b},\widetilde{\tau},H}$, although in the present work we do not evaluate their magnitudes. In the MSSM, the most viable CP-violating source is $S^{\not{CP}}_{\widetilde{H}}$, arising from CP-violating Higgsino-Wino or Higgsino-Bino mixing within the expanding bubble wall [45]. The constant $v_w \simeq 0.05$ is the velocity of the expanding bubble wall. The $k$-factors, e.g.

$$k_R \equiv k_{\tau_R} + k_{\widetilde{\tau}_R} \ , \quad k_Q \equiv k_q + k_{\widetilde{q}}, \ \ldots \ , \tag{6.19}$$

follow the same notation as in Eqs. (6.11). The diffusion constants are, e.g.,

$$D_Q \equiv \frac{k_q \, D_q + k_{\widetilde{q}} \, D_{\widetilde{q}}}{k_Q} \ , \ \ldots \ , \tag{6.20}$$

again following Eqs. (6.11).

These Boltzmann equations are different from those in the established literature [20], because of the inclusion of bottom and tau Yukawa interactions. Below, we will show how ours reduce to those in the limit that $y_b, y_\tau \to 0$.

## 6.2 Yukawa equilibrium

Top, bottom, and tau Yukawa interactions may all be in chemical equilibrium during EWB. The corresponding chemical equilibrium conditions allow one to express all charge densities in terms of a single charge density. Instead of expressing them in terms of $Y$, we will express them all in terms of $H$, the Higgs and Higgsino charge density, which has been the convention in previous work.

First, we consider the lepton densities. When tau Yukawa interactions are in chemical

equilibrium condition, the relation

$$\frac{L}{k_L} - \frac{H}{k_H} - \frac{R}{k_R} = 0 \; . \tag{6.21}$$

is satisfied. The sum of the Boltzmann equations for $L$ and $R$ (6.18) is

$$v_w \, (R + L)' + (D_R \, R'' + D_L \, L'') = 0 \; . \tag{6.22}$$

Since the left- and right-handed lepton diffusion constants are not equal, there is no simple relation that would allow us to relate $R$ to $L$. However, in the limit that $v_w \to 0$, Eq. (6.22) implies that

$$D_L \, L = - \, D_R \, R \; . \tag{6.23}$$

(We have assumed the boundary conditions $L(\infty) = L'(\infty) = R(\infty) = R'(\infty) = 0$.) Therefore, we have

$$L(z) \;\equiv\; \kappa_L \, H(z) + \Delta L(z) = \frac{k_L}{k_H} \, \frac{D_R \, k_R}{D_L \, k_L + D_R \, k_R} \, H(z) + \Delta L(z) \tag{6.24a}$$

$$R(z) \;\equiv\; \kappa_R \, H(z) + \Delta R(z) = -\frac{k_R}{k_H} \, \frac{D_L \, k_L}{D_L \, k_L + D_R \, k_R} \, H(z) + \Delta R(z) \; , \tag{6.24b}$$

where $\Delta L$ and $\Delta R$ are the $\mathcal{O}(v_w)$ corrections to these relations, derived below.

Let us now describe the physics of Eqs. (6.24) through two limiting cases. Case (i): set $D_R = D_L$. In this limit, Eq. (6.22) implies that lepton number is *locally* conserved: $L + R = 0$. Higgs density $H$, created by the CP-violating source, is converted into $L$ through tau Yukawa interactions, until chemical equilibrium (6.21) is reached, when

$$L(z) = \frac{k_L}{k_H} \, \frac{k_R}{k_L + k_R} \, H(z) \; . \tag{6.25}$$

Case (ii): take $D_R \to \infty$, keeping $D_L$ finite. Any $R$ density created by tau Yukawa interactions instantly diffuses away to $z = \pm\infty$; therefore, we set $R = 0$. Now, tau Yukawa

chemical equilibrium (6.21) implies

$$L(z) = \frac{k_L}{k_H} H(z) \ . \tag{6.26}$$

In other words, tau Yukawa interactions will enforce chemical equilibrium locally. Since RH lepton density is diffusing away, reducing the local $R$, more conversion of $H$ into $R$ and $L$ occurs to compensate, thereby resulting in more LH lepton density. This conversion ceases when Eq. (6.26) is reached. Therefore, a large diffusion constant for RH leptons *enhances* the density for LH leptons close to the bubble wall. This enhancement, maximized for $D_R \to \infty$, lies in the range

$$\frac{5}{3} \ \leq \ \frac{k_R + k_L}{k_R} \ \leq \ 7 \ , \tag{6.27}$$

since $1 \leq k_R \leq 3$ and $2 \leq k_L \leq 6$. The lower (upper) bound is reached when $m_{\tilde{e}_3} \gg T \gg m_{\tilde{\ell}_3}$ ($m_{\tilde{e}_3} \ll T \ll m_{\tilde{\ell}_3}$).

Next, consider the case of physical relevance, where $D_R \gg D_L$, but keeping both $D_R, D_L$ finite. Close to the bubble wall, LH lepton density will be enhanced, as argued above. However, far from the bubble wall, an additional effect occurs: RH lepton density, having diffused far into the unbroken phase, is converted into $L$ and $H$ by tau Yukawa interactions. This effect *suppresses* $L$. Close to the bubble wall, Higgsinos created by the CP-violating source (e.g., $H > 0$) will be converted into LH leptons ($L > 0$) and RH anti-leptons ($R < 0$), and then, far from the wall, the RH anti-leptons will be converted into LH anti-leptons, thereby suppressing $L$. This physics is incorporated in the $\mathcal{O}(v_w)$ corrections $\Delta L$ and $\Delta R$, which we now derive. Using Eqs. (6.21, 6.22, 6.24), we can derive differential equations for these densities:

$$-D_{LR}\,\Delta L'' + v_w\,\Delta L' \ = \ v_w\,\frac{k_R\,k_L^2}{k_H(k_L+k_R)^2}\,\frac{D_L - D_R}{D_{LR}}\,H' \tag{6.28a}$$

$$-D_{LR}\,\Delta R'' + v_w\,\Delta R' \ = \ v_w\,\frac{k_R^2\,k_L}{k_H(k_L+k_R)^2}\,\frac{D_L - D_R}{D_{LR}}\,H' \ , \tag{6.28b}$$

where $D_{LR} \equiv (D_L\,k_L + D_R\,k_R)/(k_L + k_R)$. With the boundary conditions $\Delta L(\pm\infty) =$

$\Delta R(\pm\infty) = 0$, the solutions to these equations are

$$\Delta L(z) = v_w \frac{k_L^2\, k_R}{k_H\,(k_R + k_L)^2} \frac{D_L - D_R}{D_{LR}^2} \int_z^\infty dz'\, H(z')\, e^{v_w(z-z')/D_{LR}} \quad (6.29a)$$

$$\Delta R(z) = v_w \frac{k_L\, k_R^2}{k_H\,(k_R + k_L)^2} \frac{D_L - D_R}{D_{LR}^2} \int_z^\infty dz'\, H(z')\, e^{v_w(z-z')/D_{LR}}\,. \quad (6.29b)$$

Using Eqs. (6.24,6.29), it is straight-forward to show that these solutions for $L$ and $R$ satisfy

$$\int_{-\infty}^{\infty} dz\,(L + R) = 0\,, \quad (6.30)$$

so lepton number is globally conserved, even though $L(z) + R(z) \neq 0$ locally. Regions of net lepton-number can arise due to the different diffusion constants of left- and right-handed (s)leptons. Numerically, as we show in Sec. 7, the impact from $\Delta L$ and $\Delta R$ on the analytic computation of $n_B/s$ is only $\mathcal{O}(10\%)$. Since there are much larger uncertainties in the analytic computation, it is safe to neglect $\Delta L$ and $\Delta R$ from Eqs. (6.24).

Next, we consider the quark densities. When top and bottom Yukawa interactions are in chemical equilibrium, the relations

$$\frac{Q}{k_Q} + \frac{H}{k_H} - \frac{T}{k_T} = 0\,, \quad (6.31a)$$

$$\frac{Q}{k_Q} - \frac{H}{k_H} + \frac{B}{k_B} = 0\,. \quad (6.31b)$$

are satisfied; *cf.* Eqns. (3.2, 3.4). These equations imply that

$$2\,\frac{Q}{k_Q} - \frac{T}{k_T} - \frac{B}{k_B} = 0\,. \quad (6.32)$$

First and second generation quark densities only couple to third generation densities, via strong sphaleron interactions, through the linear combination $(2Q/k_Q - T/k_T - B/k_B)$, as can be seen from Eqns. (6.16). Since this combination vanishes, third generation quark densities do not source 1st/2nd generation quark densities. Mathematically, if we impose

Eq. (6.32), the $Q_1$ Boltzmann equation (6.16c) becomes

$$v_w\, Q_1' - D_q\, Q_1'' \;\propto\; -\,\Gamma_{\rm ss}\, Q_1 \;, \tag{6.33}$$

which, with the boundary conditions $Q_1(\pm\infty) = 0$, implies $Q_1(z) = 0$. According to Eq. (6.14), we have $U_i = D_i = -Q_i/2 = 0$, for $i = 1, 2$. Therefore, we conclude that all first and second generation quark and squark charge densities vanish in the presence of fast top and bottom Yukawa interations. Strong sphalerons only induce first and second generation densities in order to wash out an asymmetry between left- and right-handed quark chemical potentials; when bottom Yukawas are active, this asymmetry vanishes and strong sphalerons have no effect. Eqns. (6.31) imply

$$\begin{aligned} T &\equiv \kappa_T\, H = \frac{k_T}{k_H}\,\frac{2k_B + k_Q}{k_B + k_Q + k_T}\, H \\ Q &\equiv \kappa_Q\, H = \frac{k_Q}{k_H}\,\frac{k_B - k_T}{k_B + k_Q + k_T}\, H \\ B &\equiv \kappa_B\, H = -\,\frac{k_B}{k_H}\,\frac{2k_T + k_Q}{k_B + k_Q + k_T}\, H \;. \end{aligned} \tag{6.34}$$

To summarize, we have expressed all quark and lepton charge densities in terms of $H$, the Higgs and Higgsino charge density, assuming that their generation Yukawa interactions are in chemical equilibrium.

Using these Yukawa chemical equilibrium relations, it is now possible to see how hypercharge is converted into $n_L$. The contribution to $n_L$ from third generation LH quarks is

$$n_{u_L^3} + n_{d_L^3} = \frac{k_q}{k_H}\,\frac{k_B - k_T}{k_B + k_Q + k_T}\, H \;, \tag{6.35}$$

while that from first and second generation LH quarks is suppressed. Furthermore, the contribution to $n_L$ from third generation leptons is

$$n_{\ell_3} = \frac{k_{\ell_3}}{k_H}\,\frac{D_R\, k_R}{D_L\, k_L + D_R\, k_R}\, H(z) + \frac{k_{\ell_3}}{k_L}\,\Delta L(z) \;. \tag{6.36}$$

It is by convention that these densities are expressed in terms of $H$. Neglecting the non-

local $\Delta L, \Delta R$ terms, we can express $H$ in terms of $Y$ using

$$Y = \left( \frac{\kappa_Q}{6} + \frac{2\kappa_T}{3} - \frac{\kappa_B}{3} - \frac{\kappa_L}{2} - \kappa_R + \frac{1}{2} \right) H \ . \tag{6.37}$$

To the extent that the non-local lepton terms can be neglected, the charge densities are proportional to the total hypercharge $Y$, generated by the CP-violating source; the constants of proportionality describe how much hypercharge is converted into each species, which depends on which interactions are in chemical equilibrium.

Let us contrast these results to previous work that neglected bottom Yukawa interactions [20]:

$$n_{u_L^3} + n_{d_L^3} = \frac{k_q}{k_H} \frac{k_B - 9k_T}{k_B + 9k_Q + 9k_T} H \ , \tag{6.38a}$$

$$n_{u_L^i} + n_{d_L^i} = \frac{k_{q_i}}{k_H} \frac{2k_Q(k_B - 9k_T) + 2k_T(9k_T + 2k_B)}{k_B + 9k_Q + 9k_T} H \ , \quad i = 1, 2 \ , \tag{6.38b}$$

The formulae are completely different. Whereas in previous work significant baryon asymmetry could arise from first and second generation LH quarks, the presence of bottom Yukawa interactions completely changes the picture: no first and second generation quark density is created. In addition, with fast bottom Yukawa interactions, the third generation quark charge vanishes when $k_T \simeq k_B$, or equivalenty $m_{\tilde{t}_R} \simeq m_{\tilde{b}_R}$; without them, this cancellation never occurs. Let us explain the physical origin of this cancellation. Suppose that the CP-violating source creates positive Higgs/Higgsino density, such that $H > 0$. Due to hypercharge conservation, top Yukawa interactions will convert Higgsinos and Higgs bosons into LH quark and squark antiparticles (driving $Q < 0$), while bottom Yukawa interactions will convert Higgsinos and Higgs bosons into LH quark and squark particles (driving $Q > 0$). Which effect wins depends on the masses $m_{\tilde{t}_R}$ and $m_{\tilde{b}_R}$, since the equipartition of $H$ charge density prefers lighter degrees of freedom in the plasma. In the lepton-mediated scenario, the quark contribution is suppressed by choosing $m_{\tilde{t}_R} \approx m_{\tilde{b}_R}$, or $m_{\tilde{t}_R}, m_{\tilde{b}_R} \gg T$.

## 6.3 Solving the Boltzmann equation

In terms of $H$, the left-handed fermion charge density (6.46) becomes

$$n_L(z) = \frac{k_q}{k_H}\,\frac{k_B - k_T}{k_B + k_Q + k_T}\,H(z) + \frac{k_\ell}{k_H}\,\frac{k_R\,D_R}{k_L\,D_L + k_R\,D_R}\,H(z) + \frac{k_\ell}{k_L}\,\Delta L(z)\;, \qquad (6.39)$$

where $\Delta L$ is given in Eq. (6.24a). The first term is the contribution to $n_L$ from third generation quarks, while the second and third terms are contributions from third generation leptons. The lepton contribution is predominantly given by the second term only; the third term, as discussed above, is suppressed for $v_w \ll 1$. This equation is the main result of this paper; from it, we infer several conclusions:

- The lepton contribution is enhanced for $m_{\tilde{\tau}_R} \ll m_{\tilde{\tau}_L}$, when $k_R$ is largest and $k_L$ smallest; (*cf.* Eqs. (6.19,3.4)). It is also enhanced for $D_R \gg D_L$. Its sign is fixed with respect to $H$, which in turn is fixed by the sign of the CP-violating source, as we show below. Therefore, in a lepton-mediated EWB scenario, where $n_L$ is predominantly leptonic, the sign of the CP-violating phase most relevant for EWB uniquely fixes the sign of $n_B/s$.

- Left-handed charge comes from third generation quarks and leptons, and not first and second generation quarks and leptons. The form of $n_L$ is qualitatively different than in previous treatments that neglected $\Gamma_{yb}$ and $\Gamma_{y\tau}$, where left-handed charge came from quarks of all generations, and not from leptons.

- Furthermore, the quark contribution to $n_L$ vanishes for $k_B = k_T$, which occurs (i) when $m_{\tilde{t}_R}, m_{\tilde{b}_R} \gg T$, or (ii)when $m_{\tilde{t}_R} = m_{\tilde{b}_R}$. If either or both squarks are light, then the sign of this contribution is opposite to that of the leptonic contribution for $m_{\tilde{t}_R} < m_{\tilde{b}_R}$ and the same for $m_{\tilde{t}_R} > m_{\tilde{b}_R}$.

We explore these implications in more detail numerically in Chapter 7.

We emphasize that our conclusions are quite general, although it appears that our Boltzmann equations (6.16-6.18) have been specialized to the MSSM. In any extention of the MSSM, if the following conditions hold — (i) that third generation Yukawa interaction

rates are faster than the diffusion rate, (ii) CP-violation is communicated to the first and second generation quark sectors solely through strong sphalerons, and (iii) any beyond-the-MSSM supermultiplets carry no hypercharge — then Eq. (6.39) and its conclusions remain valid.

Since $n_B/s$ is determined by $n_L$, all that remains is to solve for the Higgs charge density $H$. We can reduce the Boltzmann equations (6.16-6.18) into a single equation for $H$ by taking the appropriate linear combination of equations

$$\text{(6.16a)} + 2 \times \text{(6.16b)} + \text{(6.17)} + \text{(6.18a)} \ , \tag{6.40}$$

such that the Yukawa and strong sphaleron rates all cancel, and expressing the densities $L, Q, T$ in terms of $H$ using Eqs. (6.24,6.34). This master Boltzmann equation equation is an integro-differential equation for $H(z)$, due to the presence of the $\Delta L$ term. Therefore, for simplicity, we treat $\Delta L$ perturbatively: first, we neglect $\Delta L$ in our solution for $H$, and then, given our solution $H$, we include the $\Delta L$ contribution in Eq. (6.39) for $n_L$. Neglecting $\Delta L$, the master Boltzmann equation is

$$v_w \, H' - \bar{D} \, H'' = \ - \bar{\Gamma} \, H + \bar{S} \ , \tag{6.41}$$

where

$$\bar{D} = \frac{D_H + D_Q(\kappa_T - \kappa_B) + D_L \, \kappa_L}{1 + \kappa_T - \kappa_B + \kappa_L} \tag{6.42a}$$

$$\bar{\Gamma} = \frac{\Gamma_h + \Gamma_{mt} + \Gamma_{mb} + \Gamma_{m\tau}}{k_H(1 + \kappa_T - \kappa_B + \kappa_L)} \tag{6.42b}$$

$$\bar{S} = \frac{S_{\tilde{H}}^{\not{CP}} + S_{\tilde{t}}^{\not{CP}} - S_{\tilde{b}}^{\not{CP}} - S_{\tilde{\tau}}^{\not{CP}}}{1 + \kappa_T - \kappa_B + \kappa_L} \ . \tag{6.42c}$$

Although the form of Eq. (6.41) is identical to that in the established literature [20, 22], the form of Eqs. (6.42) is dramatically different. We note that there is no dependence on the first/second generation quark sector, owing to the fact that they do not participate in the dynamics which determines $n_L$.

To solve Eq. (6.41), we follow Ref. [20] making the approximations (a) that the true spatial dependence of the chiral relaxation rates may be replaced by a step-function, so that we may write $\bar{\Gamma}(z) = \bar{\Gamma}\,\theta(z)$; and (b) that $\bar{S}(z) \simeq 0$ for $z < -L_w/2$. For the symmetric phase, where $z < -L_w/2$, we obtain

$$H = \mathcal{A}\, e^{v_w z/\bar{D}} \,, \tag{6.43}$$

where

$$\mathcal{A} = \int_0^\infty dy\; \bar{S}(y) \frac{e^{-\gamma_+ y}}{\bar{D}\gamma_+} + \int_{-Lw/2}^0 dy\; \bar{S}(y) \left[ \frac{\gamma_-}{v_w \gamma_+} + \frac{e^{-v_w y/\bar{D}}}{v_w} \right] . \tag{6.44}$$

Furthermore, we have defined

$$\gamma_\pm \equiv \frac{1}{2\bar{D}} \left[ v_w \pm \sqrt{v_w^2 + 4\bar{\Gamma}\bar{D}} \right] . \tag{6.45}$$

Although the form of Eqns. (6.43-6.45) is similar to that in previous work [20], our results for $\bar{D}$, $\bar{\Gamma}$, and $\bar{S}$ are different, due to the modified structure of the Boltzmann equations in the presence of fast bottom and tau Yukawa rates.

After solving the system of Boltzmann equations (6.16-6.18) for each density, the left-handed fermion charge density is

$$n_L = \left( \frac{k_q}{k_Q} \right) Q + \sum_{i=1,2} \left( \frac{k_{q_i}}{k_{Q_i}} \right) Q_1 + \left( \frac{k_\ell}{k_L} \right) L \,, \tag{6.46}$$

where $k_q \equiv k_{t_L} + k_{b_L}$, $k_\ell \equiv k_{\nu_L^\tau} + k_{\tau_L}$, *etc.* The three terms in Eq. (6.46) correspond to the contributions to $n_L$ from third generation quarks, first/second generation quarks, and third generation leptons, respectively. If the masses of all left-handed squarks and sleptons is much above the temperature of the phase transition, only fermions contribute to the left-handed density and we have

$$n_L \simeq Q + 2\,Q_1 + L \,. \tag{6.47}$$

Finally, we show how our Boltzmann equations reproduce those given in previous work in the limit $y_b,\, y_\tau \to 0$. In this limit, we can neglect the rates $\Gamma_{yb,\tau}$ and $\Gamma_{mb,\tau}$, and CP-

violating sources $S^{\not{C}\not{P}}_{\widetilde{b},\widetilde{\tau}}$. First, since there is no source for lepton charge, we have $L = R = 0$. Second, the only source for $B$ density is strong sphaleron processes; therefore, we have

$$-2\,B = Q_1 \tag{6.48}$$

in analogy with Eq. (6.12). Thus, Eqs. (6.15,6.48) imply that $Q_1 = 2(Q + T)$. Therefore, by Eq. (6.47), we have the often-used relation $n_L = 5Q + 4T$; this relation is no longer valid for $\tau_{yb}, \tau_{y\tau} \lesssim \tau_{\rm diff}$. In addition, the Boltzmann equations of Refs. [20, 22, 23] follow from Eqs. (6.16a,b,6.17); they too are no longer valid for $\tau_{yb}, \tau_{y\tau} \lesssim \tau_{\rm diff}$.

## 6.4 Baryons at last

Baryon number generation is decoupled from the dynamics that determines $n_L$ because $\Gamma_{ws}^{-1} \gg \tau_{\rm diff}$. The Boltzmann equation for $n_B$ is [21]

$$v_w\, n_B' - D_Q\, n_B'' + \mathcal{R}\, n_B = -\frac{3}{2}\,\Gamma_{ws}\, n_L(z) \tag{6.49}$$

where $\Gamma_{ws}$ is the weak sphaleron rate, and the relaxation term

$$\mathcal{R} \equiv \Gamma_{ws}\,\left[\frac{9}{4}\left(1 + \frac{n_{sq}}{6}\right)^{-1} + \frac{3}{2}\right] \tag{6.50}$$

describes how baryon-number generation ceases when weak sphalerons reach chemical equilibrium, when $\sum_i \mu_{q_i} + \mu_{\ell_i} = 0$. (Also, $n_{sq}$ is the number of light squarks.) The weak sphaleron rate is spacetime-dependent; here, we take

$$\Gamma_{ws} \;\to\; \Gamma_{ws}\,\theta(-L_w/2 - z) \tag{6.51}$$

so that weak sphalerons are active only in the unbroken phase, for $z < -L_w/2$. The solution to Eq. (6.49) is

$$n_B = -\frac{3\Gamma_{ws}}{2D_Q\lambda_+}\int_{-\infty}^{-L_w/2} dz\; n_L(z)\, e^{-\lambda_- z}\;. \tag{6.52}$$

with

$$\lambda_{\pm} = \frac{1}{2D_Q}\left(v_w \pm \sqrt{v_w^2 + 4D_Q\,\mathcal{R}}\right) \ , \tag{6.53}$$

The entropy density is given by

$$s = \frac{2\pi^2}{45}\, g_{*S}\, T^3 \ , \tag{6.54}$$

where $g_{*S} \sim 130$, for the parameters given in the text. Given $n_L$, either numerically or analytically, we can compute $n_B/s$.

# Chapter 7

# Computing the Baryon Asymmetry, Part II: Numerical Results

In the preceding chapter, we showed how the Boltzmann equations may be solved analytically. We argued that bottom and tau Yukawa interactions are not only relevant to EWB dynamics, but dramatically change how hypercharge is converted into left-handed quark and lepton density. Independent of the nature of the CP-violating source, this collisional effect can suppress or flip the sign of the baryon asymmetry. In some regions of parameter space, these interactions will be crucial for connecting EWB to experiments.

We now investigate these claims by studying the Boltzmann equations numerically. We assume that superequilibrium is maintained (assuming gaugino masses $m_{\widetilde{V}} \lesssim 1$ TeV); therefore, we work with the reduced system of Boltzmann equations given in Eqs. (6.16-6.18). First, we study a "lepton-mediated scenario" that strongly illustrates the key features described above: (i) the quark contribution to $n_L$ is suppressed for $m_{\widetilde{t}_R} \simeq m_{\widetilde{b}_R}$, and (ii) the baryon asymmetry, driven by left-handed leptons, has opposite sign compared to what one would predict if neglecting bottom and tau Yukawa interactions.

Next, we investigate other regions of parameter space: (i) a "light-stop scenario," similar to that in Ref. [46], and (ii) a heavy squark and slepton scenario, which may be relevant for EWB the NMSSM. In the latter case, we find that lepton-mediated EWB is the default scenario over a wide range of parameter space.

| | | | | | | | |
|---|---|---|---|---|---|---|---|
| $\mu$ | 120 GeV | $M_T^2$ | $-(60\text{ GeV})^2$ | $T$ | 100 GeV | $D_Q$ | $6/T$ |
| $M_1$ | 120 GeV | $M_B^2$ | $(100\text{ GeV})^2$ | $v(T)$ | 125 GeV | $D_H$, $D_L$ | $100/T$ |
| $M_2$ | 250 GeV | $M_R^2$ | $(300\text{ GeV})^2$ | $\Delta\beta$ | 0.015 | $D_R$ | $380/T$ |
| $\tan\beta$ | 20 | $m_A$ | 150 GeV | $v_w$ | 0.05 | $L_w$ | $25/T$ |

Table 7.1: Important parameters for electroweak baryogenesis.

## 7.1 Lepton-mediated electroweak baryogenesis: input parameters

We now consider an MSSM scenario that illustrates some of the novel features discussed in Sec. 6. As we will see, the picture here is that the BAU is induced predominantly by leptonic left-handed charge: hence, lepton-mediated. The key parameters that govern the behavior of this scenario are (i) $\tan\beta \gtrsim 20$ and pseudoscalar Higgs mass (at zero temperature) $m_A \lesssim 500$ GeV, ensuring $\tau_{y\tau}$, $\tau_{y\tau} \ll \tau_{\rm diff}$, and (ii) right-handed top and bottom squarks with approximately equal mass, thereby suppressing the quark contribution to $n_L$. Here, we take both squarks to be light, with $\mathcal{O}(100\text{ GeV})$ masses, since a strong first-order phase transition requires a light top squark.

Although we work within the context of the MSSM, many of our conclusions are much more general. In EWB scenarios beyond the MSSM, light squarks are not required for a strong first-order phase transition (see e.g. Refs. [49, 50, 51]). Even if the squarks are very heavy, EWB is still mediated by leptons as long as the previous two conditions are met.

The computation of $n_B/s$ relies upon many numerical inputs, described here. We have evaluated the masses of particles during the EWPT assuming that electroweak symmetry is unbroken, as discussed in Chapter 2. This approximation is motivated by the fact that most of the charge transport dynamics takes place outside the bubble, in the region of unbroken symmetry. These masses receive contributions from the mass parameters in Tab. 7.1 and from finite-temperature corrections, listed in the Tab. 2.2. The right-handed stop, sbottom, and stau SUSY-breaking mass-squared parameters are $M_T^2$, $M_B^2$, and $M_R^2$, respectively. The RH stop is required to be light to achieve a strong first-order phase transition [46]; taking the RH sbottom and stau to be light as well ensures that the quark contribution to $n_L$ is suppressed, while the lepton contribution is enhanced, in accord with Eq. (6.39). We take

all other squark and slepton mass-squared parameters to be 10 TeV. (In addition, we take $A_t = 7$ TeV; with these parameters the lightest zero-temperature stop mass is $m_{\tilde{t}_1} \simeq 102$ GeV.)

The diffusion constants $D_i$ have been computed in Ref. [28, 29]; the fact that $D_R \gg D_L$ enhances the left-handed lepton charge, as discussed in Sec. 6. The bubble wall velocity $v_w$, thickness $L_w$, profile parameters $\Delta\beta$ and $v(T)$ describe the dynamics of the expanding bubbles during the EWPT, at temperature $T$ [40]. The spacetime-dependent vevs are approximated by

$$v(z) \simeq \frac{1}{2}\, v(T) \left[1 - \tanh\left(-\frac{3z}{L_w}\right)\right] \tag{7.1}$$

$$\beta(z) \simeq \beta(T) - \frac{1}{2}\,\Delta\beta \left[1 + \tanh\left(-\frac{3z}{L_w}\right)\right] , \tag{7.2}$$

following Ref. [32].

We consider a CP-violating source $S_{\widetilde{H}}^{\not{C}\not{P}}$ arising solely from Higgsino-Bino mixing, enhanced for $\mu = M_1$, and calculated following Refs. [31, 22]. The relevant CP-violating phase $\phi_1 \equiv \arg(M_1 \mu b^*)$ virtually unconstrained from electric dipole moment searches if we assume that the gaugino phases are non-universal, such that $\phi_1 \gg \phi_2$ [45]. The Higgsino and Bino thermal widths are $\Gamma_{\widetilde{H}} \simeq 0.025\, T$ and $\Gamma_{\widetilde{H}} \simeq 0.020\, T$ [48]. Numerically, we find

$$S_{\widetilde{H}}^{\not{C}\not{P}} \simeq -0.15 \text{ GeV} \times \beta'(z)\, v(z)^2 \sin\phi_1 . \tag{7.3}$$

The magnitude of $S_{\widetilde{H}}^{\not{C}\not{P}}$ — and thus $n_B/s$ — is proportional to $\Delta\beta$, which itself goes as $\Delta\beta \propto 1/m_A^2$. Therefore, within this computation, viable EWB requires $m_A$ to be sufficiently light; this leads to significant bottom and tau Yukawa interaction rates. (In other computations, there exist contributions to $S_{\widetilde{H}}^{\not{C}\not{P}}$ that are not suppressed as $m_A \to \infty$ [41, 46].)

The CP-conserving relaxation rates wash-out CP-violating asymmetries within the bro-

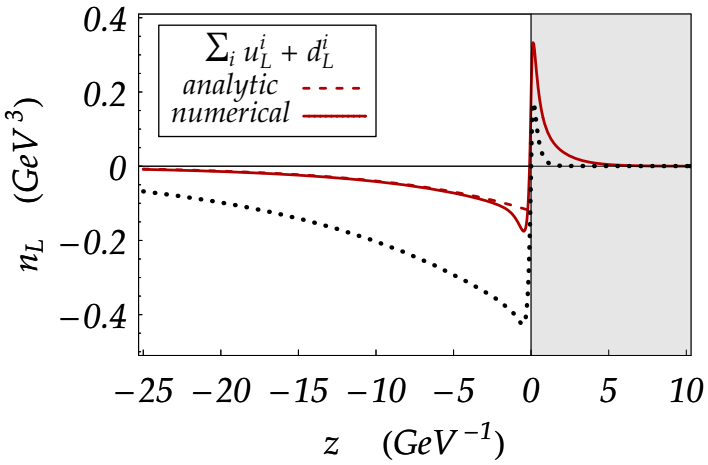


Figure 7.1: Left-handed charge densities for quarks that source $n_B/s$, for lepton-mediated scenario. Solid (dashed) curve is our numerical (analytic) result, as function of distance $z$ from bubble wall. Shaded region denotes broken electroweak symmetry. Dotted curve are numerical results obtained neglecting tau/bottom Yukawa interactions. The effect of these interactions is to suppress LH quark charge, while enhancing LH lepton charge, thereby flipping the sign of $n_L$ and $n_B/s$ compared to previous computations.

ken phase. Computed following Ref. [22], these rates are

$$\Gamma_h(z) \simeq 2.5 \times 10^{-3}\ \text{GeV}^{-1} \times v(z)^2 \tag{7.4}$$

$$\Gamma_{mt}(z) \simeq 3.0 \times 10^{-3}\ \text{GeV}^{-1} \times v(z)^2 \sin^2\beta(z) \tag{7.5}$$

$$\Gamma_{mb}(z) \simeq \left(\frac{y_b}{y_t}\right)^2 \cot^2\beta(z)\,\Gamma_{mt}(z)\ . \tag{7.6}$$

We neglect additional CP-violating relaxation rates from squarks, (s)leptons, and Higgs scalars.

## 7.2 Lepton-mediated scenario: results

We now solve the Boltzmann equations (6.16-6.18) numerically for the lepton-mediated EWB scenario, with input parameters defined above. In Fig. 7.1, we show the left-handed charge density $n_L$ that arises from quarks, for maximal CP-violating phase $\phi_1 = -\pi/2$. Our numerical results are shown by the solid curves, plotted as a function of the distance $z$

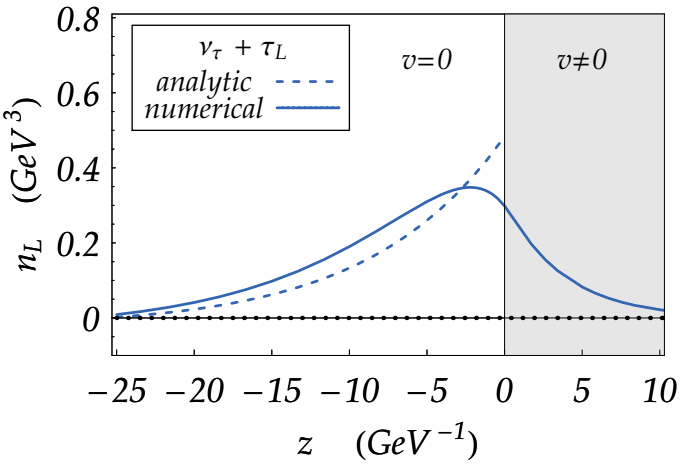


Figure 7.2: Left-handed charge densities for leptons and quarks (right) that source $n_B/s$, for lepton-mediated scenario. Solid (dashed) curve is our numerical (analytic) result, as function of distance $z$ from bubble wall. Shaded region denotes broken electroweak symmetry. Dotted curve (at zero) is our numerical result obtained neglecting tau/bottom Yukawa interactions. The effect of these interactions is to suppress LH quark charge, while enhancing LH lepton charge, thereby flipping the sign of $n_L$ and $n_B/s$ compared to previous computations.

to the moving bubble wall. The region of broken electroweak symmetry (denoted $v \neq 0$) is for $z > 0$, while unbroken symmetry is for $z < 0$ (denoted $v = 0$). As advertised, the total left-handed quark charge is suppressed compared to our computation neglecting bottom and tau Yukawa interactions (dotted curve).

In Fig. 7.2, we show the left-handed, third generation lepton charge density, for $\phi_1 = -\pi/2$. Without tau Yukawa interactions, no lepton charge density is generated; this is indicated by the dotted curve at zero. However, our numerical (solid) and analytic (dashed) results indicate that tau Yukawa interactions do generate significant lepton charge. In fact, as promised, $n_L$ is predominantly leptonic, while the quark contribution is suppressed.

The resulting baryon asymmetry depends crucially upon whether or not bottom and tau Yukawa interactions have been incorporated into the Boltzmann equations. We find

$$n_B/s \;\approx\; \begin{cases} 6 \times \sin\phi_1 \; (n_B/s)_{\rm CMB} & \text{Bottom/tau included} \\ -\,11 \times \sin\phi_1 \; (n_B/s)_{\rm CMB} & \text{Bottom/tau neglected} \end{cases} \tag{7.7}$$

where $(n_B/s)_{\rm CMB} = 8.84 \times 10^{-11}$ is the central value obtained from the CMB [2], re-

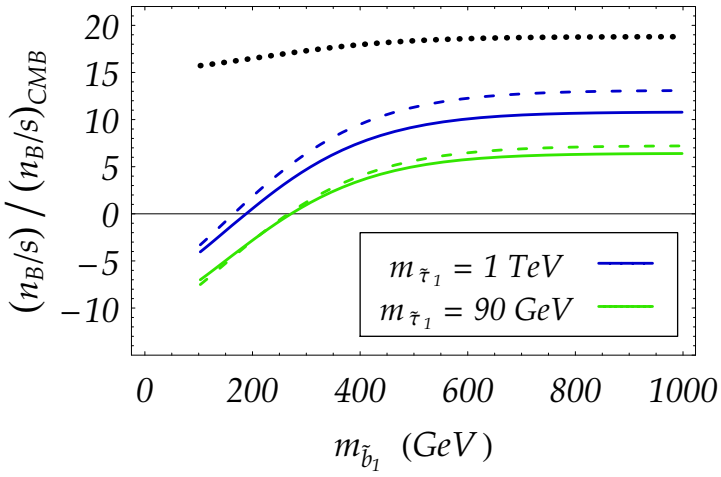


Figure 7.3: Baryon asymmetry $(n_B/s)$, normalized to $(n_B/s)_{\rm CMB}$, for $\sin\phi_1 = \pi/2$, as a function of lightest (RH) bottom squark mass at zero temperature, for lightest (RH) stau mass $m_{\tilde{\tau}} = 90$ GeV (lower solid and dashed curves) and $m_{\tilde{\tau}} = 1$ TeV (middle solid and dashed). The uppermost, dotted curve is numerical results neglecting bottom and tau Yukawa interactions.

quiring $\sin\phi_1 \approx 1/6$. However, if we had neglected bottom/tau Yukawa interactions, we would have required $\sin\phi_1 \approx -1/11$. If electric dipole moment searches uncover new CP-violating phases, such as $\phi_1$, the inclusion $\Gamma_{yb}$ and $\Gamma_{y\tau}$ will clearly be essential in testing the consistency of supersymmetric EWB scenarios.

The agreement in the unbroken phase between our numerical and analytic results is good. (The latter has been plotted only for $z < 0$.) However, close to the bubble wall, there is some disagreement between numerical and analytic lepton charge densities. For $|z| \lesssim \sqrt{\tilde{D}\,\tau_{y\tau}} \simeq 2$ GeV, the lepton density has not had enough time to reach chemical equilibrium; here, our analytic approximation is breaking down, as discussed in Chapter 3.

## 7.3 MSSM parameter exploration

In the preceding section, the lepton-mediated scenario dramatically illustrated the novel effects from bottom and tau Yukawa interactions. However, this scenario relied up having $m_{\tilde{t}_R} \simeq m_{\tilde{b}_R}$, so that the quark contribution to $n_L$ would be suppressed. Now we ask: as we deviate away from these parameters, what happens to the baryon asymmetry? In Fig. 7.3,

we show how the baryon asymmetry is affected by increasing $m_{\tilde{b}_R}$, while keeping the right-handed stop mass fixed. There are two pairs of solid and dashed curves; the upper and lower solid curves correspond to our numerical results, with a lightest (mostly right-handed) stau mass $m_{\tilde{\tau}_1} = 1$ TeV and 90 GeV, respectively. The dashed curves are the corresponding analytic results, in good agreement with our numerical curves. As $m_{\tilde{b}_R}$ is increased, the baryon asymmetry is reduced in magnitude and then flips sign. For $m_{\tilde{b}_R} \gg m_{\tilde{t}_R}$, the quark contribution to $n_L$ is no longer suppressed and has opposite sign compared to the lepton contribution; the former overwhelms the latter. The mass of the right-handed tau slepton also plays a minor role; from Eq. (6.36), we see that the lepton contribution to $n_L$ is enhanced slightly when the right-handed stau is light, i.e., not Boltzmann suppressed. Our numerical result neglecting bottom and tau Yukawa interactions is shown by the uppermost, dotted curve.

The favored region of MSSM parameter space for EWB is the so-called "light-stop scenario," where all squarks and sleptons, except the right-handed stop, have TeV-scale masses [46]. In Fig. 7.3, this corresponds to the region where $m_{\tilde{b}_1} = m_{\tilde{\tau}_1} = 1$ TeV. (Increasing these masses further has no impact on EWB; they are effectively decoupled from the plasma.) In this region, the impact of bottom and tau Yukawa couplings is only a factor-of-two. Furthermore, if in addition we take $m_A \to \infty$, then bottom and tau Yukawa interactions will be suppressed; one regains the dotted curve.

## 7.4 Beyond the MSSM

In the MSSM, lepton-mediated EWB can occur only in a small window of parameter space, where

$$m_{\tilde{t}_R} \simeq m_{\tilde{b}_R} \simeq 100 \text{ GeV}. \tag{7.8}$$

Is there a compelling reason to expect that the SUSY-breaking right-handed stop and sbottom masses will conspire to satisfy Eq. (7.8)?

In extensions of the MSSM, lepton-mediated EWB can be much more generic, without fine-tuning between RH stop and sbottom masses — namely, when both species are Boltz-

mann suppressed in the plasma. In Eq. (6.39), we note that the left-handed quark charge vanishes when $k_B \simeq k_T$. For $m_{\tilde{t}_R},\ m_{\tilde{b}_R} \gg T$, we have

$$k_{\tilde{u}_3},\ k_{\tilde{d}_3} \ \rightarrow \ 0 \ , \tag{7.9}$$

and then

$$k_T - k_B \ \simeq \ k_{u_3} - k_{d_3} \ \simeq \ 0 \ , \tag{7.10}$$

since the plasma masses for top and bottom quarks, largely determined by QCD interactions, are approximately equal.

We previously argued that structure of EWB Boltzmann equations, which describe how hypercharge is generated and equilibrated in the plasma, is not modified in the presence of an additional gauge singlet, since the singlet carries no hypercharge. The singlet sector will modify the nature of the phase transition, the properties of the expanding bubbles, and, perhaps, the CP-violating sources. The singlet, however, will not negate the impact of Yukawa interactions. Therefore, it makes sense to decouple these issues: we can study how chemical equilibration might work in the NMSSM by going to larger $m_{\tilde{t}_R}$, assuming that a first-order phase transition is provided by the singlet and carrying the bubble wall parameters and CP-violating sources over from the MSSM.

In Fig. 7.4, we show how the lepton-mediated EWB is the default scenario for $m_{\tilde{t}_R}, m_{\tilde{b}_R} \gg T$. We plot $(n_B/s)$, normalized to $(n_B/s)_{\rm CMB}$ and taking $\phi_2 = \pi/2$, as a function of $\tan\beta$. In each panel, the three curves correspond to zero-temperature stop mass $m_{\tilde{t}_1} = 102$ GeV (solid), 323 GeV (dashed), and 612 GeV (dotted). On the left, we have $m_A = 150$ GeV; on the right, we have $m_A = 1$ TeV. All other squark and slepton masses have been taken to be TeV-scale. Where $(n_B/s)$ is negative, the $n_L$ is quark-dominated; where it is positive, $n_L$ is lepton-dominated. We have taken the CP-violating source to be fixed, despite the fact that we are varying $m_A$:

$$S_{\widetilde{H}}^{\not{CP}} \ \simeq \ -1.0 \ \text{GeV} \ \times \beta'(z)\, v(z)^2 \ , \tag{7.11}$$

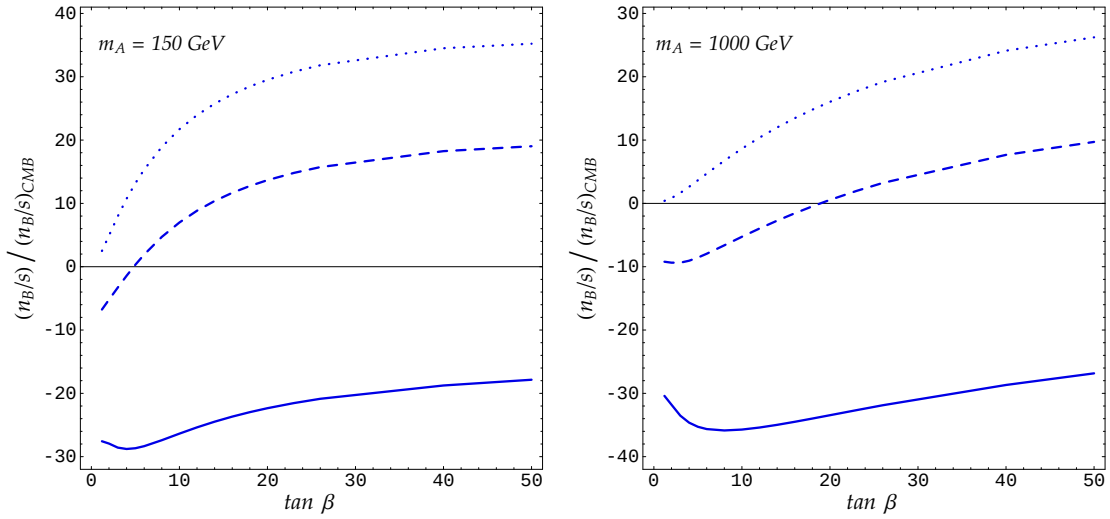


Figure 7.4: Baryon asymmetry $(n_B/s)$, normalized to $(n_B/s)_{\rm CMB}$, for $\sin\phi_1 = \pi/2$, as a function of $\tan\beta$, for $m_A = 150$ (left panel) and $m_A = 1$ TeV. The plotted curves correspond to zero-temperature stop mass $m_{\tilde{t}_1} = 102$ GeV (solid), 323 GeV (dashed), and 612 GeV (dotted), with $m_{\tilde{b}_1} = 1$ TeV. Positive $(n_B/s)$ is lepton-driven, negative $(n_B/s)$ is quark-driven.

with corresponding relaxation rate

$$\Gamma_h(z) \simeq 1.3 \times 10^{-2}\ \text{GeV}^{-1} \times v(z)^2\ . \tag{7.12}$$

All other parameters are the same as before.

The important lesson of Fig. 7.4 is not the overall magnitude of $(n_B/s)$; it is how the $n_B$ transitions from quark-driven to lepton-driven as one increases $m_{\tilde{t}_R}$. First, consider the solid curve in the left-panel, for which $m_{\tilde{t}_R} \simeq 100$ GeV $\ll m_{\tilde{b}_R}$. Here, $n_L$ is dominated by quarks. Increasing $\tan\beta$ suppresses $n_L$ slightly, as $\Gamma_{y\tau}$ turns on, generating some lepton charge that partially cancels the quark-dominated $n_L$. Next, notice the dramatic effect when we increase to $m_{\tilde{t}_R} \simeq 300$ GeV (dashed curve). At small $\tan\beta$, the magnitude of $n_L$ is suppressed in comparison to the previous curve; bottom Yukawa interactions are suppressing the quark contribution to $n_L$ as $(k_T - k_B)$ is decreased. At larger $\tan\beta$, bottom and tau Yukawa interactions become more efficient; the lepton charge density quickly overwhelms the already-suppressed left-handed quark charge. Last, we increase to $m_{\tilde{t}_R} \simeq 600$ GeV

(dotted curve). Even at small $\tan\beta$, bottom Yukawa interactions have completely suppressed the quark charge, since $(k_B - k_T) \simeq 0$. At larger $\tan\beta$, $\Gamma_{y\tau}$ turns on, generating significant lepton density.

In Fig. 7.4, right panel, we repeat this story for $m_A = 1$ TeV. Even at large $m_A$, the same story holds, albeit with a slower turn-on of tau Yukawa interactions with $\tan\beta$. For $m_{\tilde{t}_R}, m_{\tilde{b}_R} \gtrsim 500$ GeV, bottom and tau Yukawa interactions are very important. For small $\tan\beta$, the magnitude of the baryon asymmetry is suppressed because (i) bottom Yukawa interactions have suppressed the quark contribution to $n_L$, since $(k_T - k_B) \simeq 0$, and (ii) tau Yukawa interactions are still too small to generate lepton charge. For moderate $\tan\beta$, the quark charge is still suppressed, but now $\Gamma_{y\tau}$ is large enough to generate leptonic $n_L$. We emphasize that this scenario does not require any fine-tuning, as in Eq. (7.8). All that matters is that both right-handed stop and sbottom are Boltzmann suppressed in the plasma.

# Chapter 8

# Pion Decays and Supersymmetry

## 8.1 Introduction

Low-energy precision tests provide important probes of new physics that are complementary to collider experiments[54, 55, 56]. In particular, effects of weak-scale supersymmetry (SUSY) — one of the most popular extensions of the Standard Model (SM) — can be searched for in a wide variety of low-energy tests: muon $(g-2)$ [119], $\beta$- and $\mu$-decay [57, 58], parity-violating electron scattering [59], electric dipole moment searches [18], and SM-forbidden transitions like $\mu \to e\gamma$ [60], *etc.* (For a recent review, see Ref. [61].) In this chapter, we compute the SUSY contributions to pion leptonic ($\pi_{l2}$) decays and analyze the conditions under which they can be large enough to produce observable effects in the next generation of experiments. This work is somewhat tangential to the preceeding chapters: it is not directly related to the baryon asymmetry, but may provide important handles on parameters (e.g., chargino masses) that govern electroweak baryogenesis.

In particular, we consider the ratio $R_{e/\mu}$, defined by

$$R_{e/\mu} \equiv \frac{\Gamma(\pi^+ \to e^+\nu_e + e^+\nu_e\gamma)}{\Gamma(\pi^+ \to \mu^+\nu_\mu + \mu^+\nu_\mu\gamma)} \,. \tag{8.1}$$

The key advantage of $R_{e/\mu}$ is that a variety of QCD effects that bring large theoretical uncertainties— such as the pion decay constant $F_\pi$ and lepton flavor independent QCD radiative corrections — cancel from this ratio. Indeed, $R_{e/\mu}$ is one of few electroweak

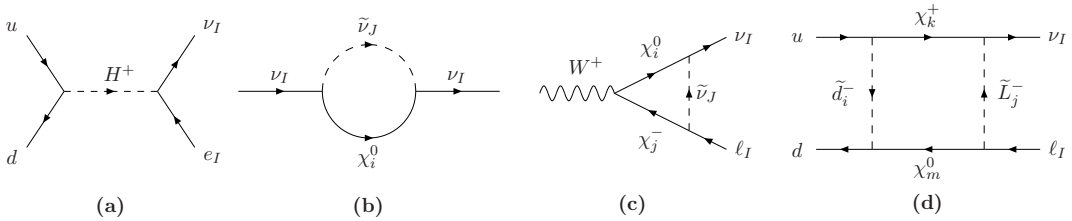


Figure 8.1: *Representative contributions to $\Delta R_{e/\mu}^{SUSY}$: (a) tree-level charged Higgs boson exchange, (b) external leg diagrams, (c) vertex diagrams, (d) box diagrams. Graph (a) contributes to the pseudoscalar amplitude, graphs (b,c) contribute to the axial vector amplitude, and graph (d) contributes to both amplitudes.*

observables that involve hadrons and yet are precisely calculable (see [62] for discussion and Refs. [63, 64] for explicit computations). Moreover, measurements of this quantity provide unique probes of deviations from lepton universality of the charged current (CC) weak interaction in the SM that are induced by loop corrections and possible extensions of the SM. In the present case, we focus on contributions from SUSY that can lead to deviations from lepton universality [74].

The current, state-of-the-art SM computation of $R_{e/\mu}$ is

$$R_{e/\mu}^{SM} = (1.2352 \ \pm \ 0.0001) \times 10^{-4} \, , \tag{8.2}$$

following a recent, improved treatment of hadronic effects through Chiral Perturbation Theory [65, 66].

Experimentally, the most precise measurements of $R_{e/\mu}$ have been obtained at TRIUMF [67] and PSI [68]. Taking the average of these results gives [1]

$$R_{e/\mu}^{EXPT} = (1.230 \ \pm \ 0.004) \times 10^{-4} \, , \tag{8.3}$$

in agreement with the SM. Future experiments at these facilities will make more precise measurements of $R_{e/\mu}$, aiming for precision at the level of $< 1 \times 10^{-3}$ (TRIUMF [69]) and $5 \times 10^{-4}$ (PSI [70]). These projected uncertainties are close to the conservative estimate of theoretical uncertainties given in Ref. [63].

Deviations $\Delta R_{e/\mu}$ from the SM predictions in Eq. (8.2) would signal the presence of

new, lepton flavor-dependent physics. In the Minimal Supersymmetric Standard Model (MSSM), a non-vanishing $\Delta R_{e/\mu}^{SUSY}$ may arise from either tree-level or one-loop corrections. In section 8.2, we consider contributions to $\Delta R_{e/\mu}^{SUSY}$ arising from R-parity conserving interactions (Fig. 8.1). Although tree-level charged Higgs exchange can contribute to the rate $\Gamma[\pi^+ \to \ell^+\nu(\gamma)]$, this correction is flavor-independent and cancels from $R_{e/\mu}$. One-loop corrections induce both scalar and vector semileptonic dimension six four-fermion operators. Such interactions contribute via pseudoscalar and axial vector pion decay amplitudes, respectively. We show that the pseudoscalar contributions are negligible unless the ratio of the up- and down-type Higgs vacuum expectation values (vevs) is huge ($v_u/v_d \equiv \tan\beta \gtrsim 10^3$). For smaller $\tan\beta$ the most important effects arise from one-loop contributions to the axial vector amplitude, which we analyze in detail by performing a numerical scan over MSSM parameter space. We find that experimental observation of SUSY loop-induced deviations at a significant level would require further reductions in both the experimental error and theoretical SM uncertainty. Such improvements could lead to stringent tests of "slepton universality" of the charged current sector of the MSSM, for which it is often assumed that the left-handed first and second generation sleptons $\widetilde{e}_L$ and $\widetilde{\mu}_L$ are degenerate (see e.g. [52] ) and thus $\Delta R_{e/\mu}^{SUSY} \simeq 0$.

In section 8.3, we consider corrections to $R_{e/\mu}$ from R-parity violating (RPV) processes. These corrections enter at tree-level, but are suppressed by couplings whose strength is contrained by other measurements. In order to analyze these constraints, we perform a fit to the current low energy precision observables. We find that, at 95% C.L., the magnitude of RPV contributions to $\Delta R_{e/\mu}^{SUSY}$ could be several times larger than the combined theoretical and anticipated experimental errors for the future $R_{e/\mu}$ experiments. Details regarding the calculation of one-loop corrections are given in Section 8.4. We summarize the main results and provide conclusions in Section 8.5.

## 8.2 R-parity conserving interactions

### 8.2.1 Pseudoscalar contributions

The tree-level amplitude for $\pi^+ \to \ell^+ \nu_\ell$ that arises from the $(V-A)\otimes(V-A)$ four fermion operator is

$$\begin{aligned} i\mathcal{M}^{(0)}_{AV} &= -i2\sqrt{2}\, G_\mu V_{ud} \,\langle 0|\, \bar{d}\gamma^\lambda P_L\, u\,\left|\pi^+\right\rangle\, \overline{u}_\nu \gamma_\lambda P_L\, v_\ell \\ &= 2V_{ud} F_\pi G_\mu m_\ell\, \overline{u}_\nu P_R\, v_\ell\ , \end{aligned} \tag{8.4}$$

where $P_{L,R}$ are the left- and right-handed projection operators,

$$F_\pi = 92.4 \pm 0.07 \pm 0.25 \quad \text{MeV} \tag{8.5}$$

is the pion decay constant, $G_\mu$ is the Fermi constant extracted from the muon lifetime, and $V_{ud}$ is the $(1,1)$ component of the CKM matrix. The first error in Eq. (8.5) is experimental while the second arises from uncertainties associated with QCD effects in the one-loop SM electroweak radiative corrections to the $\pi_{\mu 2}$ decay rate. The superscript "$(0)$" and subscript "$AV$" in Eq. (8.4) denote a tree-level, axial vector contribution. At one-loop order, one must subtract the radiative corrections to the muon-decay amplitude — since $G_\mu$ is obtained from the muon lifetime — while adding the corrections to the semileptonic CC amplitude. The corrections to the muon-decay amplitude as well as lepton flavor-independent contributions to the semileptonic radiative corrections cancel from $R_{e/\mu}$.

Now consider the contribution from an induced pseudoscalar four fermion effective operator of the form

$$\Delta\mathcal{L}_{PS} = -\frac{G_{PS} V_{ud}}{\sqrt{2}}\, \overline{\nu}(1+\gamma^5)\ell\, \bar{d}\gamma^5 u\ . \tag{8.6}$$

Contributions to $R_{e/\mu}$ from operators of this form were considered in a model-independent operator framework in Ref. [71] and in the MSSM in Ref. [72]. In the MSSM, such an operator can arise at tree-level (Fig. 8.1a) through charged Higgs exchange and at one-loop through box graphs (Fig. 8.1d). These amplitudes determine the value of $G_{PS}$. The total

amplitude is

$$i\mathcal{M}_{AV}^{(0)} + i\mathcal{M}_{PS} = V_{ud}F_\pi G_\mu m_\ell\, \overline{u}_\nu(1+\gamma^5)v_\ell \left[1 + \frac{G_{PS}}{G_\mu}\,\omega_\ell\right] \tag{8.7}$$

where

$$\omega_\ell \equiv \frac{m_\pi^2}{m_\ell(m_u+m_d)} \simeq \begin{cases} 5\times 10^3 & \ell = e \\ 20 & \ell = \mu \end{cases} \tag{8.8}$$

is an enhancement factor reflecting the absence of helicity suppression in pseudoscalar contributions as compared to $(V-A)\otimes(V-A)$ contributions [73]. Pseudoscalar contributions will be relevant to the interpretation of $R_{e/\mu}$ if

$$\left|\frac{G_{PS}}{G_\mu}\right|\,\omega_\ell \gtrsim 0.0005\;, \tag{8.9}$$

and if $G_{PS}\,\omega_\ell$ is lepton-flavor dependent.

The tree-level pseudoscalar contribution (Fig. 8.1a) gives

$$G_{PS}^{(0)} = \frac{m_\ell \tan\beta(m_u\cot\beta - m_d\tan\beta)}{\sqrt{2}m_{H^+}^2 v^2}\;, \tag{8.10}$$

where $m_{H^+}$ is the mass of the charged Higgs boson. Thus, we have

$$\frac{G_{PS}^{(0)}}{G_\mu}\,\omega_\ell = \frac{m_\pi^2\tan\beta(m_u\cot\beta - m_d\tan\beta)}{(m_u+m_d)m_{H^+}^2}\;. \tag{8.11}$$

It is indeed possible to satisfy (8.9) for

$$\tan\beta \;\gtrsim\; 20\,\left(\frac{m_{H^+}}{100\text{ GeV}}\right)\;. \tag{8.12}$$

Note that the combination $G_{PS}^{(0)}/G_\mu \times \omega_\ell$ entering Eq. (8.7) is independent of lepton flavor and will cancel from $R_{e/\mu}$. In principle, however, the extraction of $F_\pi$ from $\pi_{\mu 2}$ decay could be affected by tree-level charged Higgs exchange if the correction in Eq. (8.9) is $\gtrsim 0.003$ in magnitude, corresponding to a shift comparable to the theoretical SM uncertainty as estimated in Ref. [63]. In the case of charged Higgs exchange, one would require $\tan\beta \gtrsim$

$120\,(m_{H^+}/100\text{ GeV})$ to generate such an effect.

One-loop contributions to $G_{PS}$ are generated by box graphs (Fig. 8.1d). The magnitude of these contributions is governed by the strength of chiral symmetry breaking in both the quark and lepton sectors. Letting $\epsilon$ generically denote either a Yukawa coupling $y_f$ or a ratio $m_f/M_{SUSY}$ (where $f = e,\ \mu,\ u$, or $d$), we find that

$$\frac{G_{PS}^{(1)}}{G_\mu} \sim \frac{\alpha}{8\pi s_W^2}\left(\frac{m_W}{M_{SUSY}}\right)^2 \epsilon^2\ , \tag{8.13}$$

where the superscript "$(1)$" denotes one loop induced pseudoscalar interaction. We have verified by explicit computation that the $\mathcal{O}(\epsilon)$ contributions vanish. The reason is that in each pair of incoming quarks or outgoing leptons the two fermions must have opposite chirality in order to contribute to $G_{PS}^{(1)}$. Since CC interactions in the MSSM are purely left-handed, the chirality must change at least twice in each graph, with each flip generating a factor of $\epsilon$. For example, we show one pseudoscalar contribution in Fig. 8.2 that is proportional to $\epsilon^2 = y_\mu y_d$. Here, the chirality changes at the $u\widetilde{d}\widetilde{H}$ and $\nu\widetilde{\mu}\widetilde{H}$ vertices. Potentially, this particular contribution can be enhanced for large $\tan\beta$; however, to satisfy (8.9), we need

$$\tan\beta \gtrsim 10^3\left(\frac{M_{SUSY}}{100\text{ GeV}}\right)^3\ . \tag{8.14}$$

These extreme values of $\tan\beta$ can be problematic, leading $y_b$ and $y_\tau$ to become nonperturbatively large. To avoid this scenario, we need roughly $\tan\beta \lesssim 65$ (see [52] and references therein).

Pseudoscalar contributions can also arise through mixing of left- and right-handed scalar superpartners. Since each left-right mixing insertion introduces a factor of $\epsilon$, the leading contributions to $G_{PS}^{(1)}$ will still be $\mathcal{O}(\epsilon^2)$. However, if the triscalar SUSY-breaking parameters $a_f$ are not suppressed by $y_f$ as normally assumed, it is possible to have $\epsilon \sim \mathcal{O}(1)$, potentially leading to significant contributions. This possibility, although not experimentally excluded, is considered theoretically "unnatural" as it requires some fine-tuning to avoid spontaneous color and charge breaking (see Ref. [58] for discussion). Neglecting this possibility and extremely large values of $\tan\beta$, we conclude that loop-induced pseu-

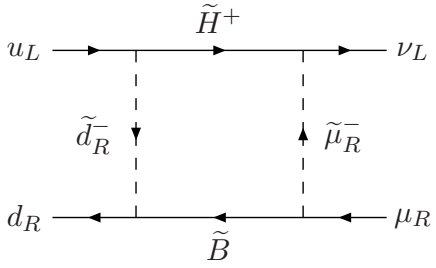


Figure 8.2: *This contribution to $G_{PS}^{(1)}$ is suppressed by $\epsilon^2 = y_\mu y_d$.*

doscalar contributions are much too small to be detected at upcoming experiments. These conclusions are consistent with an earlier, similar analysis in Ref. [72].

### 8.2.2 Axial vector contributions

One-loop radiative corrections also contribute to the axial vector amplitude. The total amplitude can be written as

$$i\mathcal{M}_{AV} = V_{ud} f_\pi G_\mu m_\ell \, \overline{u}_\nu (1+\gamma^5) v_\ell \left[1 + \Delta\hat{r}_\pi - \Delta\hat{r}_\mu\right] \ , \tag{8.15}$$

where $\Delta\hat{r}_\pi$ and $\Delta\hat{r}_\mu$ denote one-loop contributions to the semileptonic and $\mu$-decay amplitudes, respectively and where the hat indicates quantities renormalized in the modified dimensional reduction ($\overline{DR}$) scheme. Since $\Delta\hat{r}_\mu$ cancels from $R_{e/\mu}$, we concentrate on the SUSY contributions to $\Delta\hat{r}_\pi$ that do not cancel from $R_{e/\mu}$. It is helpful to distinguish various classes of contributions

$$\Delta\hat{r}_\pi^{SUSY} = \Delta_L^\ell + \Delta_V^\ell + \Delta_L^q + \Delta_V^q + \Delta_B + \Delta_{GB} \ , \tag{8.16}$$

where $\Delta_L^\ell$ ($\Delta_L^q$), $\Delta_V^\ell$ ($\Delta_V^q$), $\Delta_B$, and $\Delta_{GB}$ denote leptonic (hadronic) external leg (Fig. 8.1b), leptonic (hadronic) vertex (Fig. 8.1c), box graph (Fig. 8.1d), and gauge boson propagator contributions, respectively. The corrections $\Delta_{L,V}^q$ and $\Delta_{GB}$ cancel from $R_{e/\mu}$, so we do not discuss them further (we henceforth omit the "$\ell$" superscript). The explicit general formulae for $\Delta_{L,\,V,\,B}$, calculated in $\overline{DR}$, are given in Section 8.4. We have verified that $\Delta_L$ and $\Delta_V$ agree with Ref. [75] for case of a pure SU(2)$_L$ chargino/neutralino sector.

At face value, it appears from equations (8.37-8.39) that $\Delta R_{e/\mu}^{\rm SUSY}$ carries a non-trivial dependence on MSSM parameters since the SUSY masses enter both explicitly in the loop functions and implicitly in the mixing matrices $Z$, defined in equations (8.32-8.36). Nevertheless, we are able to identify a relatively simple dependence on the SUSY spectrum.

We first consider $\Delta R_{e/\mu}^{SUSY}$ in a limiting case obtained with three simplifying assumptions: (1) no flavor mixing among scalar superpartners; (2) no mixing between left- and right-handed scalar superpartners; and (3) degeneracy between $\widetilde{\ell}_L$ and $\widetilde{\nu}_\ell$ and no gaugino-Higgsino mixing. Our first assumption is well justified; experimental bounds on flavor violating processes constrain the contributions to $R_{e/\mu}$ from lepton flavor violation in the slepton soft-breaking sector to be less than the sensitivies at upcoming experiments by a factor of $10-20$ [72].

Our second assumption has minimal impact. In the absence of flavor mixing, the charged slepton mass matrix decomposes into three $2\times 2$ blocks; thus, for flavor $\ell$, the mass matrix in the $\{\widetilde{\ell}_L, \widetilde{\ell}_R\}$ basis is

$$\begin{pmatrix} M_L^2 + \left(s_W^2 - \frac{1}{2}\right) m_Z^2 \cos 2\beta & m_\ell \left(\frac{a_\ell}{y_\ell} - \mu \tan\beta\right) \\ m_\ell \left(\frac{a_\ell}{y_\ell} - \mu \tan\beta\right) & M_R^2 - s_W^2 m_Z^2 \cos 2\beta \end{pmatrix},$$

where $M_L^2$ ($M_R^2$) is the SUSY-breaking mass parameter for left-handed (right-handed) sleptons, $a_\ell$ is the coefficient for the SUSY-breaking triscalar interaction, $y_\ell$ is the Yukawa coupling, and $\mu$ is the Higgsino mass parameter. Under particular models of SUSY-breaking mediation, it is usually assumed that $a_\ell/y_\ell \sim M_{SUSY}$, and thus left-right mixing is negligible for the first two generations due to the smallness of $m_e$ and $m_\mu$. Of course, $a_\ell$ could be significantly larger and induce significant left-right mixing [58]. For reasons discussed above, we neglect this possibility.

We have adopted the third assumption for purely illustrative purposes; we will relax it shortly. Clearly, fermions of the same weak isospin doublet are not degenerate; their

masses obey

$$m^2_{\tilde{\ell}_L} = m^2_{\tilde{\nu}_\ell} - m^2_W \cos 2\beta + m^2_\ell \tag{8.17}$$

$$m^2_{\tilde{d}_L} = m^2_{\tilde{u}_L} - m^2_W \cos 2\beta + m^2_d - m^2_u \; . \tag{8.18}$$

In addition, gaugino mixing is certainly always present, as the gaugino mass matrices contain off-diagonal elements proportional to $m_Z$ [see Eqs. (8.33, 8.34)]. However, the third assumption becomes valid for $M_{SUSY} \gg m_Z$.

Under our three assumptions, the SUSY vertex and external leg corrections sum to a constant that is independent of the superpartner masses, leading to considerable simplifications. The Bino [U(1)$_Y$ gaugino] vertex and external leg corrections exactly cancel. The Wino [SU(2)$_L$ gaugino] vertex and leg corrections do not cancel; rather, $\Delta_V + \Delta_L = \alpha/4\pi s^2_W$, a constant that carries no dependence on the slepton, gaugino, or Higgsino mass parameters. The occurrence of this constant is merely an artifact of our use of the $\overline{\rm DR}$ renormalization scheme. (In comparison, in modified minimal subtraction, we find $\Delta_V + \Delta_L = 0$ in this same limit.[1]) This dependence on renormalization scheme cancels in $R_{e/\mu}$. (In addition, this scheme-dependent constant enters into the extraction of $G_\mu$; hence, the individual decay widths $\Gamma(\pi \to \ell\nu_\ell)$ are also independent of renormalization scheme.)

The reason for this simplification is that under our assumptions, we have effectively taken a limit that is equivalent to computing the one-loop corrections in the absence of electroweak symmetry breaking. In the limit of unbroken SU(2)$_L \times$U(1)$_Y$, the one-loop SUSY vertex and external leg corrections sum to a universal constant which is renormalization scheme-dependent, but renormalization scale-independent [75]. (For unbroken SU(2)$_L$, the SM vertex and external leg corrections yield an additional logarithmic scale dependence; hence, the SU(2)$_L$ $\beta$-function receives contributions from both charge and wavefunction renormalization.) In addition, virtual Higgsino contributions are negligible, since their interactions are suppressed by small first and second generation Yukawa couplings. Setting all external momenta to zero and working in the limit of unbroken SU(2)$_L$ symmetry, we

[1] Technically, since $\overline{MS}$ breaks SUSY, it is not the preferred renormalization scheme for the MSSM. However, this aspect is not important in the present calculation.

find that the Higgsino contributions to $\Delta_L + \Delta_V$ are $y_\ell^2/32\pi^2$.

In this illustrative limit, the only non-zero contributions to $\Delta R_{e/\mu}^{\rm SUSY}$ come from two classes of box graphs (Fig. 8.1d) — one involving purely Wino-like interactions and the other with both a virtual Wino and Bino. The sum of these graphs is

$$\Delta_B^{(\ell)} = \frac{\alpha}{12\pi s_W^2}\left(\frac{m_W^2}{M_2^2}\right)\left[F_1(x_L, x_Q) + t_W^2 F_2(x_B, x_L, x_Q)\right] \tag{8.19}$$

where we have defined

$$\begin{aligned} F_1(x_L, x_Q) \equiv\ & \frac{3}{2}\left[\frac{x_L(x_L-2)\ln x_L}{(x_L-x_Q)(1-x_L)^2}\right. \\ & \left. + \frac{x_Q(x_Q-2)\ln x_Q}{(x_Q-x_L)(1-x_Q)^2} - \frac{1}{(1-x_L)(1-x_Q)}\right] \end{aligned} \tag{8.20}$$

and

$$\begin{aligned} F_2(x_B, x_L, x_Q) \equiv \frac{1}{2}\ & \left[\frac{x_B(x_B+2\sqrt{x_B})\ln x_B}{(1-x_B)(x_B-x_L)(x_B-x_Q)}\right. \\ & + \frac{x_L(x_L+2\sqrt{x_B})\ln x_L}{(1-x_L)(x_L-x_B)(x_L-x_Q)} \\ & \left. + \frac{x_Q(x_Q+2\sqrt{x_B})\ln x_Q}{(1-x_Q)(x_Q-x_L)(x_Q-x_B)}\right], \end{aligned} \tag{8.21}$$

where $x_B \equiv M_1^2/M_2^2$, $x_L \equiv m_{\tilde{\ell}}^2/M_2^2$, and $x_Q \equiv m_{\widetilde{Q}}^2/M_2^2$, with masses $M_1$, $M_2$, $m_{\tilde{\ell}}$, and $m_{\widetilde{Q}}$ of the Bino, Wino, left-handed $\ell$-flavored slepton, and left-handed 1st generation squark, respectively. Numerically, we find that always $F_1 \gg F_2$; the reason is that the sum of Bino-Wino graphs tend to cancel, while the sum of pure Wino graphs all add coherently. Hence, Bino exchange (through which the term proportional to $F_2$ arises) does not significantly contribute to $\Delta R_{e/\mu}^{\rm SUSY}$.

In Fig. 8.3, we show $F_1(x_L, x_Q)$ as a function of $x_L$ for fixed $x_Q$. Since $F_1$ is symmetric under $x_L \leftrightarrow x_Q$, Fig. 8.3 also shows $F_1$ as a function of $x_Q$, and hence how $\Delta_B$ depends on $m_{\tilde{u}_L}$. For $x_L,\ x_Q \sim 1$, we have $F_1 \sim \mathcal{O}(1)$, while if either $x_L \gg 1$ or $x_Q \gg 1$, then $F_1 \to 0$, which corresponds to the decoupling of heavy sleptons or squarks. There is no enhancement of $\Delta_B$ for $x_L \ll 1$ or $x_Q \ll 1$ (i.e. if $M_2$ is very heavy) due to the overall

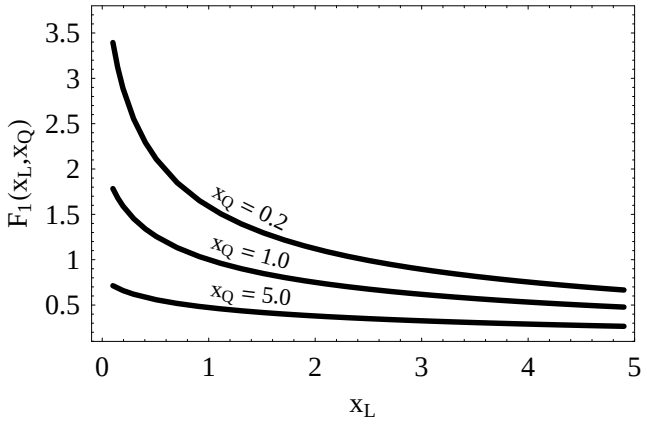


Figure 8.3: *The box graph loop function $F_1(x_L, x_Q)$ as a function of $x_L \equiv m^2_{\widetilde{L}}/M_2^2$ for several values of $x_Q \equiv m^2_{\widetilde{Q}}/M_2^2$. For $x_L \sim x_Q \sim 1$ (i.e. SUSY masses degenerate), $F_1(x_L, x_Q) \sim 1$. For $x_L \gg 1$ or $x_Q \gg 1$ (i.e. very massive sleptons or squarks), $F_1(x_L, x_Q) \to 0$.*

$1/M_2^2$ suppression in (8.19).

The total box graph contribution is

$$\begin{aligned}\frac{\Delta R^{\rm SUSY}_{e/\mu}}{R^{\rm SM}_{e/\mu}} &= 2\,{\rm Re}[\Delta_B^{(e)} - \Delta_B^{(\mu)}] \\ &\simeq \frac{\alpha}{6\pi s_W^2}\left(\frac{m_W}{M_2}\right)^2 \\ &\quad \times \left[F_1\left(\frac{m^2_{\widetilde{e}}}{M_2^2},\ \frac{m^2_{\widetilde{Q}}}{M_2^2}\right) - F_1\left(\frac{m^2_{\widetilde{\mu}}}{M_2^2},\ \frac{m^2_{\widetilde{Q}}}{M_2^2}\right)\right] .\end{aligned} \tag{8.22}$$

Clearly $\Delta R^{\rm SUSY}_{e/\mu}$ vanishes if both sleptons are degenerate and is largest when they are far from degeneracy, such that $m_{\widetilde{e}_L} \gg m_{\widetilde{\mu}_L}$ or $m_{\widetilde{e}_L} \ll m_{\widetilde{\mu}_L}$. In the latter case, we have

$$\left|\frac{\Delta R^{\rm SUSY}_{e/\mu}}{R^{\rm SM}_{e/\mu}}\right| \lesssim 0.001 \times \left(\frac{100\ {\rm GeV}}{M_{SUSY}}\right)^2 \tag{8.23}$$

for e.g. $M_{SUSY} \equiv M_2 \sim m_{\widetilde{u}_L} \sim m_{\widetilde{e}_L} \ll m_{\widetilde{\mu}_L}$.

We now relax our third assumption to allow for gaugino-Higgsino mixing and non-degeneracy of $\widetilde{\ell}$ and $\widetilde{\nu}_\ell$. Both of these effects tend to spoil the universality of $\Delta_V + \Delta_L$, giving

$$\Delta_V + \Delta_L - \frac{\alpha}{4\pi s_W^2} \equiv \frac{\alpha}{8\pi s_W^2}\, f \simeq 0.001\, f\ . \tag{8.24}$$

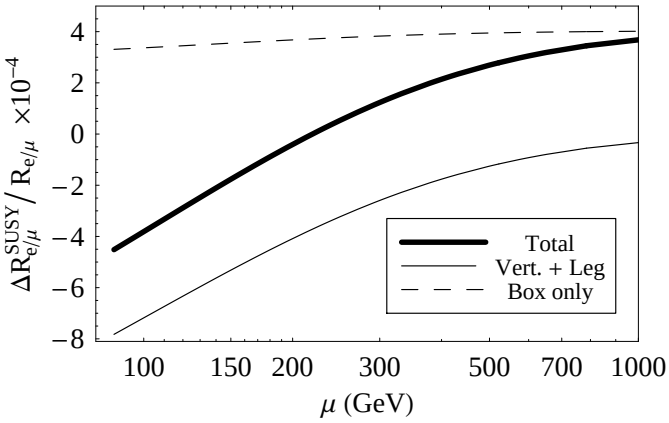


Figure 8.4: $\Delta R^{SUSY}_{e/\mu}$ *versus* $\mu$*, with fixed parameters* $M_1 = 100$ *GeV,* $M_2 = 150$ *GeV,* $m_{\tilde{e}_L} = 100$ *GeV,* $m_{\tilde{\mu}_L} = 500$ *GeV,* $m_{\tilde{u}_L} = 200$ *GeV. Thin solid line denotes contributions from* $(\Delta_V + \Delta_L)$ *only; dashed line denotes contributions from* $\Delta_B$ *only; thick solid line shows the sum of both contributions to* $\Delta R^{SUSY}_{e/\mu}$.

The factor $f$ measures the departure of $\Delta_V + \Delta_L$ from universality. If the SUSY spectrum is such that our third assumption is valid, we expect $f \to 0$ . For realistic values of the SUSY parameters, two effects lead to a non-vanishing $f$: (a) splitting between the masses of the charged and neutral left-handed sleptons that results from breaking of SU(2)$_L$, and (b) gaugino-Higgsino mixing. The former effect is typically negligible. To see why, we recall from Eq. (8.17) that

$$m_{\tilde{\ell}} = m_{\tilde{\nu}_\ell} \left[ 1 + \mathcal{O}\left( \frac{m_W^2}{m_{\tilde{\ell}}^2} \right) \right] , \tag{8.25}$$

where we have neglected the small non-degeneracy proportional to the square of the lepton Yukawa coupling. We find that the leading contribution to $f$ from this non-degeneracy is at least $\mathcal{O}(m_W^4/m_{\tilde{\ell}}^4)$, which is $\lesssim 0.1$ for $m_{\tilde{\ell}} \gtrsim 2m_W$.

Significant gaugino mixing can induce $f \sim \mathcal{O}(1)$. The crucial point is that the size of $f$ from gaugino mixing is governed by the size of $M_2$. If $M_2 \gg m_Z$, then the Wino decouples from the Bino and Higgsino, and contributions to $\Delta_V + \Delta_L$ approach the case of unbroken SU(2)$_L$. On the other hand, if $M_2 \sim m_Z$, then $\Delta_V + \Delta_L$ can differ substantially from $\alpha/4\pi s_W^2$.

In the limit that $m_{\tilde{\ell}_L} \gg M_2$ ($\ell = e, \mu$), we also have a decoupling scenario where $\Delta_B =$

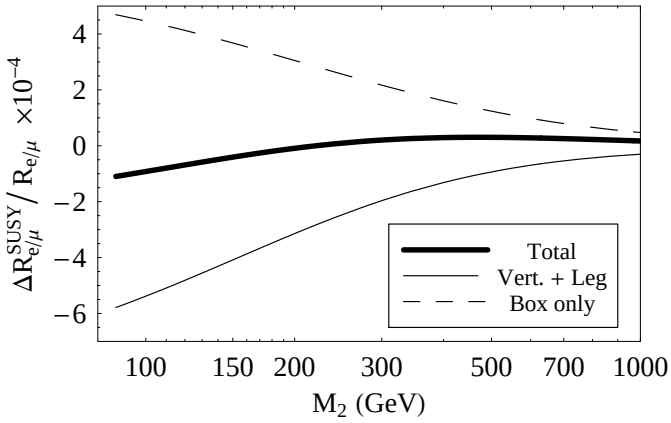


Figure 8.5: $\Delta R^{SUSY}_{e/\mu}/R^{SM}_{e/\mu}$ *as a function of* $M_2$*, with* $\mu = 200$ *GeV and all other parameters fixed as in Fig. 8.4. Each line shows the contribution indicated as in the caption of Fig. 8.4.*

0, $\Delta_V + \Delta_L = \frac{\alpha}{4\pi s_W^2}$, and thus $f = 0$. Hence, a significant contribution to $\Delta R_{e/\mu}$ requires at least one light slepton. However, regardless of the magnitude of $f$, if $m_{\tilde{e}_L} = m_{\tilde{\mu}_L}$, then these corrections will cancel from $R_{e/\mu}$.

It is instructive to consider the dependence of individual contributions $\Delta_B$ and $\Delta_V + \Delta_L$ to $\Delta R^{SUSY}_{e/\mu}$, as shown in Figs. 8.4 and 8.5. In Fig. 8.4, we plot the various contributions as a function of the supersymmetric mass parameter $\mu$, with $M_1 = 100$ GeV, $M_2 = 150$ GeV, $m_{\tilde{e}_L} = 100$ GeV, $m_{\tilde{\mu}_L} = 500$ GeV, $m_{\tilde{u}_L} = 200$ GeV. We see that the $\Delta_V + \Delta_L$ contributions (thin solid line) vanish for large $\mu$, since in this regime gaugino-Higgsino mixing is suppressed and there is no $\Delta_V + \Delta_L$ contribution to $\Delta R^{SUSY}_{e/\mu}$. However, the $\Delta_B$ contribution (dashed line) is nearly $\mu$-independent, since box graphs with Higgsino exchange (which depend on $\mu$) are suppressed in comparison to those with only gaugino exchange. In Fig. 8.5, we plot these contributions as a function of $M_2$, with $\mu = 200$ GeV and all other parameters fixed as above. We see that both $\Delta_V + \Delta_L$ and $\Delta_B$ contributions vanish for large $M_2$.

One general feature observed from these plots is that $\Delta_V + \Delta_L$ and $\Delta_B$ contributions tend to cancel one another; therefore, the largest total contribution to $\Delta R^{SUSY}_{e/\mu}$ occurs when either $\Delta_V + \Delta_L$ or $\Delta_B$ is suppressed in comparison to the other. This can occur in the following ways: (1) if $\mu \gg m_Z$, then $\Delta_B$ may be large, while $\Delta_V + \Delta_L$ is suppressed, and (2) if $m_{\tilde{u}_L},\ m_{\tilde{d}_L} \gg m_Z$, then $\Delta_V + \Delta_L$ may be large, while $\Delta_B$ is suppressed. In Fig. 8.5,

we have chosen parameters for which there is a large cancellation between $\Delta_V + \Delta_L$ and $\Delta_B$. However, by taking the limits $\mu \to \infty$ or $m_{\widetilde{u}_L},\ m_{\widetilde{d}_L} \to \infty$, $\Delta R_{e/\mu}^{SUSY}$ would coincide with the $\Delta_B$ or $\Delta_V + \Delta_L$ contributions, respectively.

Because the $\Delta_V + \Delta_L$ and $\Delta_B$ contributions tend to cancel, it is impossible to determine whether $\widetilde{e}_L$ or $\widetilde{\mu}_L$ is heavier from $R_{e/\mu}$ measurements alone. For example, a positive deviation in $R_{e/\mu}$ can result from two scenarios: (1) $\Delta R_{e/\mu}^{SUSY}$ is dominated by box graph contributions with $m_{\widetilde{e}_L} < m_{\widetilde{\mu}_L}$, or (2) $\Delta R_{e/\mu}^{SUSY}$ is dominated by $\Delta_V + \Delta_L$ contributions with $m_{\widetilde{e}_L} > m_{\widetilde{\mu}_L}$.

Guided by the preceding analysis, we expect for $\Delta R_{e/\mu}^{SUSY}$:

- The maximum contribution is $\left|\Delta R_{e/\mu}^{SUSY}/R_{e/\mu}\right| \sim 0.001$.
- Both the vertex + leg and box contributions are largest if $M_2 \sim \mathcal{O}(m_Z)$ and vanish if $M_2 \gg m_Z$. If $M_2 \sim \mathcal{O}(m_Z)$, then at least one chargino must be light.
- The contributions to $\Delta R_{e/\mu}^{SUSY}$ vanish if $m_{\widetilde{e}_L} = m_{\widetilde{\mu}_L}$ and are largest if either $m_{\widetilde{\mu}_L} \ll m_{\widetilde{e}_L}$ or $m_{\widetilde{\mu}_L} \gg m_{\widetilde{e}_L}$.
- The contributions to $\Delta R_{e/\mu}^{SUSY}$ are largest if $\widetilde{e}_L$ or $\widetilde{\mu}_L$ is $\mathcal{O}(m_Z)$.
- If $\mu \gg m_Z$, then the lack of gaugino-Higgsino mixing suppresses the $\Delta_V + \Delta_L$ contributions to $\Delta R_{e/\mu}^{SUSY}$.
- If $m_{\widetilde{u}_L},\ m_{\widetilde{d}_L} \gg m_Z$, then the $\Delta_B$ contributions to $\Delta R_{e/\mu}^{SUSY}$ are suppressed due to squark decoupling.
- If $\widetilde{u}_L$, $\widetilde{d}_L$, and $\mu$ are all $\mathcal{O}(m_Z)$, then there may be cancellations between the $\Delta_V + \Delta_L$ and $\Delta_B$ contributions. $\Delta R_{e/\mu}^{SUSY}$ is largest if it is dominated by *either* $\Delta_V + \Delta_L$ *or* $\Delta_B$ contributions.

We now study $\Delta R_{e/\mu}^{SUSY}$ quantitatively by making a numerical scan over MSSM param-

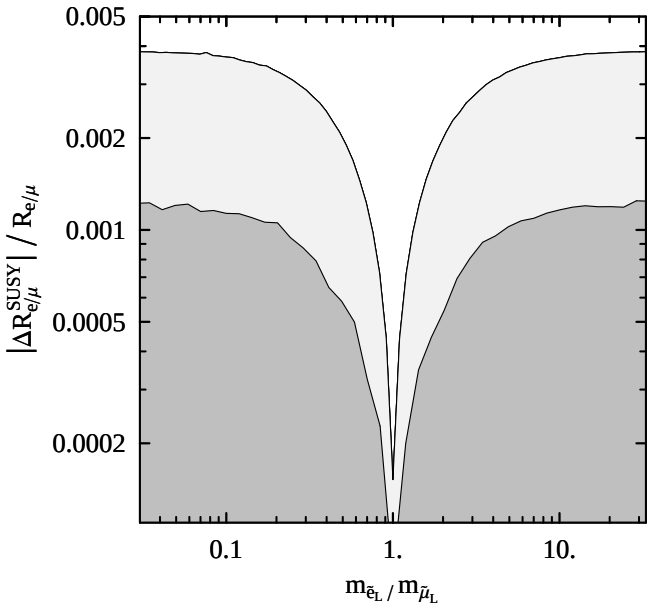


Figure 8.6: $\Delta R^{SUSY}_{e/\mu}$ *as a function of the ratio* $m_{\tilde{e}_L}/m_{\tilde{\mu}_L}$. *The dark and light regions denote the regions of MSSM parameter space consistent and inconsistent, respectively, with the LEP II bound.*

eter space, using the following ranges:

$$\begin{aligned} m_Z/2 \;<\; \{M_1,\; |M_2|, |\mu|,\; m_{\tilde{u}_L}\} \;<\; 1 \text{ TeV} \\ m_Z/2 \;<\; \{m_{\tilde{\nu}_e}, m_{\tilde{\nu}_\mu}\} \;<\; 5 \text{ TeV} \\ 1 \;<\; \tan\beta \;<\; 50 \\ \text{sign}(\mu),\; \text{sign}(M_2) = \pm 1 \;, \end{aligned} \tag{8.26}$$

where $m_{\tilde{e}_L}$, $m_{\tilde{\mu}_L}$, and $m_{\tilde{d}_L}$ are determined from Eqs. (8.17,8.18).

Direct collider searches impose some constraints on the parameter space. Although the detailed nature of these constraints depends on the adoption of various assumptions and on interdependencies on the nature of the MSSM and its spectrum [1], we implement them in a coarse way in order to identify the general trends in corrections to $R_{e/\mu}$. First, we include only parameter points in which there are no SUSY masses lighter than $m_Z/2$. (However, the current bound on the mass of lightest neutralino is even weaker than this.) Second, parameter points which have no charged SUSY particles lighter than 103 GeV are

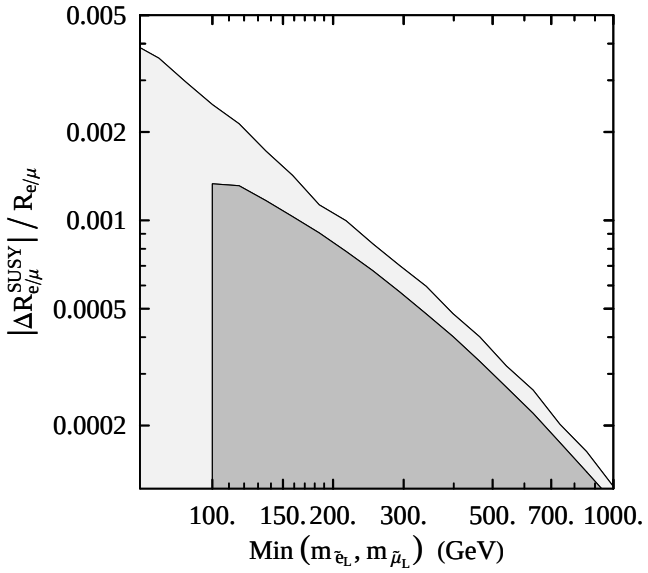


Figure 8.7: $\Delta R^{SUSY}_{e/\mu}$ *as a function of Min[*$m_{\tilde{e}_L}$, $m_{\tilde{\mu}_L}$*], the mass of the lightest first or second generation charged slepton. The dark and light regions denote the regions of MSSM parameter space consistent and inconsistent, respectively, with the LEP II bound.*

said to satisfy the "LEP II bound." (This bound may also be weaker in particular regions of parameter space.)

Additional constraints arise from precision electroweak data. We consider only MSSM parameter points whose contributions to the oblique parameters $S$, $T$, and $U$ [76] agree with electroweak precision observables (EWPO). A recent fit to both high- and low-energy EWPO using the value of $m_t = 170.9 \pm 1.8$ GeV [77] has been reported in Ref. [78], yielding

$$\begin{aligned} T &= -0.111 \pm 0.109 \\ S &= -0.126 \pm 0.096 \\ U &= 0.164 \pm 0.115 \end{aligned} \tag{8.27}$$

where the errors quoted are one standard deviation and where the value of the Standard Model Higgs boson mass has been set to the LEP lower bound $m_h = 114.4$ GeV. Using the correlation matrix given in Ref. [78] and the computation of superpartner contributions

to the oblique parameters reported in Ref. [59], we determine the points in the MSSM parameter space that are consistent with EWPO at 95% confidence. Because we have neglected the 3rd generation and right-handed scalar sectors in our analysis and parameter scan, we do not calculate the entire MSSM contributions to $S$, $T$, and $U$. Rather, we only include those from charginos, neutralinos, and the first two generation left-handed scalar superpartners. Although incomplete, this serves as a conservative lower bound; in general, the contributions to $S$, $T$, and $U$ from the remaining scalar superpartners (that we neglect) only causes further deviations from the measured values of the oblique parameters. In addition, we have assumed that the lightest CP-even Higgs mass is the same as the SM Higgs mass reference point: $m_h = 114.4$ GeV, neglecting the corrections due to the small mass difference, and the typically small contributions from the remaining heavier Higgs bosons.

We do not impose other electroweak constraints in the present study, but note that they will generally lead to further restrictions. For example, the results of the E821 measurement of the muon anomalous magnetic moment [79] tend to favor a positive sign for the $\mu$ parameter and relatively large values of $\tan\beta$. Eliminating the points with $\text{sign}(\mu) = -1$ will exclude half the parameter space in our scan, but the general trends are unaffected.

We show the results of our numerical scan in Figs. 8.6–8.9. In Figs. 8.6–8.8, the dark regions contain all MSSM parameter points within our scan consistent with the LEP II bound, while the light regions contain all MSSM points inconsistent with the LEP II bound, but with no superpartners lighter than $m_Z/2$. In effect, the dark (light) regions show how large $\Delta R_{e/\mu}^{SUSY}/R_{e/\mu}$ can be, assuming consistency (inconsistency) with the LEP II bound, as a function of a given parameter. In Fig. 8.6, we show $\Delta R_{e/\mu}^{SUSY}/R_{e/\mu}$ as a function of the ratio of slepton masses $m_{\widetilde{e}_L}/m_{\widetilde{\mu}_L}$. If both sleptons are degenerate, then $\Delta R_{e/\mu}^{SUSY}$ vanishes. Assuming the LEP II bound, in order for a deviation in $R_{e/\mu}$ to match the target precision at upcoming experiments, we must have

$$\delta R_{e/\mu} \equiv \left|\Delta R_{e/\mu}^{SUSY}/R_{e/\mu}\right| \gtrsim 0.0005 \,, \tag{8.28}$$

and thus $m_{\widetilde{e}_L}/m_{\widetilde{\mu}_L} \gtrsim 2$ or $m_{\widetilde{\mu}_L}/m_{\widetilde{e}_L} \gtrsim 2$. (This result is consistent with an earlier anal-

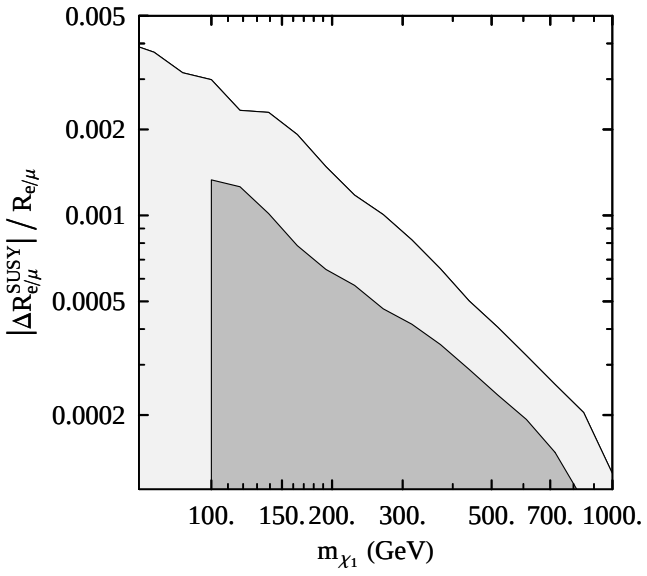


Figure 8.8: $\Delta R^{SUSY}_{e/\mu}$ *versus* $m_{\chi 1}$*, the mass of the lightest chargino. The dark and light regions denote the regions of MSSM parameter space consistent and inconsistent, respectively, with the LEP II bound.*

ysis [72], where the authors conclude that $\Delta R^{SUSY}_{e/\mu}$ would be unobservably small if $m_{e_L}$ and $m_{\mu_L}$ differ by less than 10%.)

In Fig. 8.7, we show $\Delta R^{SUSY}_{e/\mu}/R_{e/\mu}$ as a function of Min[$m_{\tilde{e}_L}$, $m_{\tilde{\mu}_L}$], the mass lightest first or second generation slepton. If the lighter slepton is extremely heavy, then both heavy sleptons decouple, causing $\Delta R^{SUSY}_{e/\mu}$ to vanish. Assuming the LEP II bound, to satisfy (8.28), we must have $m_{\tilde{e}_L} \lesssim 300$ GeV or $m_{\tilde{\mu}_L} \lesssim 300$ GeV.

In Fig. 8.8, we show $\Delta R^{SUSY}_{e/\mu}/R_{e/\mu}$ as a function of $m_{\chi 1}$, the lightest chargino mass. If $m_{\chi 1}$ is large, $\Delta R^{SUSY}_{e/\mu}$ vanishes because $M_2$ must be large as well, suppressing $\Delta_B$ and forcing $\Delta_V$ and $\Delta_L$ to sum to the flavor independent constant discussed above. Assuming the LEP II bound, to satisfy (8.28), we must have $m_{\chi 1} \lesssim 250$ GeV.

Finally, we illustrate the interplay between $\Delta_V + \Delta_L$ and $\Delta_B$ by considering $\delta R^{SUSY}_{e/\mu}$ as a function of $|\mu|$ and $m_{\tilde{u}_L}$. In Fig. 8.9, we show the largest values of $\delta R^{SUSY}_{e/\mu}$ obtained in our numerical parameter scan, restricting to parameter points which satisfy the LEP II bound. The solid shaded areas correspond to regions of the $|\mu|$-$m_{\tilde{u}_L}$ plane where the largest value of $\delta R^{SUSY}_{e/\mu}$ lies within the indicated ranges. It is clear that $\delta R^{SUSY}_{e/\mu}$ can be largest

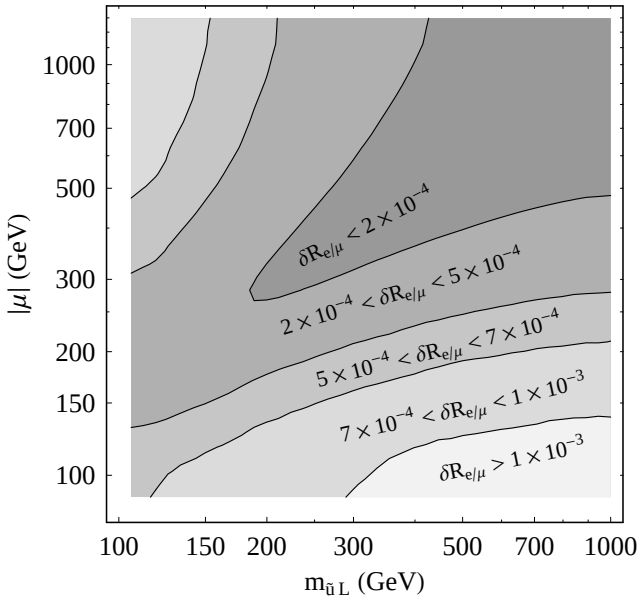


Figure 8.9: *Contours indicate the largest values of $\delta R_{e/\mu}^{SUSY}$ obtained by our numerical parameter scan (8.26), as a function of $|\mu|$ and $m_{\tilde{u}_L}$. The solid shaded regions correspond to the largest values of $\delta R_{e/\mu}^{SUSY}$ within the ranges indicated. All values of $\delta R_{e/\mu}^{SUSY}$ correspond to parameter points which satisfy the LEP II bound.*

in the regions where either (1) $\mu$ is small, $m_{\tilde{u}_L}$ is large, and the largest contributions to $\Delta R_{e/\mu}^{SUSY}$ are from $\Delta_V + \Delta_L$, or (2) $\mu$ is large, $m_{\tilde{u}_L}$ is small, and the largest contribution to $\Delta R_{e/\mu}^{SUSY}$ is from $\Delta_B$. If both $\mu$ and $m_{\tilde{u}_L}$ are light, then $\Delta R_{e/\mu}^{SUSY}$ can still be very small due to cancellations, even though both $\Delta_V + \Delta_L$ and $\Delta_B$ contributions are large individually. More precisely, to satisfy (8.28), we need either $\mu \lesssim 250$ GeV, or $\mu \gtrsim 300$ GeV and $m_{\tilde{u}_L} \lesssim 200$ GeV.

## 8.3 Contributions from R-parity Violating Processes

In the presence of RPV interactions, tree-level exchanges of sfermions (shown in Fig. 8.10), lead to violations of lepton universality and non-vanishing effects in $R_{e/\mu}$. The magnitude of these tree-level contributions is governed by both the sfermion masses and by the pa-

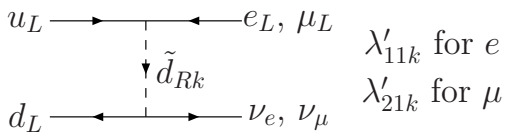


Figure 8.10: Tree-level RPV contributions to $R_{e/\mu}$.

rameters $\lambda'_{11k}$ and $\lambda'_{21k}$ that are the coefficients in RPV interactions:

$$\mathcal{L}_{RPV,\ \Delta L=1} = \lambda'_{ijk} L_i Q_j \tilde{\bar{d}}^{\dagger}_k + \ldots \tag{8.29}$$

Defining [81, 82]

$$\Delta'_{ijk}(\tilde{f}) = \frac{|\lambda'_{ijk}|^2}{4\sqrt{2} G_\mu m^2_{\tilde{f}}} \geq 0, \tag{8.30}$$

contributions to $R_{e/\mu}$ from RPV interactions are

$$\frac{\Delta R^{RPV}_{e/\mu}}{R^{SM}_{e/\mu}} = 2\Delta'_{11k} - 2\Delta'_{21k}. \tag{8.31}$$

Note that RPV contribution to the muon lifetime (and, thus, the Fermi constant $G_\mu$) cancels in $R_{e/\mu}$, therefore does not enter the expression.

The quantities $\Delta'_{ijk}$ *etc.* are constrained by existing precision measurements and rare decays. A summary of the low energy constraints is given in Table III of Ref. [61], which includes tests of CKM unitarity (primarily through RPV effects in superallowed nuclear $\beta$-decay that yields a precise value of $|V_{ud}|$ [80]), atomic parity violating (PV) measurements of the cesium weak charge $Q^{\rm Cs}_W$ [83], the ratio $R_{e/\mu}$ itself [67, 68], a comparison of the Fermi constant $G_\mu$ with the appropriate combination of $\alpha$, $m_Z$, and $\sin^2\theta_W$ [84], and the electron weak charge determined from SLAC E158 measurement of parity violating Møller scattering[85].

In Fig. 8.11 we show the present 95% C.L. constraints on the quantities $\Delta'_{11k}$ and $\Delta'_{21k}$ obtained from the aforementioned observables (interior of the blue curve). Since the $\Delta'_{ijk}$ are positive semidefinite quantities, only the region of the contour in the upper right hand quadrant are shown. The green curve indicates the possible implication of a future mea-

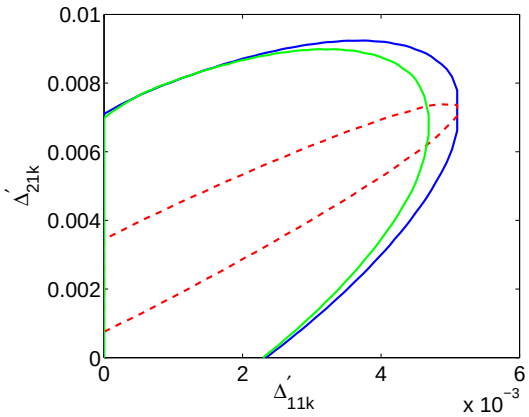


Figure 8.11: Present 95% C.L. constraints on RPV parameters $\Delta'_{j1k}$, $j = 1, 2$ that enter $R_{e/\mu}$ obtained from a fit to precision electroweak observables. Interior of the dark blue contour corresponds to the fit using the current value of $\Delta R_{e/\mu}/R^{SM}_{e/\mu}$ [67, 68], while the dashed red contour corresponds to the fit using the future expected experimental precision [69], assuming the same central value. The light green curve indicates prospective impact of a future measurement of the proton weak charge at Jefferson Lab [86].

surement of the proton weak charge planned at Jefferson Lab [86], assuming agreement with the Standard Model prediction for this quantity and the anticipated experimental uncertainty. The dashed red curve shows the possible impact of future measurements of $R_{e/\mu}$, assuming agreement with the present central value but an overall error reduced to the level anticipated in Ref. [69]; with the error anticipated in Ref. [70] the width of the band would be a factor of two smaller than shown.

Two general observations emerge from Fig. 8.11. First, given the present constraints, values of $\Delta'_{21k}$ and $\Delta'_{11k}$ differing substantially from zero are allowed. For values of these quantities inside the blue contour, $\Delta R^{SUSY}_{e/\mu}$ could differ from zero by up to five standard deviations for the error anticipated in Ref. [69]. Such RPV effects could, thus, be considerably larger than the SUSY loop corrections discussed above. On the other hand, agreement of $R_{e/\mu}$ with the SM would lead to considerable tightening of the constraints on this scenario, particularly in the case of $\Delta'_{21k}$, which is currently constrained only by $R_{e/\mu}$ and deep inelastic $\nu$ ($\bar{\nu}$) scattering [87].

The presence of RPV interactions would have significant implications for both neutrino physics and cosmology. It has long been known, for example, that the existence of

$\Delta L = \pm 1$ interactions — such as those that could enter $R_{e/\mu}$ — will induce a Majorana neutrino mass [88], while the presence of non-vanishing RPV couplings would imply that the lightest supersymmetric particle is unstable and, therefore, not a viable candidate for cold dark matter. The future measurements of $R_{e/\mu}$ could lead to substantially tighter constraints on these possibilities or uncover a possible indication of RPV effects. In addition, we note that the present uncertainty associated with RPV effects entering the $\pi_{\mu 2}$ decay rate would affect the value of $F_\pi$ at a level about half the theoretical SM uncertainty as estimated by Ref. [63].

## 8.4 General Radiative Corrections in the MSSM

In this section, we present the complete formulae for the R-parity conserving vertex, external leg, and box graphs. The reader that wishes to avoid these technicalities is advised to move to our conclusions in Section 8.5.

The MSSM Lagrangian and Feynman rules [89] are expressed in terms of chargino and neutralino mixing matrices $Z_\pm$ and $Z_N$, respectively, which diagonalize the superpartner mass matrices, defined as follows. The four neutralino mass eigenstates $\chi_i^0$ are related to the gauge eigenstates $\psi^0 \equiv (\widetilde{B}, \widetilde{W}^3, \widetilde{H}_d^0, \widetilde{H}_u^0)$ by

$$\psi_i^0 = Z_N^{ij}\, \chi_j^0 \,, \tag{8.32}$$

where

$$Z_N^T \begin{pmatrix} M_1 & 0 & -c_\beta\, s_W m_Z & s_\beta\, s_W m_Z \\ 0 & M_2 & c_\beta\, c_W m_Z & -s_\beta\, c_W m_Z \\ -c_\beta\, s_W m_Z & c_\beta\, c_W m_Z & 0 & -\mu \\ s_\beta\, s_W m_Z & -s_\beta\, c_W m_Z & -\mu & 0 \end{pmatrix} Z_N = \begin{pmatrix} m_{\chi_1} & & 0 \\ & \ddots & \\ 0 & & m_{\chi_4} \end{pmatrix}$$

is the diagonalized neutralino mass matrix. The chargino mass eigenstates $\chi_i^\pm$ are related

to the gauge eigenstates $\psi^+ \equiv (\widetilde{W}^+, \widetilde{H}_u^+)$ and $\psi^- \equiv (\widetilde{W}^-, \widetilde{H}_d^-)$ by

$$\psi_i^\pm = Z_\pm^{ij}\, \chi_j^\pm \ , \tag{8.33}$$

where

$$Z_-^T \begin{pmatrix} M_2 & \sqrt{2}s_\beta m_W \\ \sqrt{2}c_\beta m_W & \mu \end{pmatrix} Z_+ = \begin{pmatrix} m_{\chi_1} & 0 \\ 0 & m_{\chi_2} \end{pmatrix} \tag{8.34}$$

is the diagonalized chargino mass matrix. We note that the off-diagonal elements which mix gauginos and Higgsinos stem solely from electroweak symmetry breaking.

The charged slepton mass eigenstates $\widetilde{L}_i$ are related to the gauge eigenstates $\widetilde{\ell} \equiv (\widetilde{e}_L, \widetilde{\mu}_L, \widetilde{\tau}_L, \widetilde{e}_R, \widetilde{\mu}_R, \widetilde{\tau}_R)$ by

$$\widetilde{\ell}_i = Z_L^{ij}\, \widetilde{L}_j \ , \tag{8.35}$$

where

$$Z_L^\dagger\, \mathbf{M}_{\widetilde{\ell}}^{\mathbf{2}}\, Z_L = \begin{pmatrix} m^2_{\widetilde{L}_1} & & 0 \\ & \ddots & \\ 0 & & m^2_{\widetilde{L}_6} \end{pmatrix} \tag{8.36}$$

is the diagonalized slepton mass matrix. There are two classes of off-diagonal elements in $\mathbf{M}_{\widetilde{\ell}}^{\mathbf{2}}$ which can contribute to slepton mixing: mixing between flavors and mixing between left- and right-handed components of a given flavor, both of which arise through SUSY-breaking terms. (Left-right mixing due to SUSY-preserving terms will be suppressed by $m_\ell / m_{\widetilde{\ell}}$ and is irrelevant for the first two generations.)

Similarly, up-type squarks, down-type squarks, and sneutrinos have mixing matrices $Z_U$, $Z_D$, and $Z_\nu$, respectively, defined identically to $Z_L$ — except for the fact that there are no right-handed sneutrinos in the MSSM and thus there are only three sneutrino mass eigenstates.

There are three types of contributions to $\Delta R_{e/\mu}^{SUSY}$ in the MSSM: external leg, vertex,

and box graph radiative corrections. The leptonic external leg corrections (Fig. 8.1b) are

$$\Delta_L^{(i)} = -\frac{\alpha}{16\pi s_W^2}\Big( \; |Z_N^{1j} t_W - Z_N^{2j}|^2 \; B(m_{\chi_j^0}, m_{\tilde{\nu}_i}) + \; 2\,|Z_-^{1k}|^2 \; B(m_{\chi_k}, m_{\tilde{L}_i}) \qquad (8.37)$$
$$+ \; |Z_N^{1j} t_W + Z_N^{2j}|^2 \; B(m_{\chi_j^0}, m_{\tilde{L}_i}) + \; 2\,|Z_+^{1k}|^2 \; B(m_{\chi_k}, m_{\tilde{\nu}_i}) \; \Big) \; ,$$

where the loop function is [91]

$$B(m_1, m_2) = \int_0^1 dx\; x \; \ln\left(\frac{M^2}{m_1^2(1-x) + m_2^2 x}\right) \; .$$

The leptonic vertex corrections (Fig. 8.1c) are

$$\Delta_V^{(I)} = \frac{\alpha}{8\pi s_W^2}\Big( \; (Z_N^{1j} t_W + Z_N^{2j})\,(Z_N^{1j*} t_W - Z_N^{2j*})\; C_2(m_{\tilde{\nu}_i}, m_{\chi_j^0}, m_{\tilde{L}_i}) \qquad (8.38)$$
$$+ 2\,(Z_N^{2j*} - t_W\; Z_N^{1j*})\; Z_+^{1k} \; \Big[ \; (Z_N^{2j} Z_+^{1k} - \frac{1}{\sqrt{2}} Z_N^{4j} Z_+^{2k})\; C_2(m_{\chi_j^0}, m_{\tilde{\nu}_i}, m_{\chi_k})$$
$$+ \; (Z_N^{2j*} Z_-^{1k} + \frac{1}{\sqrt{2}} Z_N^{3j*} Z_-^{2k}) \;\; m_{\chi_j^0} m_{\chi_k} \; C_1(m_{\chi_j^0}, m_{\tilde{\nu}_i}, m_{\chi_k}) \; \Big]$$
$$+ 2\,(Z_N^{2j} + t_W\; Z_N^{1j})\; Z_-^{1k} \; \Big[ \; (Z_N^{2j*} Z_-^{1k} + \frac{1}{\sqrt{2}} Z_N^{3j*} Z_-^{2k})\; C_2(m_{\chi_k}, m_{\tilde{L}_i}, m_{\chi_j^0})$$
$$+ \; (Z_N^{2j} Z_+^{1k} - \frac{1}{\sqrt{2}} Z_N^{4j} Z_+^{2k}) \;\; m_{\chi_j^0} m_{\chi_k} \; C_1(m_{\chi_k}, m_{\tilde{L}_i}, m_{\chi_j^0}) \; \Big] \; \Big) \; ,$$

with loop functions

$$C_1(m_1, m_2, m_3) = \int_0^1 dx\; dy\; \frac{1}{m_1^2 x + m_2^2 y + m_3^2(1-x-y)}$$
$$C_2(m_1, m_2, m_3) = \int_0^1 dx\; dy\; \ln\left(\frac{M^2}{m_1^2 x + m_2^2 y + m_3^2(1-x-y)}\right) \; .$$

The corrections from box graphs (Fig. 8.1d) are

$$\Delta_B^{(I)} = \frac{\alpha m_W^2}{8\pi s_W^2} \times \tag{8.39}$$
$$\Big( \; |Z_-^{1k}|^2 \; (Z_N^{2m*} + t_W Z_N^{1m*}) \; (Z_N^{2m} - \frac{1}{3} t_W Z_N^{1m}) \;\; D_1(m_{\chi_m^0}, m_{\tilde{d}_L}, m_{\chi_k}, m_{\tilde{L}_i})$$
$$+ \; |Z_+^{1j}|^2 \; (Z_N^{2m} - t_W Z_N^{1m}) \; (Z_N^{2m*} + \frac{1}{3} t_W Z_N^{1m*}) \; D_1(m_{\chi_j}, m_{\tilde{u}_L}, m_{\chi_m^0}, m_{\tilde{\nu}_i})$$
$$+ \; Z_-^{1j} Z_+^{1j} \; (Z_N^{2m} - t_W Z_N^{1m}) \; (Z_N^{2m} - \frac{1}{3} t_W Z_N^{1m}) \; m_{\chi_m^0} m_{\chi_j} \; D_2(m_{\chi_m^0}, m_{\tilde{d}_L}, m_{\chi_j}, m_{\tilde{\nu}_i})$$
$$+ \; Z_-^{1k} Z_+^{1k} \; (Z_N^{2m*} + t_W Z_N^{1m*}) \; (Z_N^{2m*} + \frac{1}{3} t_W Z_N^{1m*})$$
$$\times \; m_{\chi_m^0} m_{\chi_k} \; D_2(m_{\chi_k}, m_{\tilde{u}_L}, m_{\chi_m^0}, m_{\tilde{L}_i}) \; \Big) \; ,$$

with loop functions

$$D_n(m_1, m_2, m_3, m_4) = \int_0^1 dx \, dy \, dz \; \frac{1}{[m_1^2 x + m_2^2 y + m_3^2 z + m_4^2 (1 - x - y - z)]^n} \; .$$

In formulae (8.37-8.39), $I = 1$ corresponds to $\pi \to e \, \nu_e$ and $I = 2$ corresponds to $\pi \to \mu \, \nu_\mu$. All other indeces are summed over. We use $\overline{\rm DR}$ renormalization at scale $M$. We have defined $t_W \equiv \tan\theta_W$ and $s_W \equiv \sin\theta_W$. We have neglected terms proportional to either Yukawa couplings or external momenta (which will be suppressed by $\mathcal{O}(m_\pi / M_{SUSY})$). Finally, the SUSY contribution to $R_{e/\mu}$ is

$$\frac{\Delta R_{e/\mu}^{\rm SUSY}}{R_{e/\mu}} = 2 \; {\rm Re}[\Delta_V^{(1)} - \Delta_V^{(2)} + \Delta_L^{(1)} - \Delta_L^{(2)} + \Delta_B^{(1)} - \Delta_B^{(2)}] \; . \tag{8.40}$$

In addition, the following are some useful formulae needed to show the cancellations of vertex and leg corrections in the limit of no superpartner mixing:

$$C_2(m_1, m_2, m_1) = B(m_2, m_1)$$
$$2 m_1^2 \, C_1(m_1, m_2, m_1) - 2 \, B(m_1, m_2) + 2 \, B(m_2, m_1) = 1 \; .$$

## 8.5 Conclusions

Given the prospect of two new studies of lepton universality in $\pi_{\ell 2}$ decays [69, 70] with experimental errors that are substantially smaller than for existing measurements and possibly approaching the $5 \times 10^{-4}$ level, an analysis of the possible implications for supersymmetry is a timely exercise. In this study, we have considered SUSY effects on the ratio $R_{e/\mu}$ in the MSSM both with and without R-parity violation. Our results indicate that in the R-parity conserving case, effects from SUSY loops can be of order the planned experimental error in particular, limited regions of the MSSM parameter space. Specifically, we find that a deviation in $R_{e/\mu}$ due to the MSSM at the level of

$$0.0005 \lesssim \left| \frac{\Delta R_{e/\mu}^{SUSY}}{R_{e/\mu}} \right| \lesssim 0.001 \ , \tag{8.41}$$

implies (1) the lightest chargino $\chi_1$ is sufficiently light

$$m_{\chi 1} \ \lesssim \ 250 \text{ GeV} \quad ,$$

(2) the left-handed selectron $\widetilde{e}_L$ and smuon $\widetilde{\mu}_L$ are highly non-degenerate:

$$\frac{m_{\widetilde{e}_L}}{m_{\widetilde{\mu}_L}} \ \gtrsim \ 2 \quad \text{or} \quad \frac{m_{\widetilde{e}_L}}{m_{\widetilde{\mu}_L}} \ \lesssim \ \frac{1}{2} \ ,$$

(3) at least one of $\widetilde{e}_L$ or $\widetilde{\mu}_L$ must be light, such that

$$m_{\widetilde{e}_L} \lesssim 300 \text{ GeV} \quad \text{or} \quad m_{\widetilde{\mu}_L} \lesssim 300 \text{ GeV},$$

and (4) the Higgsino mass parameter $\mu$ and left-handed up squark mass $m_{\widetilde{u}_L}$ satisfy either

$$|\mu| \lesssim 250 \text{ GeV}$$

or

$$|\mu| \gtrsim 300 \text{ GeV}, \; m_{\tilde{u}_L} \lesssim 200 \text{ GeV}.$$

Under these conditions, the magnitude $\Delta R_{e/\mu}^{SUSY}$ may fall within the sensitivity of the new $R_{e/\mu}$ measurements.

In conventional scenarios for SUSY-breaking mediation, one expects the left-handed slepton masses to be comparable, implying no substantial corrections to SM predictions for $R_{e/\mu}$. Significant reductions in both experimental error and theoretical, hadronic physics uncertainties in $R_{e/\mu}^{SM}$ would be needed to make this ratio an effective probe of the superpartner spectrum.

On the other hand, constraints from existing precision electroweak measurements leave considerable latitude for observable effects from tree-level superpartner exchange in the presence of RPV interactions. The existence of such effects would have important consequences for both neutrino physics and cosmology, as the presence of the $\Delta L \neq 0$ RPV interactions would induce a Majorana mass term for the neutrino and allow the lightest superpartner to decay to SM particles too rapidly to make it a viable dark matter candidate. Agreement between the results of the new $R_{e/\mu}$ measurements with $R_{e/\mu}^{SM}$ could yield significant new constraints on these possibilities.

# Chapter 9

# Supersymmetric Signatures in Muon and Beta Decays

## 9.1 Introduction

The search for physics beyond the Standard Model (SM) lies at the forefront of particle and nuclear physics. Among the prospective candidates for SM extensions, low-energy supersymmetry (SUSY) remains one of the most attractive possibilities. Its elegant solution to the naturalness problem associated with stability of the electroweak scale, its generation of coupling unification near the GUT scale, and its viable particle physics explanations for the abundance of matter (both visible and dark), have motivated a plethora of phenomenological studies over the years. With the advent of the Large Hadron Collider (LHC), direct evidence for low-energy SUSY may become available in the near future.

In the search for new physics, studies of precision electroweak observables and rare or SM-forbidden processes provide an important and complementary probe to collider searches (for recent discussions, see Refs. [54, 55]). Indeed, precise measurements of $Z$-pole observables and other electroweak precision measurements, as well as the branching ratios of rare decays such as $b \to s\gamma$ or $B_s \to \mu^+\mu^-$ have placed important constraints on supersymmetric models. At low energies, the recent evidence for a possibly significant deviation of the muon anomalous magnetic moment, $(g_\mu - 2)$, from SM expectations provides at least a tantalizing hint of low-energy SUSY in the regime of large $\tan\beta$ [79, 92]. Similarly, new searches for the permanent electric dipole moments of various systems will

probe SUSY (and other) CP-violation sources at a level of interest to explaining the baryon asymmetry of the universe[18, 54], while precision studies of fixed target, parity-violating electron scattering will be strongly sensitive to the existence lepton-number violating supersymmetric interactions[93].

In this paper, we study the implications of SUSY for weak decays of the muon, neutron, and nuclei. Our work is motivated by the prospect of significantly higher precision in future measurements of the muon lifetime ($\tau_\mu$) and decay correlation parameters, as well as of considerably higher precision in studies of neutron and nuclear $\beta$-decay at various laboratories, including the Spallation Neutron Source (SNS), Los Alamos Neutron Science Center (LANSCE), NIST, the Institut Laue-Langevin (ILL), and a possible high-intensity radioactive ion beam facility. Recent experimental progress including: new measurements of muon decay parameters at TRIUMF and PSI[94, 95, 96]; new measurements of the muon lifetime at PSI[97, 98]; Penning trap studies of nuclear $\beta$-decay[99]; the development of cold and ultracold neutron technology for the study of neutron decay; and plans for new measurements of the leptonic decays of the pion[100, 101] – point to the high level of experimental activity in this direction.

Theoretically, recent efforts have focused on the use of such experiments to test the unitarity of the Cabibbo-Kobayashi-Maskawa matrix, including analyses of SUSY corrections to the $(V-A)\otimes(V-A)$ structure of the SM charged current (CC) interaction [57, 81, 102] and improved limits on hadronic structure effects in neutron and nuclear $\beta$-decays[103]. Going beyond the $(V-A)\otimes(V-A)$ structure of the SM CC interaction, it has recently been shown that the scale of neutrino mass implied by neutrino oscillation experiments and the cosmic microwave background implies stringent bounds on chirality-changing scalar and tensor operators that could contribute to weak decays[104, 105, 106]. Comprehensive reviews of non-$(V-A)\otimes(V-A)$ effects in $\beta$-decay have been given in Refs. [107, 108, 109]

Here, we study the effects of supersymmetric interactions that give rise to non-$(V-A)\otimes(V-A)$ interactions but evade the neutrino mass bounds. Such effects can arise through radiative corrections in supersymmetric models containing only left-handed neutrinos. For concreteness, we focus on the minimal supersymmetric Standard Model (MSSM). We do

not consider simple extensions of the MSSM with right-handed or Majorana neutrinos and their superpartners as required by non-vanishing neutrino mass, as the effects of the corresponding neutrino sector on weak decays is highly constrained.[1]. We show that in the MSSM, radiatively-induced non-$(V-A)\otimes(V-A)$ interactions are particularly sensitive to flavor and left-right mixing among first and second generation sleptons and squarks. The flavor structure of the MSSM has been the subject of extensive scrutiny, and as we show below, experimental studies of lepton flavor violation (LFV) lead to tight constraints on the corresponding effects in weak decays. In contrast, there exist few independent probes of left(L)-right(R) mixing among scalar fermions. It is generally assumed that this mixing is proportional to the relevant Yukawa couplings, implying that it is highly suppressed in processes involving only first and second generation sfermions. However, this "alignment" assumption is not inherent in the structure of the SUSY–breaking sector of the MSSM, and while its use can simplify MSSM phenomenology, it is of interest to explore experimental observables that may test this assumption. In what follows, we argue that studies of weak decay correlations may provide such experimental tests. Specifically, we find that:

(i) Supersymmetric box graph corrections to the $\mu$-decay amplitude generates a non-vanishing scalar interaction involving right handed charged leptons ($g^S_{RR}\neq 0$ in the standard parameterization used below) in the presence of flavor mixing among left-handed (LH) sneutrinos and among right-handed (RH) sleptons, or flavor-diagonal mixing among LH and RH sleptons.

(ii) Analogous box graph effects can give rise to non-vanishing scalar and tensor interactions in light quark $\beta$-decay. The generation of these interactions requires non-vanishing left-right mixing among first generation sleptons and squarks. Studies of the energy-dependence of $\beta$-decay correlations and $\beta$-polarization – as well as of the energy-independent spin-polarization correlation – provide a probe of these interactions and the requisite L-R mixing.

(iii) Flavor-mixing among the LH sleptons ($\tilde{\nu}_L$, $\tilde{\ell}_L$) is highly constrained by searches for

[1] In see-saw scenarios, for example, the scale of the additional sneutrino mass is sufficiently large that these degrees of freedom decouple from low-energy observables.

lepton flavor violation in processes such as $\mu \to e\gamma$ and $\mu \to e$ conversion. Thus, any observable departure from $(V-A)\otimes(V-A)$ interactions in $\mu$-decay associated with the MSSM would arise from large, flavor diagonal L-R mixing among smuons ($\tilde{\mu}$) and selectrons ($\tilde{e}$). The former are also constrained by the present value of $(g_\mu - 2)$. At present, we are not aware of any analogous constraints on L-R mixing among first generation squarks and sleptons.

(iv) The magnitude of the effects in $\mu$-decay are below the present sensitivity of decay correlation studies. However, the presence of the SUSY-induced scalar interaction could modify the extraction of the Fermi constant ($G_\mu$) from the next generation of $\tau_\mu$ measurements at PSI. Similarly, improvements in $\beta$-decay correlation precision by $\lesssim$ an order of magnitude would allow one to probe the SUSY-induced scalar and tensor interactions generated by large L-R mixing. Such measurements could in principle provide a unique test of L-R mixing among first generation superpartners.

In the remainder of the paper, we provide details of our analysis. Section 9.2 gives a general overview of weak decay correlations and our notation and conventions. In Section 9.3 we discuss the computation of the relevant SUSY corrections and give analytic expressions for the resulting operators. Section 9.4 contains a discussion of constraints resulting from other measurements and numerical implications for the $\mu$-decay and $\beta$-decay correlations. We summarize our conclusions in Section 9.5.

## 9.2 Weak Decay Correlations: General Features

Departures from the SM $(V-A)\otimes(V-A)$ structure of the low-energy leptonic and semileptonic CC weak interactions can be characterized by an effective four fermion Lagrangian containing all independent dimension six operators. In the case of $\mu$-decay, it is conventional to use

$$\mathcal{L}^{\mu-\text{decay}} = -\frac{4G_\mu}{\sqrt{2}} \sum_{\gamma,\,\epsilon,\,\mu} g^\gamma_{\epsilon\mu}\ \bar{e}_\epsilon \Gamma^\gamma \nu_e\ \bar{\nu}_\mu \Gamma_\gamma \mu_\mu \tag{9.1}$$

where the sum runs over Dirac matrices $\Gamma^\gamma = 1$ (S), $\gamma^\alpha$ (V), and $\sigma^{\alpha\beta}/\sqrt{2}$ (T) and the subscripts $\mu$ and $\epsilon$ denote the chirality ($R$,$L$) of the muon and final state lepton, respectively[2]. Note that the use of this Lagrangian is only appropriate for the analysis of processes that occur at energies below the electroweak scale, as it is not $SU(2)_L \times U(1)_Y$ invariant. At tree-level in the SM one has $g^V_{LL} = 1$ with all other $g^\gamma_{\epsilon\mu} = 0$. In the limit of vanishing lepton masses, non-QED SM electroweak radiative corrections to the tree-level amplitude are absorbed into the definition of $G_\mu$.

In the literature, there exist several equivalent parameterizations of non-Standard Model contributions to light quark $\beta$-decay[107, 108, 109]. In analogy with Eq. (9.1) we use

$$\mathcal{L}^{\beta-\mathrm{decay}} = -\frac{4G_\mu}{\sqrt{2}} \sum_{\gamma,\,\epsilon,\,\delta} a^\gamma_{\epsilon\delta}\ \bar{e}_\epsilon \Gamma^\gamma \nu_e\, \bar{u} \Gamma_\gamma d_\delta \tag{9.2}$$

where the notation is similar to that for the $\mu$-decay effective Lagrangian. As with $\mathcal{L}^{\mu-\mathrm{decay}}$, only the purely left-handed $(V-A)\otimes(V-A)$ interaction appears at tree-level in the SM. In this case, one has $a^V_{LL} = V_{ud}$, the (1,1) element of the Cabibbo-Kobayashi-Maskawa (CKM) matrix. Including electroweak radiative corrections leads to

$$a^V_{LL} = V_{ud}\ (1 + \Delta\widehat{r}_\beta - \Delta\widehat{r}_\mu) \quad , \tag{9.3}$$

where $\Delta\widehat{r}_\beta$ contains the electroweak radiative corrections to the tree-level $(V-A)\otimes(V-A)$ $\beta$-decay amplitude and $\Delta\widehat{r}_\mu$ contains the corresponding corrections for $\mu$-decay apart from the QED corrections that are explicitly factored out when definiting $G_\mu$ from the muon lifetime.

Supersymmetric contributions to $\Delta\widehat{r}_\beta - \Delta\widehat{r}_\mu$ have been computed in Refs. [57, 81, 102]. These corrections can affect tests of the unitarity of the first row of the CKM matrix, as they must be subtracted from $a^V_{LL}$ when determining $V_{ud}$ from $\beta$-decay half lives. The corresponding implications for CKM unitarity tests have been discussed in those studies. Supersymmetric corrections can also give rise to non-vanishing $g^\gamma_{\epsilon\mu}$ and $a^\gamma_{\epsilon\delta}$ that parameterize the non-$(V-A)\otimes(V-A)$ interactions in Eqs. (9.1,9.2). The presence of these

[2]The normalization of the tensor terms corresponds to the convention adopted in Ref. [110]

operators cannot be discerned using the muon lifetime or $\beta$-decay half lives alone, but they can be probed using studies of the spectrum, angular distribution, and polarization of the decay products. We consider here non-$(V-A)\otimes(V-A)$ that are generated by one-loop corrections and are, thus, suppressed by a factor of $\alpha/4\pi$. Consequently, we focus on those operators that interfere linearly with SM contributions in weak decay observables and have the largest possible phenomenological effects.

In the case of polarized $\mu^-$ ($\mu^+$) decay, the electron (positron) spectrum and polarization are characterized by the eleven Michel parameters[111, 112], four of which ($\rho$, $\eta$, $\xi$, and $\delta$) describe the spectral shape and angular distribution. An additional five ($\xi'$, $\xi''$, $\eta''$, $\alpha/A$, $\beta/A$) are used to characterize the electron (positron) transverse and longitudinal polarization, while the final two ($\alpha'/A$, $\beta'/A$) parameterize time-reversal odd correlations between the muon polarization and the outgoing charged lepton spin. In what follows, we find that SUSY box graphs generate non-vanishing contributions to $g^S_{RR}$. This coupling appears quadratically in the parameters $\xi$ and $\xi'$ and interferes linearly with the SM term $g^V_{LL}$ in $\eta$, $\eta''$, and $\beta'/A$. The linear-dependence of $\eta$ on $g^S_{RR}$ is particularly interesting, since $\eta = 0$ in the SM, and since a non-zero value for this parameter enters the extraction of $G_\mu$ from $\tau_\mu$:

$$\frac{1}{\tau_\mu} = \frac{G_\mu^2 m_\mu^5}{192\pi^3}\left[1+\delta_{\rm QED}\right]\left[1+4\eta\frac{m_e}{m_\mu}-8\left(\frac{m_e}{m_\mu}\right)^2\right]\left[1+\frac{3}{5}\left(\frac{m_\mu}{M_W}\right)^2\right] \quad , \tag{9.4}$$

where $\delta_{\rm QED}$ denote the QED corrections the decay rate in the low-energy (Fermi) effective theory.

For $\beta$-decay, it is customary to use the description of the differential decay rate written down by Jackson, Treiman, and Wyld [113] (see also [107, 108, 109]):

$$\begin{aligned} d\Gamma \;\propto\; \mathcal{N}(E_e)\Bigg\{1 + a\frac{\vec{p}_e\cdot\vec{p}_\nu}{E_e E_\nu} + b\frac{\Gamma m_e}{E_e} + \langle\vec{J}\rangle\cdot\left[A\frac{\vec{p}_e}{E_e} + B\frac{\vec{p}_\nu}{E_\nu} + D\frac{\vec{p}_e\times\vec{p}_\nu}{E_e E_\nu}\right] \\ + \vec{\sigma}\cdot\left[N\langle\vec{J}\rangle + G\frac{\vec{p}_e}{E_e} + Q'\hat{p}_e\hat{p}_e\cdot\langle\vec{J}\rangle + R\langle\vec{J}\rangle\times\frac{\vec{p}_e}{E_e}\right]\Bigg\} d\Omega_e d\Omega_\nu dE_e, \end{aligned} \tag{9.5}$$

where $\mathcal{N}(E_e) = p_e E_e (E_0 - E_e)^2$; $E_e$ ($E_\nu$), $\vec{p}_e$ ($\vec{p}_\nu$), and $\vec{\sigma}$ are the $\beta$ (neutrino) energy,

momentum, and polarization, respectively; $\vec{J}$ is the polarization of the decaying nucleus; and $\Gamma = \sqrt{1-(Z\alpha)^2}$.

As we discuss below, SUSY box graphs may generate non-zero contributions to the operators in Eq. (9.2) parameterized by $a^S_{RR}$, $a^S_{RL}$, and $a^T_{RL}$. The latter interfere linearly with the SM parameter $a^V_{LL}$ in terms in Eq. (9.5) that depend on $\beta$ energy, including the so-called Fierz interference coefficient, $b$; the parity-violating correlation involving neutrino momentum and nuclear spin, $B$; and the polarization correlation coefficient, $Q'$. In addition, the energy-independent spin-polarization correlation coefficient $N$ also contains a linear dependence on $a^S_{RR}$, $a^S_{RL}$, and $a^T_{RL}$. Specifically, one has

$$b\,\zeta = \pm\ 4\,\mathrm{Re}\left[M_F^2\, g_V g_S\, a^V_{LL}(a^S_{RL}+a^S_{RR})^* - 2M_{GT}^2\, g_A g_T\, a^V_{LL} a^{T*}_{RL}\right] \tag{9.6}$$

$$\begin{aligned} B\,\zeta = 2\,\mathrm{Re}\Bigg[ & \pm\lambda_{J'J}\, M_{GT}^2 \left((g_A^2\,|a^V_{LL}|^2 + 4\,g_T^2\,|a^T_{RL}|^2) \mp \frac{\Gamma m}{E}\,4\,g_A g_T\, a^V_{LL} a^{T*}_{RL}\right) \\ & + \delta_{J'J}\, M_F M_{GT}\sqrt{\frac{J}{J+1}}\ \Big(2\,g_V g_A\,|a^V_{LL}|^2 \\ & \qquad \mp \frac{\Gamma m}{E}\,(4\,g_V g_T\, a^V_{LL} a^{T*}_{RL} - 2\,g_A g_S\, a^V_{LL}(a^S_{RL}+a^S_{RR})^*)\ \Big)\Bigg] \end{aligned} \tag{9.7}$$

$$\begin{aligned} Q'\,\zeta = 2\,\mathrm{Re}\Bigg[ & \lambda_{J'J}\, M_{GT}^2 \left((g_A^2\,|a^V_{LL}|^2 + 4g_T^2\,|a^T_{RL}|^2) \mp \frac{\Gamma m}{E}\,2\,g_A g_T\, a^V_{LL} a^{T*}_{RL}\right) \\ & \mp \delta_{J'J}\, M_F M_{GT}\sqrt{\frac{J}{J+1}}\ \Big(2\,g_V g_A\,|a^V_{LL}|^2 \\ & \qquad \mp \frac{\Gamma m}{E}\,(4\,g_V g_T\, a^V_{LL} a^{*T}_{RL} - 2\,g_A g_S\, a^V_{LL}(a^S_{RL}+a^S_{RR})^*)\ \Big)\Bigg] \end{aligned} \tag{9.8}$$

$$\begin{aligned} N\,\zeta = 2\,\mathrm{Re}\Bigg[ & \lambda_{J'J}\, M_{GT}^2 \left(\frac{\Gamma m}{E}\,(4g_T^2\,|a^T_{RL}|^2 + g_A^2\,|a^V_{LL}|^2) \mp 4 g_T g_A\, a^T_{RL} a^{V*}_{LL}\right) \\ & + \delta_{J'J}\, M_F M_{GT}\sqrt{\frac{J}{J+1}}\ \Big((4g_V g_T\, a^V_{LL} a^{T*}_{RL} - 2g_S g_A\,(a^S_{RR}+a^S_{RL}) a^{V*}_{LL}) \\ & \qquad \pm \frac{\Gamma m}{E}\,(4 g_S g_T\,(a^S_{RR}+a^S_{RL}) a^{T*}_{RL} - 2 g_V g_A\,|a^V_{LL}|^2)\ \Big)\Bigg] \end{aligned} \tag{9.9}$$

$$\zeta = 2M_F^2\,\left(g_V^2\,|a^V_{LL}|^2 + g_S^2\,|a^S_{RL}+a^S_{RR}|^2\right) + 2M_{GT}^2\,(g_A^2\,|a^V_{LL}|^2 + 4\,g_T^2\,|a^T_{RL}|^2)\quad , \tag{9.10}$$

$$\tag{9.11}$$

where $J$ ($J'$) are the initial (final) nuclear spin and $\lambda_{J'J} = (1, 1/J+1, -J/J+1)$ for

$J' = (J-1, J, J+1)$[3]. The quantities $M_F$ and $M_{GT}$ are Fermi and Gamow-Teller matrix elements and $g_{V,A,S,T}$ are vector, axial vector, scalar, and tensor form factors. For transitions between initial ($i$) and final ($f$) nuclear states the corresponding reduced matrix elements are

$$\begin{aligned} \langle f||\bar{u}\gamma^\lambda d + \text{H.C.}||i\rangle &= g_V(q^2)M_F \\ \langle f||\bar{u}\gamma^\lambda\gamma_5 d + \text{H.C.}||i\rangle &= g_A(q^2)M_{GT} \\ \langle f||\bar{u}d + \text{H.C.}||i\rangle &= g_S(q^2)M_F \\ \langle f||\bar{u}\sigma^{\lambda\rho} d + \text{H.C.}||i\rangle &= g_T(q^2)M_{GT} \quad . \end{aligned} \tag{9.12}$$

The conserved vector current property of the SM CC interaction implies that $g_V(0) = 1$ in the limit of exact isospin symmetry. Isospin breaking corrections imply deviations from unity of order a few $\times 10^{-4}$ [114] (for an earlier estimate, see Ref. [115]). A two parameter fit to $\beta$-decay data yields $g_A(0)/g_V(0) = 1.27293(46)$[109], assuming only a non-vanishing SM coupling, $a_{LL}^V$, and neglecting differences in electroweak radiative corrections between hadronic vector and axial vector amplitudes. Theoretical expectations for $g_S$ and $g_T$ are summarized below.

## 9.3 SUSY-Induced Scalar and Tensor Interactions

We compute the SUSY contributions to the weak decay correlations in the MSSM and obtain non-vanishing contributions to $g_{RR}^S$, $a_{RR}^S$, and $a_{RL}^{S,T}$ from the box diagrams in Figures 9.1 ($\mu$-decay) and 9.2 ($\beta$-decay). These amplitudes – as well as others not shown explicitly in Figures 9.1 and 9.2 – also contribute to the parameters $g_{LL}^V$ and $a_{LL}^V$ that arise in the SM. A complete analysis of those contributions, along with the gauge boson propagator, vertex, and external leg corrections, is given in Ref. [57]. Here, we focus on the non-$(V-A)\otimes(V-A)$ operators generated by the diagrams shown explicitly.

Since the SM CC interaction is purely left-handed (LH), the generation of operators

[3]The quantity $\zeta$ is often denoted by $\xi$ in the literature. However, we have modified the notation to avoid confusion with the Michel parameter $\xi$.

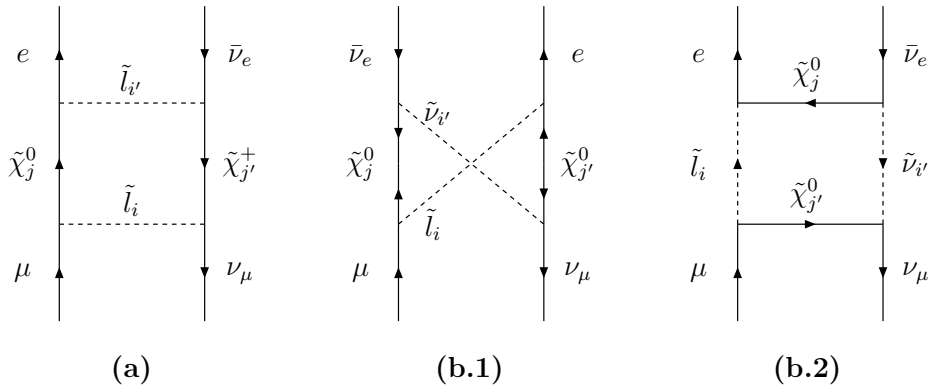


Figure 9.1: *Feynman diagrams relative to supersymmetric contributions giving rise to non* $(V-A)\otimes(V-A)$ *amplitudes in the muon decay. The amplitude relative to the diagram shown in* **(a)** *involves left-right slepton mixing, while those in* **(a)** *are non-vanishing if lepton flavor mixing is present in the slepton sector.*

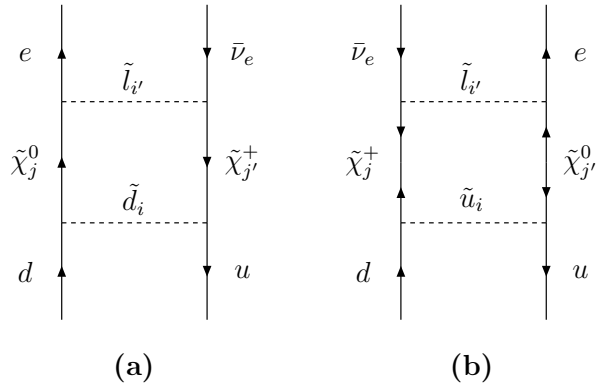


Figure 9.2: *Feynman diagrams relative to supersymmetric contributions giving rise to anomalous amplitudes in* $\beta$ *decay processes.*

involving the right-handed (RH) SM fields requires the presence of RH fermion superpartners in the one-loop graphs. These particles appear either by virtue of left-right mixing among superpartners in Figures 9.1(a) and 9.2(a,b) or through coupling of the neutralinos ($\tilde{\chi}^0_j$) to the RH sleptons as in Figures 9.1(b.1, b.2). Note that in the latter case, a given virtual slepton mass eigenstate $\tilde{l}_i$ will couple to both the first and second generation charged leptons, thereby requiring the presence of non-zero flavor mixing. In contrast, the contributions of Figures. 9.1(a) and 9.2(a,b) involve only L-R mixing but no flavor mixing among the sfermions in the loops.

To set our notation, we largely follow the conventions of Refs. [89, 90]. The L-R and

flavor mixing among the sfermions is determined by the sfermion mass matrices. In the flavor basis, one has

$$\mathbf{M}^{\mathbf{2}}_{\tilde{\mathbf{f}}} = \begin{pmatrix} \mathbf{M}^{\mathbf{2}}_{\mathbf{LL}} & \mathbf{M}^{\mathbf{2}}_{\mathbf{LR}} \\ \mathbf{M}^{\mathbf{2}}_{\mathbf{LR}} & \mathbf{M}^{\mathbf{2}}_{\mathbf{RR}} \end{pmatrix} \tag{9.13}$$

where for quark and charged slepton superpartners $\mathbf{M}^{\mathbf{2}}_{\mathbf{AB}}$ $(A, B = L, R)$ are $3 \times 3$ matrices with indices running over the three flavors of sfermion of a given chiral multiplet $(L, R)$. For sneutrinos, only $\mathbf{M}^{\mathbf{2}}_{\mathbf{LL}}$ is non-vanishing. After electroweak symmetry-breaking, the $\mathbf{M}^{\mathbf{2}}_{\mathbf{AB}}$ take the forms (using squarks as an illustration)

$$\mathbf{M}^{\mathbf{2}}_{\mathbf{LL}} = \mathbf{m}^{\mathbf{2}}_{\mathbf{Q}} + \mathbf{m}^{\mathbf{2}}_{\mathbf{q}} + \mathbf{\Delta}_{\mathbf{f}} \tag{9.14}$$

$$\mathbf{M}^{\mathbf{2}}_{\mathbf{RR}} = \mathbf{m}^{\mathbf{2}}_{\tilde{\mathbf{f}}} + \mathbf{m}^{\mathbf{2}}_{\mathbf{q}} + \bar{\mathbf{\Delta}}_{\mathbf{f}} \tag{9.15}$$

with

$$\mathbf{\Delta}_{\mathbf{f}} = \left( I_3^f - Q_f \sin^2 \theta_W \right) \cos 2\beta M_Z^2 \tag{9.16}$$

$$\bar{\mathbf{\Delta}}_{\mathbf{f}} = Q_f \sin^2 \theta_W \cos 2\beta M_Z^2 \tag{9.17}$$

and

$$\mathbf{M}^{\mathbf{2}}_{\mathbf{LR}} = \mathbf{M}^{\mathbf{2}}_{\mathbf{RL}} = \begin{cases} v \left[ \mathbf{a_f} \sin\beta - \mu \mathbf{Y_f} \cos\beta \right] , & \tilde{u} - \text{type sfermion} \\ v \left[ \mathbf{a_f} \cos\beta - \mu \mathbf{Y_f} \sin\beta \right] , & \tilde{d} - \text{type sfermion} \end{cases} , \tag{9.18}$$

where $\tan\beta = v_u/v_d$ gives the ratio of the vacuum expectation value of the two neutral Higgs fields, $\mathbf{Y_f}$ and $\mathbf{a_f}$ are the $3 \times 3$ Yukawa and soft triscalar couplings and $\mu$ is the supersymmetric coupling between the two Higgs supermultiplets. The matrices $\mathbf{m}^{\mathbf{2}}_{\mathbf{Q}}$, $\mathbf{m}^{\mathbf{2}}_{\tilde{\mathbf{f}}}$, and $\mathbf{m}^{\mathbf{2}}_{\mathbf{q}}$ are the mass matrices for the LH squarks, RH squarks, and quarks, respectively. It is often customary to assume that $\mathbf{a_f} \propto \mathbf{Y_f}$, in which case one may diagonalize $\mathbf{M}^{\mathbf{2}}_{\mathbf{LR}}$ by the same rotation that diagonalizes the fermion mass matrices and leads to a magnitude for L-R mixing proportional to the relevant fermion mass. In what follows, however, we will avoid making this assumption. Indeed, studies of the decay correlation parameters may provide a means of testing this alignment hypothesis.

The matrix $\mathbf{M}^{\mathbf{2}}_{\tilde{\mathbf{f}}}$ can be diagonalized by the unitary matrix $\mathbf{Z}_{\mathbf{f}}$. The corresponding sfermion mass eigenstates $\tilde{F}_j$ are given as a linear combination of the flavor eigenstates $\tilde{f}_I$ as

$$\tilde{F}_j = Z_f^{jI}\, \tilde{f}_I \tag{9.19}$$

where $I = 1, 2, 3$ indicate the flavor states $\tilde{f}_{L_I}$ and $I = 4, 5, 6$ refer to the RH flavor states $\tilde{f}_{R_{I-3}}$.

In general, the charginos ($\tilde{\chi}_j^+$) and neutralinos entering the loop graphs are mixtures of the electroweak gauginos and Higgsinos. Since the characteristics of this mixing are not crucial to our analysis and a detailed discussion can be found elsewhere (*e.g.*, Refs. [89, 90]), we simply give our notation for the relevant mixing:

$$\chi_i^0 = N_{ij}\psi_i^0 \quad i, j = 1 \ldots 4 \tag{9.20}$$

for the neutralinos and

$$\begin{pmatrix} \chi_1^+ \\ \chi_2^+ \end{pmatrix} = \mathbf{V} \begin{pmatrix} \tilde{W}^+ \\ \tilde{H}_u^+ \end{pmatrix} \quad , \quad \begin{pmatrix} \chi_1^- \\ \chi_2^- \end{pmatrix} = \mathbf{U} \begin{pmatrix} \tilde{W}^- \\ \tilde{H}_d^- \end{pmatrix} ; \tag{9.21}$$

for the charginos. Here, the fields $\psi_i^0$ denote the $(\tilde{B}, \tilde{W}^0, \tilde{H}_d^0, \tilde{H}_u^0)$ fields.

Using the foregoing conventions, we obtain the following contributions to the $g_{RR}^S$, $a_{RR}^S$, and $a_{RL}^{S,T}$:

$$\begin{aligned} g_{RR}^S &= \tilde{\delta}_\mu^{(a)} + \tilde{\delta}_\mu^{(b.1)} + \tilde{\delta}_\mu^{(b.2)} \\ a_{RR}^S &= \tilde{\delta}_\beta^{(a)} \\ a_{RL}^S = -2a_{RL}^T &= \tilde{\delta}_\beta^{(b)} \end{aligned} \tag{9.22}$$

where

$$\tilde{\delta}_{\mu}^{(a)} = \frac{\alpha M_Z^2}{\pi} |U_{m1}|^2 Z_L^{2i*} Z_L^{5i} Z_L^{1k} Z_L^{4k*} |N_{j1}|^2 \mathcal{F}_1\left(M_{\chi_j^0}, M_{\chi_m^+}, M_{\tilde{l}_i}, M_{\tilde{l}_k}\right) \quad (9.23)$$

$$\tilde{\delta}_{\mu}^{(b.1)} = \frac{-\alpha M_Z^2}{2\pi} N_{j1}(N_{j2}^* - \tan\theta_W N_{j1}^*) N_{k1}^*(N_{k2} - \tan\theta_W N_{k1}) \quad (9.24)$$
$$\times Z_\nu^{1m*} Z_\nu^{2m} Z_L^{4i*} Z_L^{5i} \mathcal{F}_1\left(M_{\chi_j^0}, M_{\chi_k^0}, M_{\tilde{l}_i}, M_{\tilde{\nu}_m}\right)$$

$$\tilde{\delta}_{\mu}^{(b.2)} = \frac{-\alpha M_Z^2}{2\pi} N_{j1}(N_{j2} - \tan\theta_W N_{j1}) N_{k1}^*(N_{k2}^* - \tan\theta_W N_{k1}^*) \quad (9.25)$$
$$\times Z_\nu^{1m*} Z_\nu^{2m} Z_L^{4i*} Z_L^{5i} M_{\chi_j^0} M_{\chi_k^0} \mathcal{F}_2\left(M_{\chi_j^0}, M_{\chi_k^0}, M_{\tilde{l}_i}, M_{\tilde{\nu}_m}\right)$$

$$\tilde{\delta}_{\beta}^{(a)} = \frac{\alpha M_Z^2 V_{ud}}{3\pi} |U_{k1}|^2 Z_D^{1i*} Z_D^{4i} Z_L^{1m} Z_L^{4m*} |N_{j1}|^2 \quad (9.26)$$
$$\times \mathcal{F}_1\left(M_{\chi_j^0}, M_{\chi_k^+}, M_{\tilde{d}_i}, M_{\tilde{l}_m}\right)$$

$$\tilde{\delta}_{\beta}^{(b)} = \frac{-\alpha M_Z^2 V_{ud}}{3\pi} U_{j1} V_{j1}^* Z_U^{1i*} Z_U^{4i} Z_L^{1m} Z_L^{4m*} |N_{k1}|^2 \quad (9.27)$$
$$\times M_{\chi_j^+} M_{\chi_k^0} \mathcal{F}_2\left(M_{\chi_j^+}, M_{\chi_k^0}, M_{\tilde{u}_i}, M_{\tilde{l}_m}\right)$$

and where we have defined the loop functions

$$\mathcal{F}_n\left(m_a, m_b, m_c, m_d\right) \equiv \int_0^1 \mathrm{d}x \int_0^{1-x} \mathrm{d}y \int_0^{1-x-y} \mathrm{d}z \quad (9.28)$$
$$\left[x\, m_a^2 + y\, m_b^2 + z\, m_c^2 + (1-x-y-z) m_d^2\right]^{-n} \quad .$$

## 9.4 Phenomenological Constraints and Implications

We now analyze the possible magnitude of the box graph contributions. At first glance, the results in Eqs. (9.23-9.27) exhibit the expected scaling with masses and couplings: $\tilde{\delta} \sim (\alpha/4\pi) \times (M_Z/\tilde{M})^2$, where $\tilde{M}$ is a generic superpartner mass. Thus, one expects these contributions to be of order $10^{-3}$ when $\tilde{M}$ is comparable to the electroweak scale. However, the prefactors involving products of the sfermion mixing matrices can lead to substantial departures from these expectations. (The impact of the neutralino and chargino mixing matrices $N_{jk}$, $U_{jk}$ *etc.* is less pronounced). In particular, there are two general classes box graph contributions: those which depend on slepton flavor mixing ($\delta_\mu^{(b.1,2)}$) and those which depend on L-R mixing ($\delta_\mu^{(a)}$ and $\delta_\beta^{(a,b)}$). We examine each class of contributions

independently by performing a numerical scan over MSSM parameter space while taking into consideration the results of direct searches for superpartners, precision electroweak data, and LFV studies. In particular, we attempt to constrain the viable parameter space – and thus the magnitude of these box graph contributions – by requiring consistency with the experimental bounds for the branching ratio for $\mu \to e\gamma$ and for $(g_\mu - 2)$.

### 9.4.1 Lepton Flavor Mixing Contributions

The contributions to $g^S_{RR}$ from $\delta^{(b.1,2)}_\mu$ depend on the products of stermion mixing matrices $Z^{1m*}_\nu Z^{2m}_\nu$ and $Z^{5i}_L Z^{4i*}_L$, which are non-vanishing only in the presence of flavor mixing among the first two generations of sneutrinos and RH charged sleptons, respectively. The existence of such flavor mixing also gives rise to lepton flavor violating (LFV) processes such as $\mu \to e\gamma$ and $\mu \to e$ conversion and, indeed, the products $Z^{1m*}_\nu Z^{2m}_\nu$ and $Z^{5i}_L Z^{4i*}_L$ enter the rates for such processes at one-loop order. Consequently, the non-observation of LFV processes leads to stringent constraints on these products of mixing matrix elements.

To estimate the order of magnitude for these constraints, we focus on the rate for the decay $\mu \to e\gamma$, which turns out to be particularly stringent. In principle, one could also analyze the constraints implied by limits on the $\mu \to e$ conversion and $\mu \to 3e$ branching ratios. This would possibly make our conclusions on the maximal size of the flavor violating contributions to $g^S_{RR}$ more severe, but it would not change our main conclusion: lepton flavor mixing contributions to $g^S_{RR}$ are unobservably small.

Experimentally, the most stringent bound on the corresponding branching ratio has been obtained by the MEGA collaboration[116]:

$$Br(\mu \to e\gamma) \equiv \frac{\Gamma(\mu^+ \to e^+\gamma)}{\Gamma(\mu^+ \to e^+\nu\bar{\nu})} < 1.2 \times 10^{-11} \qquad 90\% \text{ C.L.} \tag{9.29}$$

Theoretically, a general analysis in terms of slepton and sneutrino mixing matrices has been given in Ref. [60]. Using the notation of that work, we consider those contributions to the $\mu \to e\gamma$ amplitude that contain the same combinations for LFV mixing matrices as appear in the $\tilde{\delta}^{(b)}_\mu$. For simplicity, we also set (in the present analytical estimate, but not in the following numerical computation) the chargino and neutralino mixing matrices

to unity and neglect contributions that are suppressed by factors of $m_\mu/M_W$. With these approximations, the combination $Z_\nu^{1m} Z_\nu^{2m}$ appears only in the first term of the chargino loop amplitude $A_2^{(c)R}$ according to the notation of Ref. [60]. Setting the chargino mixing to 1 (or, equivalently, considering the pure wino contribution alone), gives

$$A_2^{(c)R} \simeq \frac{\alpha}{8\pi \sin^2\theta_W} \frac{1}{m^2_{\widetilde{\nu}_m}} \left(Z_\nu^{1m} Z_\nu^{2m}\right) f^{(c)}(x_m) + \cdots , \quad x_m = \left(\frac{m_{\widetilde{\nu}_m}}{m_{\widetilde{W}}}\right) \tag{9.30}$$

where $f^{(c)}(x)$ is a loop function. Analogously, the combination $Z_L^{4i} Z_L^{5i}$ appears only in the first term of the neutralino loop amplitude $A_2^{(n)L}$. This time the amplitude reads (again considering only the pure *bino* loop)

$$A_2^{(n)L} \simeq \frac{\alpha}{4\pi \cos^2\theta_W} \frac{1}{m^2_{\widetilde{L}_i}} \left(Z_L^{4i} Z_L^{5i}\right) f^{(n)}(x_i) + \cdots , \quad x_i = \left(\frac{m_{\widetilde{L}_i}}{m_{\widetilde{B}}}\right) \tag{9.31}$$

The resulting muon decay widths respectively read

$$\Gamma^{(c)}(\mu \to e\gamma) \simeq \frac{\alpha}{4} \frac{\alpha^2}{(8\pi \sin^2\theta_W)^2} \frac{m_\mu^5}{m^4_{\widetilde{\nu}_m}} \left(Z_\nu^{1m} Z_\nu^{2m}\right)^2 \left(f^{(c)}(x_m)\right)^2 \tag{9.32}$$

and

$$\Gamma^{(n)}(\mu \to e\gamma) \simeq \frac{\alpha}{4} \frac{\alpha^2}{(4\pi \cos^2\theta_W)^2} \frac{m_\mu^5}{m^4_{\widetilde{L}_i}} \left(Z_L^{4i} Z_L^{5i}\right)^2 \left(f^{(n)}(x_i)\right)^2 \tag{9.33}$$

For simplicity, we consider two extremes: $m_{\widetilde{\nu}_m} \approx m_{\widetilde{L}_i} \approx m_{\widetilde{W}} \approx m_{\widetilde{B}}$=100, 1000 GeV $\equiv \tilde{M}$. For either choice, we find

$$\left(f^{(c)}(1)\right)^2 \simeq \left(f^{(n)}(1)\right)^2 \simeq 0.007 \tag{9.34}$$

Inserting the numerical values, and requiring that $\Gamma^{(n,c)} \lesssim 10^{-30}$ GeV as required by the limit (9.29), we find that

$$\left(Z_L^{4i} Z_L^{5i}\right)_{\max} \approx \left(Z_\nu^{1m} Z_\nu^{2m}\right)_{\max} < \begin{cases} 10^{-3} & \text{for } \tilde{M} = 100 \text{ GeV} \\ 10^{-1} & \text{for } \tilde{M} = 1000 \text{ GeV} \end{cases} \tag{9.35}$$

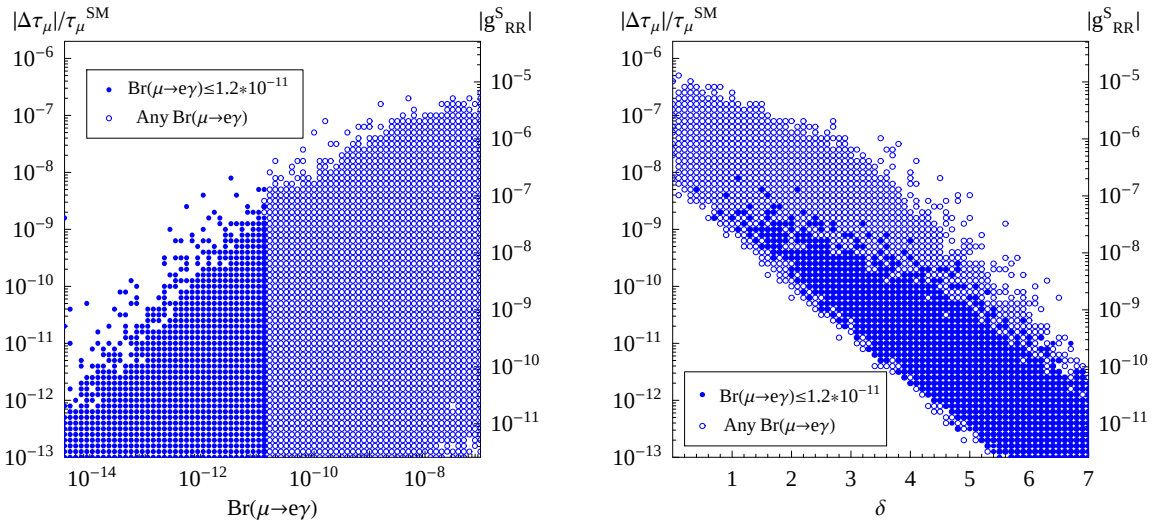


(a) (b)

Figure 9.3: *A scatter plot showing* $|\Delta\tau_\mu|/\tau_\mu^{\rm SM}$ *(left vertical axis) and* $|g^S_{\rm RR}|$ *(right vertical axis), as functions of Br*$(\mu \to e\gamma)$ *(a) and of* $\delta_{\rm LFV}$ *(b) (smaller* $\delta_{\rm LFV}$ *means more lepton flavor mixing; see the text for the precise definition). Filled circles represent models consistent with the current bound Br*$(\mu \to e\gamma) \leq 1.2 \times 10^{-11}$*, while empty circles denote all other models.*

This implies that for superpartner masses of the order of 100 GeV, the amplitudes $\tilde{\delta}_\mu^{(b.1,b.2)}$ are suppressed by a factor $10^{-6}$ relative to the naive expectations discussed above, while for 1000 GeV masses by a factor $10^{-2}$. In this latter case, however, the loop functions in the amplitudes $\tilde{\delta}_\mu^{(b)}$ experience a further suppression factor of order $10^{-2}$. Thus, the magnitude of the $\tilde{\delta}_\mu^{(b)}$ should be no larger than $\sim 10^{-7}$.

We substantiate the previous estimates by performing a numerical scan over the parameter space of the $CP$-conserving MSSM [117]. We do not implement any universality assumption in the slepton soft supersymmetry breaking mass sector or in the gaugino mass terms. However, in this section only, we neglect L-R mixing and consider flavor mixing be-

| $\mu$ | $m_1$ | $m_2$ | $(\mathbf{M^2_{LL}})_{ij}, (\mathbf{M^2_{RR}})_{ij}$ | $\tan\beta$ |
|---|---|---|---|---|
| $30 \div 10000$ | $2 \div 1000$ | $50 \div 1000$ | $10^2 \div 2000^2$ | $1 \div 60$ |

Table 9.1: *Ranges of the MSSM parameters used to generate the models shown in Fig. 9.3. Here,* $\mu$ *is the usual higgsino mass term, while* $m_{1,2}$ *indicate the soft supersymmetry breaking* $U(1)_Y$ *and SU(2) gaugino masses. The matrices* $\mathbf{M^2_{LL}}$ *and* $\mathbf{M^2_{RR}}$ *are symmetric; hence, we scanned over 6 independent masses within the specified range. All masses are in GeV.*

tween the first and second generation sleptons only. Under these assumptions, the mixing that causes non-vanishing $\tilde{\delta}_{\mu}^{(b.1,2)}$ stems solely from off-diagonal elements in the two 2×2 slepton mass matrices $\mathbf{M^2_{LL}}$ and $\mathbf{M^2_{RR}}$. We scan independently over all the parameters indicated in Table 9.1, within the specified ranges. For all models, we impose constraints from direct supersymmetric-particles searches at accelerators and require the lightest supersymmetric particle (LSP) to be the lightest neutralino (see also [118] for more details).

The result of this scan is shown in Fig. 9.3. Although general models can accommodate $g^S_{RR} \sim 10^{-5}$, the current constraint on Br($\mu \to e\gamma$) severely restricts the available parameter space and reduces the allowed upper limit on $g^S_{RR}$ by over an order of magnitude, as shown in Fig. 9.3 (a). It is also instructive to exhibit the sensitivity of $g^S_{RR}$ to the degree of flavor-mixing and to show the corresponding impact of the LFV searches. To that end, we quantify the amount of lepton flavor mixing by a parameter $\delta_{\rm LFV}$, defined as

$$\delta_{\rm LFV} = |\delta_L| + |\delta_R| \ , \tag{9.36}$$

where

$$\delta_L = \log\left(\frac{2\,(\mathbf{M^2_{LL}})_{12}}{(\mathbf{M^2_{LL}})_{11} + (\mathbf{M^2_{LL}})_{22}}\right) \qquad \delta_R = \log\left(\frac{2\,(\mathbf{M^2_{RR}})_{12}}{(\mathbf{M^2_{RR}})_{11} + (\mathbf{M^2_{RR}})_{22}}\right) \tag{9.37}$$

and *e.g.*, $(\mathbf{M^2_{LL}})_{ij}$ is the $(i,j)$-th component of left-handed slepton mass matrix. For example, if $|\delta_L|$ is close to zero, then there is a large flavor mixing contribution from left-handed sleptons; but if $|\delta_L|$ is large, then this flavor mixing is suppressed. Since the amplitudes $\tilde{\delta}_{\mu}^{(b.1,2)}$ depend on flavor mixing among *both* LH and RH sleptons, they contribute only if both $\delta_L$ and $\delta_R$ are small. (In contrast, Br($\mu \to e\gamma$) survives in the presence of flavor mixing among *either* LH or RH sleptons.) Naturally, the flavor mixing contribution to $g^S_{RR}$ is largest when $\delta_{LFV}$ is smallest, as shown in Fig. 9.3(b). We note that to obtain a large flavor mixing contribution to $g^S_{RR}$, it is not sufficient simply to have maximal mixing (i.e. $|Z^{ij}_L| = 1/\sqrt{2}$); in addition, one needs the absence of a degeneracy among the slepton mass eigenstates, or else the sum over mass eigenstates [*e.g.*, sum over $i$ and $i'$ in Eqn (9.24)] will cancel. In any case, we conclude that the flavor mixing box graph contributions are too

small to be important for the interpretation of the next generation muon decay experiments, where the precision in $\tau_\mu$ is expected to be of the order of one ppm.

### 9.4.2 Left-Right Mixing Contributions

Significantly larger contributions to $g^S_{RR}$ can arise from $\tilde{\delta}^{(a)}_\mu$, which requires only L-R mixing among same generation sleptons. In the case of smuon L-R mixing, some considerations follow from the present value for the muon anomalous magnetic moment, or $(g_\mu - 2)$, which is a chirality odd operator and which can arise from L-R mixing in one-loop graphs [119]. The only supersymmetric contribution $\delta a_\mu$ to $a_\mu \equiv (g_\mu - 2)/2$ proportional to one single power of the ratio of the muon mass and of supersymmetric particles is in fact proportional to the smuon L-R mixing, and reads

$$\delta a_\mu^{\rm LR-mix} = \frac{m_\mu}{16\pi^2} \sum_{i,m} \frac{m_{\chi_i^0}}{3m^2_{\tilde{\mu}_m}} {\rm Re}[g_1 N_{i1}(g_2 N_{i2} + g_1 N_{i1}) Z_L^{2m*} Z_L^{5m}] F_2^N(m^2_{\chi_i^0}/m^2_{\tilde{\mu}_m}), \quad (9.38)$$

where $F_2^N$ is the appropriate loop function specified in [119]. The expression features the same dependence upon the smuon mixing matrix as does Eq. (9.23). Under the widely considered alignment assumption that $\mathbf{a_f} \propto \mathbf{Y_f}$ this term is usually suppressed, as the smuon L-R mixing is also suppressed. Here, however, we drop that hypothesis, and allow for large L-R mixing: this, in general, enhances the aforementioned contribution, and we therefore expect that the experimental constraints on $(g_\mu - 2)$ will set limits on $g^S_{RR}$. In particular, assuming a common mass $\tilde{M}$ for all the supersymmetric particles, and maximal L-R mixing, Eq. (9.38) approximately reduces to

$$\delta a_\mu^{\rm LR-mix} \approx \frac{g_1^2}{4\pi} \frac{1}{12\pi} \left(\frac{m_\mu}{\tilde{M}}\right) \approx 10^{-7} \quad \text{for } \tilde{M} \sim 100 \text{ GeV}, \quad (9.39)$$

where $g_1$ indicates the $U(1)_Y$ gauge coupling. We consider here the 95% C.L. limit on beyond-the-SM contributions to $(g_\mu - 2)$ as quoted in Ref. [120],

$$a_\mu^{\rm exp} - a_\mu^{\rm th-SM} = (25.2 \pm 9.2) \times 10^{-10}, \quad (9.40)$$

bearing in mind that a more conservative approach to the evaluation of the sources of theoretical uncertainty in the SM contribution could inflate the error associated with $a_\mu^{\rm th-SM}$ (see *e.g.* Ref. [121] for the hadronic light-by-light contribution).

A large value for $\delta a_\mu$, however, does not imply automatically a large $g^S_{RR}$, since the latter also depends upon the mixing in the selectron sector, to which $\delta a_\mu$ is blind. On the other hand, large values of $|g^S_{RR}|$ in general should produce a sizable $\delta a_\mu$, although the possibility of cancellations with other terms, and the different loop function structures can lead, in principle, to a suppression of $\delta a_\mu$ even for large $g^S_{RR}$. This possibility is illustrated in Fig. 9.4, showing a scan over MSSM parameters (discussed below). As indicated by the results of this scan, imposing the $(g_\mu - 2)$ constraints restricts, but does not exclude, the possibility of obtaining relatively large values of $|g^S_{RR}|$.

The possible existence of nearly flat directions in the MSSM potential leads to additional constraints on the size of the scalar trilinear couplings from the condition of avoiding charge and color breaking minima. Quantitatively, one can express those constraints in the form [122]

$$\begin{aligned}
\mathbf{a_u^2} &\lesssim 3\,\mathbf{Y_u^2}\left(\mu_u^2 + \mathbf{m_{\tilde{Q}}^2} + \mathbf{m_{\tilde{u}}^2}\right) \\
\mathbf{a_d^2} &\lesssim 3\,\mathbf{Y_d^2}\left(\mu_d^2 + \mathbf{m_{\tilde{Q}}^2} + \mathbf{m_{\tilde{d}}^2}\right) \\
\mathbf{a_e^2} &\lesssim 3\,\mathbf{Y_e^2}\left(\mu_d^2 + \mathbf{m_{\tilde{L}}^2} + \mathbf{m_{\tilde{e}}^2}\right)
\end{aligned} \tag{9.41}$$

where $\mu^2_{u,d} \equiv m^2_{h_{u,d}} + |\mu|^2$. The conditions above can be fulfilled for large values of $\mathbf{a_f}$ for accordingly large values of $\mathbf{Y_f} \times \mathbf{m_{\tilde{f}}}$ or $\mathbf{Y_f} \times \mu_{\mathbf{u,d}}$. Since $g^S_{RR}$ depends on the product $\mathcal{F}_1 \times |(Z_L^{22})^* Z_L^{52}|$, the presence of large scalar fermion masses leads to a suppression of $g^S_{RR}$ via the loop functions $\mathcal{F}_1$. Thus, large values of $g^S_{RR}$ are possible only when L-R mixing is nearly maximal and the constraints of Eqs. (9.41) are satisfied with large values of $\mu^2_{u,d}$. Making use of the electroweak symmetry breaking (EWSB) conditions, one can express $\mu^2_{u,d}$ as functions of $M_Z$ and of the CP-odd Higgs mass, $m_A$. At the expense of introducing some fine-tuning, one may then achieve arbitrarily large values for the right hand sides of Eqs. (9.41), and hence of the trilinear scalar couplings, as long as $m_A$ is sufficiently large, independently of the other sfermion soft supersymmetry breaking mass terms. The heavy

Higgs sector does not enter in the loops contributing to any of the quantities at stake here, and the size of $m_A$ therefore does not affect our results.

While this argument cannot be applied to models such as minimal supergravity, where the sfermion and the heavy Higgs sector are connected at the GUT scale, in extended models (*e.g.*, the non-universal Higgs mass extension of mSUGRA, [123]) the size of the trilinear scalar couplings can be taken to be much larger than the size of the soft breaking sfermion mass terms. In turn, this implies the possibility of having a sizable L-R mixing not only in the third generation sfermions but, in principle, in the first two generations as well.

In contrast to the situation for $\mu$-decay, the box graph contributions to the semileptonic parameters $a^S_{RR}$ and $a^{S,T}_{RL}$ live entirely on L-R mixing among first generation sleptons and squarks. To our knowledge, there exist no strong bounds on such mixing from precision electroweak measurements or searches for rare or SM-forbidden processes. Consequently, we will consider the possibility of maximal L-R mixing which simply requires that $|M^2_{LR}| \sim |M^2_{LL} - M^2_{RR}|$. From Eqs. (9.14-9.18), this situation amounts to having $a_f$ of order the electroweak scale and $m^2_F$ not too different from $m^2_{\tilde{f}}$. The foregoing discussion of charge and color breaking minima applies to this case as well as to $\mu$-decay.

Taking into account the foregoing considerations, we carry out a numerical analysis of the magnitude of the SUSY contributions to $g^S_{RR}$, $a^S_{RR}$, and $a^{S,T}_{RL}$. As before, we consider the $CP$-conserving MSSM [117], and proceed to a random scan over its parameter space. We do not resort to any universality assumption, neither in the scalar soft supersymmetry breaking mass sector, nor in the gaugino mass terms nor in the soft-breaking

| $\mu$ | $m_1$ | $m_2$ | $m_3$ |
|---|---|---|---|
| $30 \div 10000$ | $2 \div 1000$ | $50 \div 1000$ | $m_{\rm LSP} \div 10000$ |
| $m_A$ | $m_{\widetilde{F}}$ | $A_F$ | $\tan\beta$ |
| $100 \div 10000$ | $(1 \div 10) m_{\rm LSP}$ | $\pm(m^2_{\widetilde{F}}/m_F)$ | $1 \div 60$ |

Table 9.2: *Ranges of the MSSM parameters used to generate the models shown in Figs. 9.4 and 9.5. All masses are in GeV, and* $m_{\rm LSP} \equiv \min(|\mu|, |m_1|, |m_2|)$. $m_3$ *and* $m_A$ *indicate the gluino and the* $CP$ *odd heavy Higgs boson masses, respectively. The quantity* $m_{\widetilde{F}}$ *indicates the various soft supersymmetry breaking masses, which we independently sampled; we dub the mass of the corresponding SM fermion* $F$ *as* $m_F$.

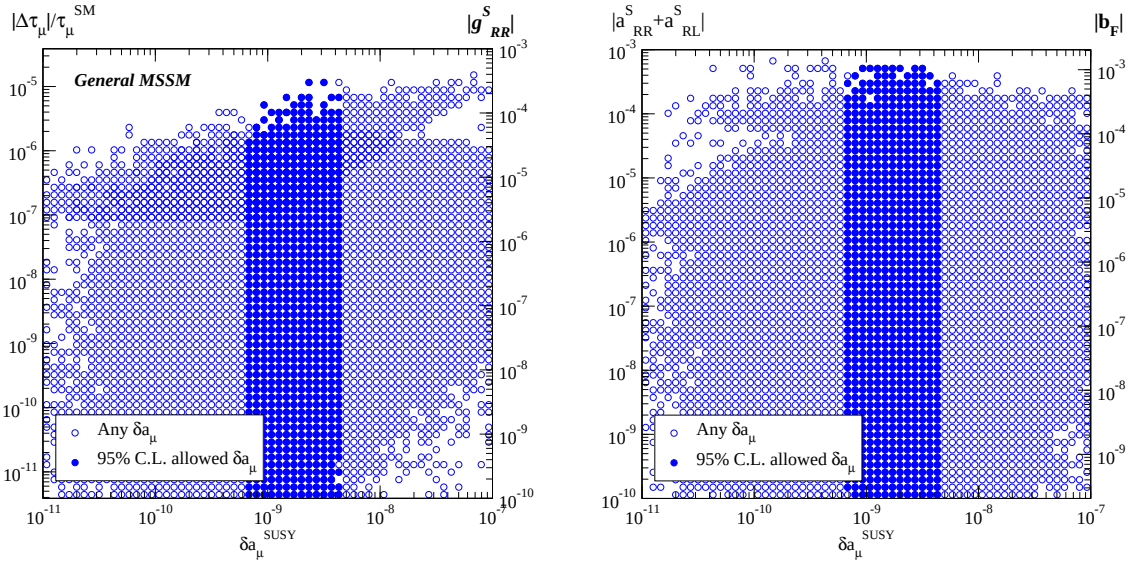


Figure 9.4: *A scatter plot showing $|\Delta\tau_\mu|/\tau_\mu^{\rm SM}$ (a) and $|g^S_{\rm RR}|$ (b), relative to muon decay, left, and $a^S_{\rm RR}+a^S_{\rm RL}$, relative to $\beta$ decay, right, as a function of the supersymmetric contribution to the muon anomalous magnetic moment $\delta a_\mu$. Filled circles represent models consistent with the current 95% C.L. range for beyond the standard model contributions to $(g_\mu-2)$, while empty circles denote all other models.*

trilinear scalar coupling sector, and scan independently over all the parameters indicated in Table 9.2, within the specified ranges. We indicate with $m_{\widetilde{F}}$ a generic scalar fermion soft mass (corresponding to a standard model fermion whose mass is $m_F$), and with $m_{\rm LSP}$ the smallest mass parameter entering the neutralino mass matrix (namely, $m_1, m_2$ and $\mu$), in absolute value. For all models, we impose constraints from direct supersymmetric-particles searches at accelerators, rare processes with a sizable potential supersymmetric contribution, the lower bound on the mass of the lightest $CP$-even Higgs boson, and precision electroweak tests. We also require the lightest supersymmetric particle (LSP) to be the lightest neutralino (see also [118] for more details) and avoid parameter choices that lead to tachyonic solutions.

We show the results of our scan in Fig. 9.4-9.6. In particular, we indicate in Fig. 9.4, (a), the values of $|\Delta\tau_\mu|/\tau_\mu^{\rm SM}$ (left axis) and $|g^S_{\rm RR}|$ (right axis) we obtained in our scan, as a function of the supersymmetric contribution to the muon anomalous magnetic moment, $\delta a_\mu$. Filled circles represent models consistent with the current 95% C.L. range for beyond

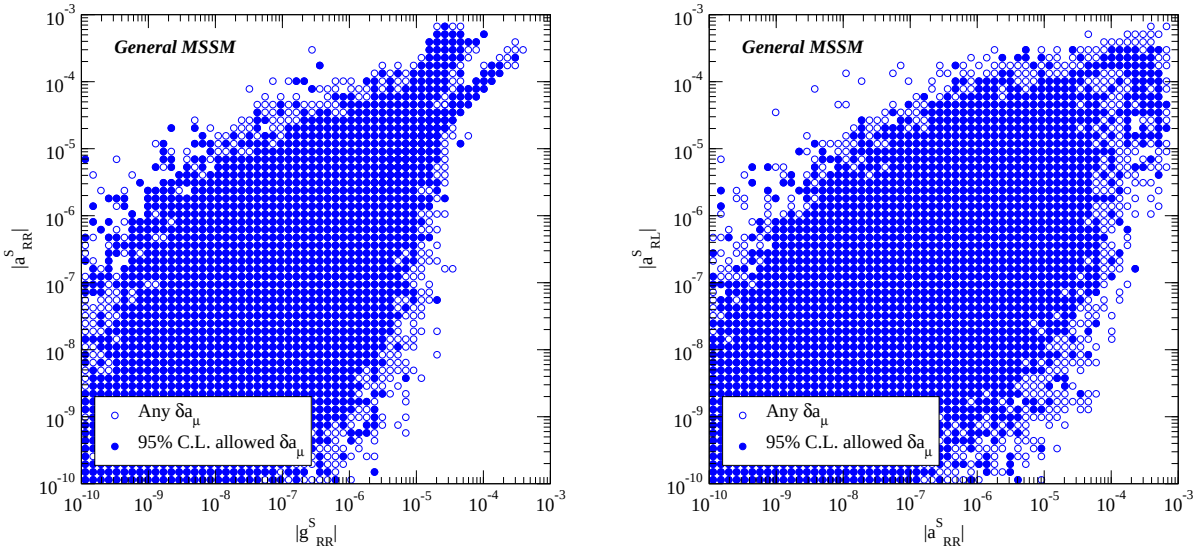


Figure 9.5: *The correlation between $a^S_{\rm RR}$ and $g^S_{\rm RR}$ (a) and between $a^S_{\rm RR}$ and $a^S_{\rm RL}$ (b). Filled circles represent models consistent with the current 95% C.L. range for beyond the standard model contributions to $(g_\mu - 2)$, while empty circles denote all other models.*

the standard model contributions to $(g_\mu - 2)$, while empty circles denote all other models. As we anticipated, large values of $\delta a_\mu$ do not always imply large $|g^S_{\rm RR}|$, and, vice-versa. The values of $|g^S_{\rm RR}|$ compatible with the limits on $(g_\mu - 2)$ and with all constraints on the supersymmetric setup can be as large as a few times $10^{-4}$, though the size of the effect could also be many orders of magnitude smaller. The models giving the largest effects tend to have large L-R mixing (and hence large trilinear scalar couplings) both in the smuon and in the selectron spectrum, and, naturally, a light supersymmetric particle spectrum. In contrast, assuming alignment between the triscalar and Yukawa matrices leads to unobservably small effects in $\mu$-decay.

Current limits on the parameter $g^S_{RR}$ obtained from direct studies of $\mu$-decay observables lead to an upper bound of $0.067$ according to the recent global analysis of Ref. [124]. Thus, improvements in precision by more than two orders of magnitude would be required to probe these non-$(V-A)\otimes(V-A)$ contributions in the large L-R mixing regime. On the other hand, the impact of $g^S_{RR}$ on the extraction of $G_\mu$ from the muon lifetime could become discernible at the level of precision of the muon lifetime measurements underway at PSI[97, 98]. These experiments expect to improve the precision on $\tau_\mu$ such that the

experimental error in $G_\mu$ is $10^{-6}$. At such a level, a contribution to $\eta$ from $g^S_{RR}$ of order $10^{-4}$ would begin to be of interest, as per Eq. (9.4). In particular, we note that there exist regions of the MSSM parameter space that generate contributions to $\Delta\tau_\mu/\tau_\mu$ as large as a few $\times 10^{-6}$ via the $\eta$ parameter in Eq. (9.4), corresponding to $\sim$ ppm corrections to $G_\mu$.

Consideration of this correction could be particularly interesting if future measurements at a facility such as GigaZ lead to comparable improvements in other electroweak parameters, such as $M_Z$ and $\sin^2\hat{\theta}_W(M_Z)$. A comparison of these quantities can provide a test of the SM (or MSSM) at the level of electroweak radiative corrections via the relation[125]

$$\sin^2\hat{\theta}_W(M_Z)\cos^2\hat{\theta}_W(M_Z) = \frac{\pi\alpha}{\sqrt{2}M_Z^2 G_\mu\left[1-\Delta\hat{r}(M_Z)\right]} \tag{9.42}$$

where $\Delta\hat{r}(M_Z)$ contains electroweak radiative corrections to the $(V-A)\otimes(V-A)$ $\mu$-decay amplitude, the $Z$-boson self energy, and the running of $\hat{\alpha}$. Any discrepancy in this relation could signal the presence of new physics contributions to $\Delta\hat{r}(M_Z)$ beyond those obtained in the SM (or MSSM). Inclusion of ppm corrections to $G_\mu$ arising from the presence of a non-zero $\eta$ in Eq. (9.4) would be important in using Eq. (9.42) to carry out a ppm self-consistency test. Resolution of other theoretical issues in the computation of $\Delta\hat{r}(M_Z)$ – such as hadronic contributions to the running of $\hat{\alpha}$ – would also be essential in performing such a test.

In the case of $\beta$-decay, we show the analogue of the figure described above for the muon decay, in Fig. 9.4, (b). We show, as a function of $\delta a_\mu$, the value of $a^S_{RR}+a^S_{RL}$. We find that values of $a^S_{RR}+a^S_{RL}$ as large as $10^{-3}$ are consistent with all phenomenological constraints. Since the amplitudes $\tilde{\delta}^{(a,b)}_\beta$ depend on L-R mixing among first, rather than second, generation sleptons and squarks (the factors $Z^{1i'}_L Z^{4i'\,*}_L$ and $Z^{1i\,*}_Q Z^{4i}_L$, $Q = U$ or $D$, respectively) the parameters $a^S_{RR}$, $a^S_{RL}$, and $a^T_{RL}$ are not as constrained by precision measurements as is $g^S_{RR}$. Thus, it is possible for the $\beta$-decay parameters to reach their naive, maximal scale $\alpha/4\pi$ in the limit of maximal L-R mixing.

The correlations between $g^S_{RR}$ and $a^S_{RR}$, and between $a^S_{RR}$ and $a^S_{RL}$, are shown in the panels (a) and (b), respectively, of Fig. 9.5. In the figure, again, filled circles represent models consistent with the current 95% C.L. range for beyond the standard model contri-

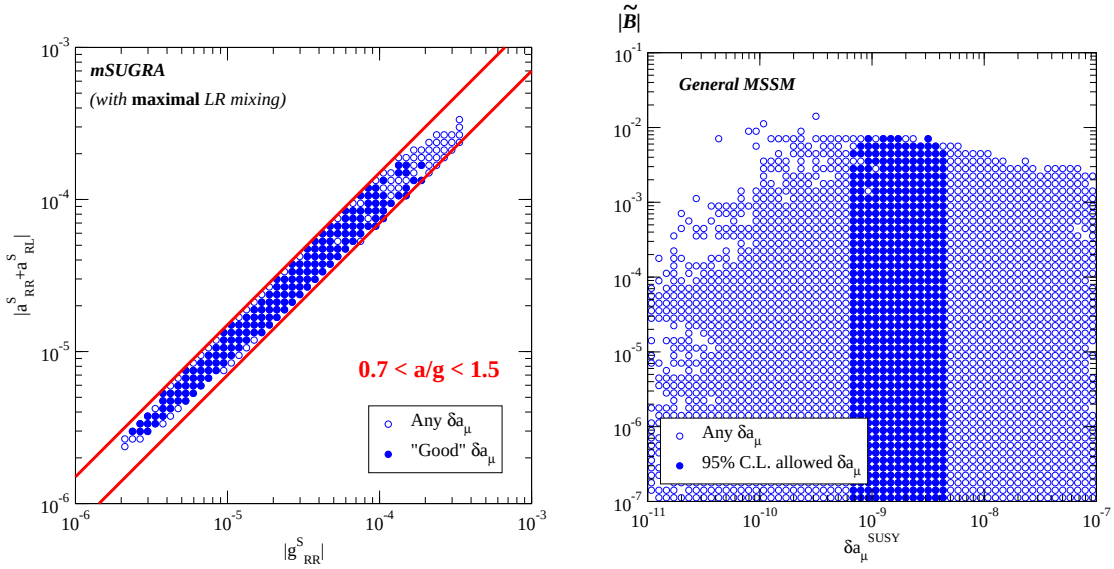


Figure 9.6: (a)*: The correlation between* $a^S_{\rm RR} + a^S_{\rm RL}$ *and* $g^S_{\rm RR}$ *in* "minimal supergravity" *models with maximal left-right mixing (i.e., where the trilinear scalar couplings have been set to the values corresponding to a maximal contribution to the quantities of interest). The scalar mass universality condition at the GUT scale dictates the strong correlation between the two quantities* $0.7 \lesssim (a^S_{\rm RR} + a^S_{\rm RL})/g^S_{\rm RR} \lesssim 1.5$. *Again, filled circles represent models consistent with the current 95% C.L. range for beyond the standard model contributions to* $(g_\mu - 2)$*, while empty circles denote all other models.* (b)*: MSSM-induced non-*$(V-A)\otimes(V-A)$ *contributions to the energy-dependence of the* $\beta$*-decay neutrino asymmetry parameter,* $B$*. Here, we have scaled out the energy-dependence and have plotted* $\tilde{B} = B/(\Gamma m/E)$ *for various randomly generated MSSM parameters. As before, dark circles indicate models consistent with* $(g_\mu - 2)$ *We have also assumed* $g_S/g_V = 1 = g_T/g_A$

butions to $(g_\mu - 2)$, while empty circles denote all other models. We notice that in general there exists no strong correlation among the various quantities, ane we find some correlation only for very large values of the quantities under investigation, in the upper right portions of the plots. Also, no hierarchy between $a^S_{RR}$ and $a^S_{RL}$ exists.

A correlation between the various quantities of interest does arise, however, when some priors are in place on the supersymmetric particle spectrum. In particular, we show the results of a scan of minimal supergravity models (where scalar soft breaking mass universality is imposed at the GUT scale) in Fig. 9.6 (a). In particular, we display on the vertical axis the values of $a^S_{RR} + a^S_{RL}$, and on the horizontal axis $g^S_{RR}$, for models where we imposed a maximal L-R mixing. In this case, we obtain that $0.7 \lesssim (a^S_{\rm RR} + a^S_{\rm RL})/g^S_{\rm RR} \lesssim 1.5$. In contrast to the model-independent parameter space scans, a nearly linear correlation be-

tween these parameters arises due to the mSUGRA-dependent relations between sfermion masses and requirement of maximal L-R mixing. Moreover, the magnitude of the $\beta$-decay couplings is generally less than $\lesssim 10^{-4}$ due to the $(g_\mu - 2)$ constraints on smuon masses and the mSUGRA sfermion mass relations. It is interesting to note that within this model scenario, the observation of a non-zero $\beta$-decay correlation at the $\sim 10^{-4}$ level would imply a non-zero $g^S_{RR}$ of similar magnitude, along with the corresponding correction to the theoretical $\mu$-decay rate.

In the more general, model-independent situation, it is important to emphasize that large L-R mixing in the first generation slepton and squark sectors can lead to $a^S_{RR}$, $a^S_{RL}$, and $a^T_{RL}$ as large as $\mathcal{O}(10^{-3})$. Coefficients of this magnitude could, in principle, be probed with a new generation of precision $\beta$-decay correlation studies. At present, the most precise tests of these quantities arises from superallowed Fermi nuclear $\beta$-decay, from which one obtains constraints on the Fierz interference coefficient $b_F = 0.0026(26)$ [126, 80]. For this transition one has

$$b_F = \pm \frac{2\, g_S}{g_V} \frac{a^S_{RL} + a^S_{RR}}{a^V_{LL}} \tag{9.43}$$

independent of the details of the nuclear matrix elements[4]. In Fig. 9.4, (b), we also show the quantity $b_F$ assuming $g_S/g_V = 1$ in the right-hand vertical axis. The present experimental sensitivity lies just above the upper end of the range of possible values of $b_F$.

It is also interesting to consider the recent global analysis of Ref. [109], where several different fits to $\beta$-decay data were performed. The fit most relevant to the presence analysis corresponds to "case 2" in that work, leading to bounds on the following quantities:

$$\begin{aligned} R_S &\equiv \frac{g_S}{g_V} \frac{a^S_{RL} + a^S_{RR}}{a^V_{LL}} \\ R_T &\equiv \frac{2\, g_T}{g_V} \frac{a^T_{RL}}{a^V_{LL}} \end{aligned} \tag{9.44}$$

In particular, including latest results for the neutron lifetime[127] that differs from the previous world average by six standard deviations leads to a non-zero $R_T$: $R_T = 0.0086(31)$ and $R_S = 0.00045(127)$ with $\chi^2/\mathrm{d.o.f.} = 1.75$. In contrast, excluding the new $\tau_n$ result

[4]Here, we have assumed all quantities are relatively real.

implies both tensor and scalar couplings consistent with zero. We note that SUSY box graphs could not account for tensor couplings of order one percent since the natural scale of the relevant correction – $\tilde{\delta}_{\beta}^{(b)}$ – is $\alpha/2\pi \sim 0.1\%$ in the case of maximal L-R mixing and SUSY masses of order $M_Z$ [see Eq. (9.27)]. Moreover, there exist no logarithmic or large $\tan\beta$ enhancements that could increase the magnitude of this amplitude over this scale.

Future improvements in experimental sensitivity by up to an order of magnitude could allow one to probe the MSSM-induced non-$(V-A)\otimes(V-A)$ contributions to the $\beta$-decay correlation coefficients in the regime of large L-R mixing. For example, future experiments using cold and ultracold neutrons could allow a determination of the energy-dependent component of the neutrino asymmetry parameter $B$ in polarized neutron decay at the level of a few $\times 10^{-4}$. As indicated by the scatter plot in Fig. 9.6 (b) – where we show the range of values for the energy-dependent part of the neutrino asymmetry – experiments with this level of sensitivity could probe well into the region of parameter space associated with large L-R mixing[128]. Similarly, prospects for significant improvements in the sensitivity to the Fierz interference term using nuclear decays at a new radioactive ion beam facility are under active consideration [129].

As with other low-energy, semileptonic observables, the theoretical interpretation of the $\beta$-decay correlation coefficients requires input from hadron structure theory. For example, the form factors that multiply the scalar and tensor couplings have not been determined experimentally, and there exists some latitude in theoretical expectations for these quantities. The current estimates are [107]

$$0.25 \lesssim g_S \lesssim 1 \qquad\qquad 0.6 \lesssim g_T \lesssim 2.3;. \tag{9.45}$$

These ranges derive from estimates for neutral current form factors assuming the quark model and spherically-symmetric wavefunctions [130]. In obtaining the dependence of $b_F$ and $B$ on MSSM parameters as in Figs. 9.4,9.6, we have assumed $g_S/g_V = 1 = g_T/g_A$, so the final sensitivities of correlation studies to MSSM-induced non-$(V-A)\otimes(V-A)$ interactions will depend on firm predictions for these ratios. Similarly, the effects of second class currents generated by the small violation of strong isospin symmetry in the SM

may generate $\beta$ energy-dependent contributions to the correlation coefficients that mimic the effects of the MSSM-induced scalar and tensor interactions discussed here. An analysis of these effects on the correlation coefficients $a$ and $A$ has been recently performed in Ref. [131]. To our knowledge, no such study has been carried out for the correlation coefficients of interest here. Carrying out such an analysis, as well as sharpening the theoretical expectations of Eq. (9.45), would clearly be important for the theoretical interpretation of future correlation studies.

## 9.5 Discussion

If supersymmetric particles are discovered at the LHC, it will be then important to draw predictions on a wide array of observables in order to determine the parameters that describe the superpartners interactions. As we have discussed above, precision studies of weak decay correlations may provide one avenue for doing so. In particular, such studies could probe a unique feature of SUSY not easily accessed elsewhere, namely, triscalar interactions involving first and second generation scalar fermions. The presence of triscalar interactions is implied by both purely supersymmetric Yukawa and bilinear components of the superpotential and by soft, SUSY-breaking triscalar interactions in the Lagrangian. The flavor and chiral structure of the latter are particularly vexing, since – in the MSSM – one has both a large number of *a priori* unknown parameters and – experimentally – a limited number of handles with which to probe them.

In light of this situation, it has been the common practice to rely on models that relate various parameters and reduce the number of inputs that must be determined from data. Conventionally, one makes the "alignment" assumption, wherein the soft-triscalar couplings for a given species of fermion are proportional to the corresponding Yukawa matrices. Under this assumption, one would expect the effects of soft triscalar interactions to be suppressed for the first and second generations. While the supersymmetric triscalar interactions are, indeed, proportional to the Yukawa couplings, the soft triscalar interactions need not be. As we have argued above, the study of weak decay correlations offer a means for testing this possibility experimentally.

The effects of triscalar couplings in weak decay correlations arise from one-loop graphs that generate scalar and tensor interactions. These interactions are forbidden in the SM CC interaction in the limit of massless fermions since it involves only LH fermions and since the scalar and tensor operators couple fields of opposite chirality. In the MSSM, such terms can arise via L-R mixing of virtual scalar fermions in one-loop box graphs, and this L-R mixing can be significant when the corresponding soft, triscalar couplings are unsuppressed. In the case of $\mu$-decay, additional contributions to scalar and tensor four-fermion operators can also be generated by flavor-mixing among same-chirality scalar leptons, but this flavor-mixing is highly constrained by LFV studies such as $\mu \rightarrow e\gamma$. Thus, for both $\mu$- and $\beta$-decay, observable, SUSY-induced scalar and tensor couplings can only be generated by flavor diagonal L-R mixing.

Probing these interactions would require improvements in precision of one- and two-orders of magnitude, respectively, for $\beta$-decay and $\mu$-decay correlation coefficients. Order of magnitude improvements for $\beta$-decay appear realistic, while the necessary advances for $\mu$-decay appear to be more daunting. On the other hand, if SUSY is discovered at the LHC, then considerations of SUSY-induced, four-fermion scalar interactions involving RH charged leptons may become necessary when extracting the Fermi constant from the muon lifetime. Doing so could become particularly important when ppm tests of electroweak symmetry become feasible.

# Chapter 10

# Conclusions

Electroweak-scale supersymmetry, if realized in nature, has many important implications for nuclear physics, particle physics, and cosmology. Supersymmetric electroweak baryogenesis may explain the origin of the baryon asymmetry. We studied how the charge transport dynamics of collisions and diffusion play an important role in determining the BAU. Gaugino, strong sphaleron, and third generation Yukawa interactions are the most important interactions that convert hypercharge, generated within the bubble wall, into left-handed quark and lepton charge that drives baryon number generation. We evaluated the gaugino and third generation Yukawa thermally-averaged interaction rates for decay and absorption processes in the plasma. We found:

- Gaugino interactions are generally in chemical equilibrium for gaugino masses $m_{\tilde{V}} \lesssim 1$ TeV. These interactions enforce superequilibrium — chemical equilibrium between a particle and its superpartner.

- Top Yukawa interactions are always in chemical equilibrium due to the large scattering rate $q_3\, H_u \leftrightarrow u_3\, g$. In addition, the decay process $\widetilde{H} \leftrightarrow \bar{q}_3\, t_R$ can be even larger, further enhancing chemical equilibrium.

- Bottom and tau Yukawa interactions can be in chemical equilibrium for large regions of parameter space. For example, the decay processes $H_d \leftrightarrow q_3 \bar{d}_3\, (\ell_3 \bar{e}_3)$ are in chemical equilibrium for $\tan\beta \gtrsim 5(15)$, and $m_A \lesssim 800$ GeV (600 GeV).

These interaction rates enter into the system of Boltzmann equations that governs the charge densities.

Next, we solved the Boltzmann equations for the charge densities. Our main result was to show how the resulting charge densities depend strongly on the inclusion of bottom and tau Yukawa interactions, which had been previously neglected. We found:

- Bottom Yukawa interactions suppress the conversion of charge from third generation quarks to the first and second generations, via strong sphalerons. Without bottom Yukawa interactions, strong sphalerons generate significant first and second generation left-handed quark charge.

- Bottom Yukawa interactions lead to a suppression of third generation left-handed quark charge when (i) $m_{\tilde{t}_R}$, $m_{\tilde{b}_R} \gtrsim 500$ GeV, or (ii) $m_{\tilde{t}_R} \simeq m_{\tilde{b}_R}$. Without bottom Yukawa interactions, this suppression does not occur.

- Tau Yukawa interactions allow for the generation of significant left-handed lepton charge; without them, no lepton charge is generated.

One interesting possibility that emerges is that the baryon asymmetry is "lepton-mediated," i.e., induced by left-handed lepton charge, rather than left-handed quarks, as previously considered. Phenomenologically, the baryon asymmetry in this scenario can differ in both magnitude and sign from what one would have computed neglecting these Yukawa interactions. To the extent that electric dipole moment searches and collider studies can give information about the CP-violating phases and supersymmetric spectrum, these interactions play a crucial in making connections with experiment.

Lastly, we investigated how supersymmetry can be studied experimentally through precision measurements of weak decays. Leptonic pion decay is sensitive to R-parity violation in the first and second generations, the mass splitting between left-handed electron and muon scalar superpartners, and the Higgsino-Wino spectrum. Deviations from the SM expectation in precision studies of muon and beta decays can arise for large tri-scalar, left-right mixing parameters. If a supersymmetric signal was observed through these tests, it would point to regions of supersymmetric parameter space beyond the minimal SUSY-breaking scenarios to which theoretical prejudice has been mostly confined.

# Appendix A

# From Green's Functions to Boltzmann Equations: an Overview of the Closed-Time-Path Formalism

The standard tool for discussing particle dynamics in the early universe is the Boltzmann equation. The purpose of this section is to show how to derive it using the Closed-Time-Path (CTP) formulation of quantum field theory, and apply these techniques to supersymmetric electroweak baryogenesis. The CTP formalism is a language of finite-temperature, non-equilibrium Green's functions. These propagators are powerful tools: they contain all the information about the dynamics of the theory — from the microscopic interactions to the macroscopic evolution of the thermal plasma. After a brief review of this formalism, we describe how to extract this information, and how our results related to standard treatments of the Boltzmann equation (see, e.g., Ref. [36]).

To be concrete, we will consider the example of a single complex scalar field $\varphi$, with Lagrangian

$$\mathcal{L} = |\partial_\mu \varphi|^2 - m_\varphi^2 |\varphi|^2 + \mathcal{L}_{\rm int} \ . \tag{A.1}$$

We define $f_\varphi(\mathbf{k}, \mathbf{X}, t)$ and $f_{\bar{\varphi}}(\mathbf{k}, \mathbf{X}, t)$ to be the particle and antiparticle distribution functions, for 3-momentum $\mathbf{k}$, position $\mathbf{X}$, and time $t \equiv X^0$. The distribution function for the charge density is $f \equiv f_\varphi - f_{\bar{\varphi}}$; its Boltzmann equation is

$$\frac{\partial f}{\partial t} + \frac{\mathbf{k}}{\omega_{\mathbf{k}}} \cdot \nabla_{\mathbf{X}} f = \mathcal{C}[f_\varphi, f_{\bar{\varphi}}] \ , \tag{A.2}$$

with collision term $\mathcal{C}$, a functional of $f_\varphi$ and $f_{\bar{\varphi}}$. (We have neglected Hubble expansion and external forces.)

Ultimately, it turns out that there are two classes of interactions that arise from the collision term in Eq. (A.2). First, there are the usual elastic and inelastic collisions of particles in the plasma. The interactions in Eqs. (2.26,2.27) are all of this type. The collision terms from these interactions are the usual thermally-averaged interaction rates; here, there is little benefit for using the CTP approach. Second, there are interactions that arise from the presence of the expanding bubble of broken electroweak symmetry, giving rise to a CP-violating source. Here, the CTP approach is essential.

## A.1 Closed-time-path Green's functions

At zero temperature, perturbation theory is essentially the study of time-ordered propagators, such as

$$G^t(x,y) = \left\langle \mathcal{T}\left\{\varphi_H(x)\,\varphi_H^\dagger(y)\right\}\right\rangle \ , \tag{A.3}$$

where $\varphi_H$ is the Heisenberg-picture field. The key difference when moving to finite temperature is that the expectation value in Eq. (A.3) is taken with respect, not to the vacuum, but to the thermal bath, an ensemble of states defined by a density matrix

$$\hat{\rho} \equiv \sum_n w_n |n_h\rangle\langle n_h| \ , \tag{A.4}$$

where the time-independent Heisenberg-picture states $|n_h\rangle$ have weight $w_n$.

Now, let us move to the interaction picture. First, the interaction-picture states $|n(t)\rangle$ are functions of time; we define the interaction states at time $t = -\infty$ to coincide with the Heisenberg states: $|n_-\rangle \equiv |n(-\infty)\rangle = |n_h\rangle$. The density matrix is $\hat{\rho} = \sum_n w_n |n_-\rangle\langle n_-|$. Second, the interaction fields $\varphi$ are related to their Heisenberg counterparts by the time-evolution operator $U$

$$\varphi_h(x) = U(x_0,-\infty)^\dagger\,\varphi(x)\,U(x^0,-\infty) \ . \tag{A.5}$$

The operator $U$ obeys the usual relations:

$$U(t_1,t_2) = U(t_2,t_1)^\dagger = U(t_2,t_1)^{-1} \tag{A.6}$$

and

$$U(t_1,t_2) = \mathcal{T}\left\{\exp\left(i\int_{t_1}^{t_2} dz^0 \int d^3z\ \mathcal{L}_{\rm int}(z)\right)\right\}\ . \tag{A.7}$$

With these relations, Eq. (A.3) becomes

$$\begin{aligned} G^t(x,y) &= \sum_n w_n \left\langle\, n_- \right| \mathcal{T}\left\{\exp\left[i\int d^4z\, \mathcal{L}_{\rm int}(z)\right]\right\}^\dagger \\ &\qquad \times \mathcal{T}\left\{\varphi(x)\,\varphi^\dagger(y)\exp\left[i\int d^4z\,\mathcal{L}_{\rm int}(z)\right]\right\} \left|\, n_-\right\rangle\ , \end{aligned} \tag{A.8}$$

where $\int d^4z = \int_{-\infty}^{\infty} dz^0 \int d^3z$. Reading from right to left, Eq. (A.8) corresponds to starting with the "in"-state $|n_-\rangle$, then time-evolving from $-\infty$ to $+\infty$, acting with the field operators at times $x^0$ and $y^0$ along the way, and lastly time-evolving from $+\infty$ back to $-\infty$, returning to the "in"-state. This time-contour, denoted $\mathcal{C}$, is the "closed time path"; it is closed in the sense that the contour begins and ends at $t = -\infty$, connecting "in"-states with "in"-states. Eq. (A.8) can then be succintly written as

$$\begin{aligned} G^t(x,y) &= \left\langle \mathcal{P}\left\{\varphi_+(x)\varphi_+^\dagger(y)\exp\left[i\int_{\mathcal{C}} d^4z\,\mathcal{L}_{\rm int}(z)\right]\right\}\right\rangle \\ &= \left\langle \mathcal{P}\left\{\varphi_+(x)\varphi_+^\dagger(y)\exp\left[i\int d^4z\,\left(\mathcal{L}_{\rm int}^{(+)}(z) - \mathcal{L}_{\rm int}^{(-)}(z)\right)\right]\right\}\right\rangle \end{aligned} \tag{A.9}$$

where $\mathcal{P}$ means *path*-ordering of fields along $\mathcal{C}$. In the second line, we have broken $\mathcal{C}$ into the sum of its two branches. The notation $\varphi_\pm(x)$ and $\mathcal{L}_{\rm int}^{(\pm)}(x)$ — itself a function of $\varphi_\pm(x)$ — denotes whether $x^0$ is on the time-increasing (+), or time-decreasing (–) branch of $\mathcal{C}$. The path-ordering prescription is to time-order the (+) fields, to anti-time-order ($\mathcal{T}^\dagger$) the (–) fields, and lastly to put all the (–) fields to the left of the (+) fields.

A perturbative evaluation of $G^t(x,y)$ proceeds similarly to zero-temperature field theory. Wick's theorem applies as usual, but with $\mathcal{P}$-ordering instead of $\mathcal{T}$-ordering. Therefore, we must consider not one but four different propagators, corresponding to all possible

path-ordering of $x^0$ and $y^0$ in $\langle\varphi(x)\varphi^\dagger(y)\rangle$:

$$
\begin{aligned}
G^>(x,y) &\equiv \left\langle \mathcal{P}\left\{\varphi_-(x)\,\varphi_+^\dagger(y)\right\}\right\rangle = \left\langle\,\varphi(x)\,\varphi^\dagger(y)\,\right\rangle && \text{(A.10a)}\\
G^<(x,y) &\equiv \left\langle \mathcal{P}\left\{\varphi_+(x)\,\varphi_-^\dagger(y)\right\}\right\rangle = \left\langle\,\varphi^\dagger(y)\,\varphi(x)\,\right\rangle && \text{(A.10b)}\\
G^t(x,y) &\equiv \left\langle \mathcal{P}\left\{\varphi_+(x)\,\varphi_+^\dagger(y)\right\}\right\rangle = \left\langle\,\mathcal{T}\left\{\varphi(x)\,\varphi^\dagger(y)\right\}\,\right\rangle && \text{(A.10c)}\\
&= \theta(x^0-y^0)\,G^>(x,y) + \theta(y^0-x^0)\,G^<(x,y)\\
G^{\bar t}(x,y) &\equiv \left\langle \mathcal{P}\left\{\varphi_-(x)\,\varphi_-^\dagger(y)\right\}\right\rangle = \left\langle\,\mathcal{T}^\dagger\left\{\varphi(x)\,\varphi^\dagger(y)\right\}\,\right\rangle && \text{(A.10d)}\\
&= \theta(y^0-x^0)\,G^>(x,y) + \theta(x^0-y^0)\,G^<(x,y)\;.
\end{aligned}
$$

These Green's functions are the free or full propagators for fields in the interaction- or Heisenberg-pictures, respectively. In particular, we see from Eq. (A.9) that a perturbative expansion of $G^t(x,y)$ will necessarily involve contracting (+) and (–) fields together (i.e., those contained in $\mathcal{L}_{\rm int}^{(-)}$); these additional propagators are inescapable. These propagators can be assembled into the matrix

$$
\widetilde{G}(x,y) \equiv \begin{pmatrix} G^t(x,y) & -G^<(x,y) \\ G^>(x,y) & -G^{\bar t}(x,y) \end{pmatrix}\;. \qquad \text{(A.11)}
$$

In this form, the propagators have the simple perturbative expansion

$$
\begin{aligned}
\widetilde{G}(x,y) &= \widetilde{G}^{(0)}(x,y) + \int d^4w \int d^4z \left(\widetilde{G}^{(0)}(x,z)\;\widetilde{\Pi}(z,w)\;\widetilde{G}(w,y)\right) && \text{(A.12a)}\\
\widetilde{G}(x,y) &= \widetilde{G}^{(0)}(x,y) + \int d^4w \int d^4z \left(\widetilde{G}(x,z)\;\widetilde{\Pi}(z,w)\;\widetilde{G}^{(0)}(w,y)\right)\;. && \text{(A.12b)}
\end{aligned}
$$

These equations are the CTP version of the Schwinger-Dyson equations, where now both the propagator and the self-energy $\widetilde{\Pi}$ (defined by $\mathcal{L}_{\rm int}$) are $2\times 2$ matrices. The free propagator $\widetilde{G}^{(0)}(x,y)$ satisfies

$$
\left(\partial_x^2 + m_\varphi^2\right)\,\widetilde{G}^{(0)}(x,y) = \left(\partial_y^2 + m_\varphi^2\right)\,\widetilde{G}^{(0)}(x,y) = -i\,\delta^4(x-y)\,\widetilde{I}\;, \qquad \text{(A.13)}
$$

where $\widetilde{I}$ denotes the $2\times 2$ identity matrix in CTP propagator space.

In vacuum, the Green's functions $G^{<,>}(x,y)$ depend only on the relative coordinate $r \equiv x - y$, through plane wave factors $e^{\pm ik\cdot r}$, with frequency $\omega_{\mathbf{k}}$ and wavelength $|\mathbf{k}|^{-1}$. At finite temperature, however, expectation values are taken with respect to the thermal plasma. The plasma itself is dynamical — namely, distribution functions for species in the plasma depend on spacetime — so $G^{<,>}(x,y)$ depends also the average coordinate $X = (x+y)/2$. The Wigner transform, defined as

$$G^{<,>}(k,X) = \int d^4r\, e^{ik\cdot r}\, G^{<,>}(x,y)\ , \tag{A.14}$$

naturally separates the microscopic dynamics (relevant over scales $\omega_{\mathbf{k}}^{-1}$, $|\mathbf{k}|^{-1} \sim \mathcal{O}(T^{-1})$) from the macroscopic evolution of the plasma. This separation between macro- and microscopic scales is valid only as long as the plasma dynamics is characterized by scales much longer than $T^{-1}$. In our analysis, we rely upon this separation of scales to perform a gradient expansion; formally denoted as an expansion in $\partial_X$, it is essentially an expansion in the ratio of micro- to macroscopic scales.

The Wigner-transformed propagators in Eq. (A.14) are the functions of primary interest. In particular, we define the function

$$F(k,X) \equiv \frac{1}{2}\ (\, G^{>}(k,X) + G^{<}(k,X)\,)\ . \tag{A.15}$$

The CP-asymmetric distribution function $f = f_\varphi - f_{\bar\varphi}$ from Eq. (A.2) is

$$f(\mathbf{k},X) = \int \frac{dk^0}{2\pi}\, 2\,k^0 F(k,X)\ . \tag{A.16}$$

In addition, we can define "moments" of this distribution function. The zeroth moment is the charge density

$$n(X) \equiv \int \frac{d^3k}{(2\pi)^3}\, f(\mathbf{k},X) = \int \frac{d^4k}{(2\pi)^4}\, 2\,k^0 F(k,X)\ , \tag{A.17}$$

the difference between particle and antiparticle densities. The first moment is the charge

current

$$\mathbf{j}(X) \equiv \int \frac{d^3k}{(2\pi)^3} \frac{\mathbf{k}}{\omega_{\mathbf{k}}} f(\mathbf{k}, X) = \int \frac{d^4k}{(2\pi)^4} 2\,\mathbf{k}\, F(k, X) \ . \tag{A.18}$$

Justification of these relations follows from the fact that

$$\int \frac{d^4k}{(2\pi)^4} 2\, k^\mu\, F(k, X) = i \left\langle : \varphi^\dagger(X) \overset{\leftrightarrow}{\partial}{}^\mu_X \varphi(X) : \right\rangle \ , \tag{A.19}$$

using equations (A.10, A.15). The normal-ordered combination of fields on the RHS is precisely the current $j^\mu(X) \equiv (n, \mathbf{j})^\mu$. Lastly, the second moment is a velocity flux tensor

$$V_{ab}(X) \equiv \int \frac{d^3k}{(2\pi)^3} \frac{k_a\, k_b}{\omega^2_{\mathbf{k}}} f(\mathbf{k}, X) = \int \frac{d^4k}{(2\pi)^4} 2\, \frac{k_a k_b}{k^0} F(k, X) \ , \tag{A.20}$$

with spatial indeces $a, b = 1, 2, 3$. In what follows, our goal is to derive and solve a Boltzmann equation for $F(k, X)$.

## A.2 Spectral functions

In the preceeding section, we described the formulation of CTP propagators, and how they are related to the charge current density $j^\mu(X)$ for a complex scalar field $\varphi$. Before we derive the Boltzmann equation, we now show how the Wigner-transformed propagators $G^{<,>}(k, X)$ contain the microscopic information about the spectrum of excitations in the plasma. We will see that $G^{<,>}(k, X)$ is proportional to a spectral function that vanishes unless the appropriate dispersion relation is satisfied.

We begin with the Schwinger-Dyson equations (A.12). Acting with the Klein-Gordon operator on the full propagator, we have

$$\left(\partial_x^2 + m_\varphi^2\right) G^\lambda(x, y) = -i \int d^4z \left[\ \widetilde{\Pi}(x, z)\, \widetilde{G}(z, y) \right]^\lambda \tag{A.21a}$$

$$\left(\partial_y^2 + m_\varphi^2\right) G^\lambda(x, y) = -i \int d^4z \left[\ \widetilde{G}(x, z)\ \widetilde{\Pi}(z, y) \right]^\lambda \ , \tag{A.21b}$$

where $\lambda = <$ or $>$. Taking the Wigner transform of the sum of Eqs. (A.21), we have

$$\left(k^2 - m_\varphi^2 - \frac{1}{4}\,\partial_X^2\right)\, G^\lambda(k,X) = \frac{i}{2}\int d^4r\; e^{-ik\cdot r}\int d^4z\left[\;\widetilde{\Pi}(x,z)\,\widetilde{G}(z,y) + \widetilde{G}(x,z)\;\widetilde{\Pi}(z,y)\;\right]^\lambda \tag{A.22}$$

This is the "constraint equation"; it determines the spectra of the degrees of freedom of $\varphi$. The free propagator satisfies (setting $\widetilde{\Pi} = 0$ and neglecting the $\partial_X^2$ term)

$$\left(k^2 - m_\varphi^2\right)\, G^\lambda(k,X)^{(0)} = 0\;. \tag{A.23}$$

The free propagators $G^{<,>}(k,X)^{(0)}$ are non-zero only if the appropriate dispersion relation $k^0 = \pm\sqrt{|\mathbf{k}|^2 + m^2}$ is satisfied. Therefore, they are proportional to the free spectral function

$$\rho^{(0)}(k) = 2\pi\,\mathrm{sign}(k^0)\;\delta(k^2 - m_\varphi^2)\;. \tag{A.24}$$

Let us consider how $\rho(k)$ is modified in the presence of interactions by studying a simple example:

$$\mathcal{L}_{\rm int}(x) = -\,\frac{\lambda}{4}\,\big|\,\varphi(x)\big|^4\quad. \tag{A.25}$$

With this interaction, the self energy is

$$\widetilde{\Pi}(x,y) = i\,\lambda\,\delta^4(x-y)\begin{pmatrix} G^t(x,y) & 0 \\ 0 & G^{\bar{t}}(x,y)\end{pmatrix}\;. \tag{A.26}$$

Plugging into Eqn. (A.22), we have

$$\left(k^2 - m_\varphi^2 - \frac{1}{4}\,\partial_X^2\right)\, G^\lambda(k,X) = \frac{\lambda}{2}\int d^4r\, e^{-ik\cdot r}\,\Big(\,G^t(x,x) + G^t(y,y)\,\Big)\;G^\lambda(x,y)\;. \tag{A.27}$$

Now, by Taylor expanding

$$G^t(x,x) + G^t(y,y) = 2\,G^t(X,X) + \frac{1}{4}\frac{\partial^2 G^t(X,X)}{\partial X^\mu \partial X^\nu}\,r^\mu\,r^\nu + \mathcal{O}(\partial_X^4)\;, \tag{A.28}$$

we have at linear order in $\lambda$

$$\left(k^2 - m_\varphi^2 - \lambda\, G^t(X,X)\right)\; G^\lambda(k,X) = 0\;, \tag{A.29}$$

neglecting $\mathcal{O}(\partial_X^2)$ terms. (We return to these terms later.) The effect at $\mathcal{O}(\lambda)$ is a shift in the pole of the spectral function. Later, we will be able to evaluate this shift more explicitly; in the relativistic limit, and assuming an equilibrium distribution for $\varphi$, it has the familiar form

$$\lambda\, G^t(X,X) = \frac{\lambda}{12}\, T^2 + \int \frac{d^3p}{(2\pi)^3} \frac{1}{\omega_{\mathbf{p}}}\;. \tag{A.30}$$

The first term is the usual one-loop thermal mass, while the second term is the usual zero-temperature ultraviolet divergence that must be removed through renormalization. This is a simple example for how the spectral function is modified at one-loop and at finite temperature; other interactions can affect $\rho(k)$ in more complicated ways. For example, massless fermions develop a non-analytic dispersion relation, including the propagation of hole modes [43]; or, particles can develop a non-zero decay width. For the purposes of evaluating collision rates of particles in the plasma, the dominant corrections to the spectral function are the finite-temperature masses.

Therefore, we can write

$$G^>(k,X) \;=\; \rho(k)\, g^>(k,X) \tag{A.31a}$$

$$G^<(k,X) \;=\; \rho(k)\, g^<(k,X) \tag{A.31b}$$

where $\rho(k)$ is the one-loop spectral function. Furthermore, the canonical commutation relations

$$\left\langle \left[\varphi(t,\mathbf{x}),\, \dot\varphi^\dagger(t,\mathbf{y})\right]\right\rangle = -\left\langle \left[\dot\varphi(t,\mathbf{x}),\, \varphi^\dagger(t,\mathbf{y})\right]\right\rangle = i\,\delta^3(\mathbf{x}-\mathbf{y}) \tag{A.32}$$

imply that $g^>(k,X) - g^<(k,X) = 1$. Thus, finally, we have

$$G^>(k,X) \;=\; \rho(k)\,(1 + g(k,X)) \tag{A.33a}$$

$$G^<(k,X) \;=\; \rho(k)\, g(k,X) \tag{A.33b}$$

and

$$F(k,X) = \rho(k)\,\left(\frac{1}{2} + g(k,X)\right)\,. \tag{A.34}$$

To summarize, we have shown that the Wigner-transformed propagators $G^{<,>}(k,X)$ can be written in terms of the spectral function $\rho(k)$ and the distribution function $g(k,X)$. The form of the $\rho(k,X)$ follows from the constraint equation, and agrees with our expectations for free and 1-loop spectral functions. In the next section, we show how to solve for $g(k,X)$ by solving the Boltzmann equation. Once we know $g(k,X)$, we can evaluate the $F(k,X)$ in (A.34).

## A.3 Quantum Boltzmann equation

We now show how the Boltzmann equation emerges in the CTP formalism. The Boltzmann equation will allow us to solve for the dynamical evolution of the distribution function $g(k,X)$ in the presence of collisions and a CP-violating source. Let us begin by taking the Wigner transform of the difference of Eqs. (A.21). Thus we obtain the "kinetic equations"

$$2k\cdot\partial_X G^{\lambda}(k,X) = \mathcal{C}[g;\,k,X]^{\lambda}\,, \tag{A.35}$$

where $\lambda = <$ or $>$, and

$$\mathcal{C}[g;\,k,X]^{\lambda} = \int d^4r\, e^{ik\cdot r}\int d^4z\,\Big[\,\widetilde{\Pi}\,(x,z)\;\widetilde{G}\,(z,y) - \widetilde{G}\,(x,z)\;\widetilde{\Pi}\,(z,y)\,\Big]^{\lambda}\,. \tag{A.36}$$

Furthermore, we have

$$2k\cdot\partial_X F(k,X) = \mathcal{C}[g;\,k,X]\,, \tag{A.37}$$

defining $\mathcal{C}\equiv(\mathcal{C}^{>}+\mathcal{C}^{<})/2$. Eq. (A.37) is the CTP analog of the usual Boltzmann equation. Indeed, Eq. (A.2) follows upon integrating by $\int dk^0$.

The collision term, to zeroth order in gradients, has the simple form

$$\mathcal{C}[g;\,k,X]^{>} = \mathcal{C}[g;\,k,X]^{<} = \Pi^{>}(k,X)\,G^{<}(k,X) - \Pi^{<}(k,X)\,G^{>}(k,X)\,. \tag{A.38}$$

In writing Eq. (A.38), we have neglected terms proportional to $\partial_X G^{<,>}(k,X)$ and $\partial_X \Pi^{<,>}(k,X)$, as per the gradient expansion. There are two general classes of interactions that enter into the collision term: those that conserve $\varphi$-charge, and those that do not. The former lead to kinetic equilibrium of $\varphi$, while the latter lead to chemical equilibration of $\varphi$ with other species in the plasma. Therefore, we write $\mathcal{C} = \mathcal{C}_{\rm kin} + \mathcal{C}_{\rm ch}$ to distinguish these two classes. To be pedegogical, we will now evaluate explicitly an example for each.

First, let us consider the $|\varphi|^4$-interaction in Eq. (A.25). This collision term describes elastic scattering of $\varphi$ and $\bar{\varphi}$ in the thermal plasma, causing them to reach kinetic equilibrium. We must compute the 2PI contribution to $\widetilde{\Pi}$, arising from the diagram in Fig. We have

$$\Pi^{<,>}(x,y) = -\frac{\lambda^2}{2}\, G^{<,>}(x,y)\, G^{<,>}(x,y)\, G^{>,<}(y,x)\ . \tag{A.39}$$

The Wigner transform is

$$\begin{aligned}\Pi^{<,>}(k,X) = \left(\prod_{i=1}^{3}\int\frac{d^4p_i}{(2\pi)^4}\right)(2\pi)^4\,\delta^4(k+p_1-p_2-p_3) \\ \times\ G^{>,<}(p_1,X)\, G^{<,>}(p_2,X)\ G^{<,>}(p_3,X)\ .\end{aligned} \tag{A.40}$$

This contribution to the collision term is

$$\begin{aligned}\mathcal{C}_{\rm kin}[g;\,k,X] \;=\; & -\frac{\lambda^2}{2}\left(\prod_{i=1}^{3}\int\frac{d^4p_i}{(2\pi)^4}\,\rho(p_i,X)\right)(2\pi)^4\,\delta^4(k+p_1-p_2-p_3)\,\rho(k,X) \\ & \times\Big[\, g(k,X)\, g(p_1,X)\,(1+g(p_2,X))\,(1+g(p_3,X)) \\ & \quad -(1+g(k,X))\,(1+g(p_1,X))\, g(p_2,X)\, g(p_3,X)\,\Big]\ .\end{aligned} \tag{A.41}$$

This form is indeed reminiscent of the collision term in the usual treatment. There is the momentum conserving $\delta$-function, the $\lambda^2$ is the matrix element squared, and the terms in square brackets are familiar combination of distribution functions for a $2 \to 2$ scattering process.

Second, we consider an interaction that leads to chemical equilibrium. Suppose that $\varphi$

is coupled to complex scalars $\chi_{1,2}$ by

$$\mathcal{L}_{\rm int} = h\,\varphi\,\chi_1^\dagger\,\chi_2 + \text{h.c.} \tag{A.42}$$

with coupling constant $h$. The self-energy for this interaction is

$$\Pi^{>,<}(x,y) = -|h|^2\,G^{>,<}_{\chi_1}(x,y)\,G^{<,>}_{\chi_2}(y,x)\ , \tag{A.43}$$

with

$$G^<_{\chi_i}(p,X) = \rho_{\chi_i}(p)\,g_{\chi_i}(p,X)\ . \tag{A.44}$$

This interaction gives

$$\begin{aligned} C_{\rm ch}[g;\,k,X] \;=\; & -h^2\int\frac{d^4p}{(2\pi)^4}\int\frac{d^4q}{(2\pi)^4}\,\rho_\varphi(k,X)\,\rho_{\chi_1}(p,X)\,\rho_{\chi_2}(q,X) \\ & \times\,(2\pi)^4\,\delta^4(k-p+q)\,\Big[\,g_\varphi(k,X)\,(1+g_{\chi_1}(p,X))\,g_{\chi_2}(q,X) \\ & -\,(1+g_\varphi(k,X))\,g_{\chi_1}(p,X)\,(1+g_{\chi_2}(q,X))\Big]\ , \end{aligned} \tag{A.45}$$

which is the usual collision term for decay and inverse decay processes. We have added subscripts to $\rho$ and $g$ to clarify the species to which they correspond.

Now that we have evaluated some collision terms, it is clear why the gradient expansion is valid. According to the kinetic equation, $\partial^\mu_X G^<(k,X)$ is $\mathcal{O}(\epsilon)$, where $\epsilon$ generically denotes the square of a coupling constant (i.e. $\epsilon=\lambda^2$ or $h^2$). Therefore, our expansion in $\partial_X$ in both the constraint equation (A.22) and the collision term (A.38) corresponds to an expansion in $\epsilon$.

# Bibliography


[1] W. M. Yao *et al.* [Particle Data Group], J. Phys. G **33** (2006) 1.

[2] J. Dunkley *et al.* [WMAP Collaboration], arXiv:0803.0586 [astro-ph].

[3] S. Weinberg, *Oxford, UK: Oxford Univ. Pr. (2008) 593 p*

[4] S. Hannestad, Phys. Rev. D **70**, 043506 (2004) [arXiv:astro-ph/0403291].

[5] P. Picozza *et al.*, Astropart. Phys. **27**, 296 (2007) [arXiv:astro-ph/0608697].

[6] A. D. Sakharov, Pisma Zh. Eksp. Teor. Fiz. **5**, 32 (1967) [JETP Lett. **5**, 24 (1967)].

[7] M. E. Shaposhnikov, Nucl. Phys. B **287** (1987) 757.

[8] M. E. Shaposhnikov, Nucl. Phys. B **299** (1988) 797.

[9] M. Quiros, arXiv:hep-ph/9901312.

[10] G. 't Hooft, Phys. Rev. Lett. **37** (1976) 8.

[11] G. 't Hooft, Phys. Rev. D **14** (1976) 3432 [Erratum-ibid. D **18** (1978) 2199].

[12] N. S. Manton, Phys. Rev. D **28**, 2019 (1983).

[13] F. R. Klinkhamer and N. S. Manton, Phys. Rev. D **30** (1984) 2212.

[14] V. A. Kuzmin, V. A. Rubakov and M. E. Shaposhnikov, Phys. Lett. B **155**, 36 (1985).

[15] M. E. Shaposhnikov, JETP Lett. **44** (1986) 465 [Pisma Zh. Eksp. Teor. Fiz. **44** (1986) 364].

[16] A. G. Cohen, D. B. Kaplan and A. E. Nelson, Phys. Lett. B **336**, 41 (1994) [arXiv:hep-ph/9406345].

[17] M. B. Gavela, P. Hernandez, J. Orloff, O. Pene and C. Quimbay, Nucl. Phys. B **430**, 382 (1994) [arXiv:hep-ph/9406289]; P. Huet and E. Sather, Phys. Rev. D **51**, 379 (1995) [arXiv:hep-ph/9404302]; T. Konstandin, T. Prokopec and M. G. Schmidt, Nucl. Phys. B **679** (2004) 246 [arXiv:hep-ph/0309291].

[18] M. Pospelov and A. Ritz, Annals Phys. **318**, 119 (2005) [arXiv:hep-ph/0504231].

[19] G. F. Giudice and M. E. Shaposhnikov, Phys. Lett. B **326**, 118 (1994) [arXiv:hep-ph/9311367].

[20] P. Huet and A. E. Nelson, Phys. Rev. D **53**, 4578 (1996) [arXiv:hep-ph/9506477].

[21] J. M. Cline, M. Joyce and K. Kainulainen, JHEP **0007** (2000) 018 [arXiv:hep-ph/0006119].

[22] C. Lee, V. Cirigliano and M. J. Ramsey-Musolf, Phys. Rev. D **71**, 075010 (2005) [arXiv:hep-ph/0412354].

[23] V. Cirigliano, M. J. Ramsey-Musolf, S. Tulin and C. Lee, Phys. Rev. D **73**, 115009 (2006) [arXiv:hep-ph/0603058].

[24] D. J. H. Chung, B. Garbrecht, M. J. Ramsey-Musolf and S. Tulin, arXiv:0808.1144 [hep-ph].

[25] K. c. Chou, Z. b. Su, B. l. Hao and L. Yu, Phys. Rept. **118** (1985) 1.

[26] A. Fick, Phil. Mag. **10**, 20 (1855).

[27] A. Fick, Poggendorff's Annel. Physik. **94**, 59 (1855).

[28] M. Joyce, T. Prokopec and N. Turok, Phys. Lett. B **338** (1994) 269 [arXiv:hep-ph/9401352].

[29] M. Joyce, T. Prokopec and N. Turok, Phys. Rev. D **53**, 2930 (1996) [arXiv:hep-ph/9410281].

[30] M. S. Carena, M. Quiros, A. Riotto, I. Vilja and C. E. M. Wagner, Nucl. Phys. B **503** (1997) 387 [arXiv:hep-ph/9702409].

[31] A. Riotto, Phys. Rev. D **58**, 095009 (1998) [arXiv:hep-ph/9803357].

[32] M. S. Carena, J. M. Moreno, M. Quiros, M. Seco and C. E. M. Wagner, Nucl. Phys. B **599**, 158 (2001) [arXiv:hep-ph/0011055].

[33] M. S. Carena, M. Quiros, M. Seco and C. E. M. Wagner, Nucl. Phys. B **650**, 24 (2003) [arXiv:hep-ph/0208043].

[34] T. Konstandin, T. Prokopec and M. G. Schmidt, Nucl. Phys. B **716** (2005) 373 [arXiv:hep-ph/0410135]; T. Konstandin, T. Prokopec, M. G. Schmidt and M. Seco, Nucl. Phys. B **738**, 1 (2006) [arXiv:hep-ph/0505103].

[35] We consider the relaxation of these assumptions in D. J. H. Chung, B. Garbrecht, M. J. Ramsey-Musolf, S. Tulin, in preparation.

[36] E. W. Kolb and M. S. Turner, "The Early universe," Front. Phys. **69**, 1 (1990).

[37] L. J. Hall, R. Rattazzi and U. Sarid, Phys. Rev. D **50**, 7048 (1994) [arXiv:hep-ph/9306309].

[38] M. S. Carena, S. Mrenna and C. E. M. Wagner, Phys. Rev. D **60**, 075010 (1999) [arXiv:hep-ph/9808312]. M. S. Carena, M. Olechowski, S. Pokorski and C. E. M. Wagner, Nucl. Phys. B **426**, 269 (1994) [arXiv:hep-ph/9402253]. D. M. Pierce, J. A. Bagger, K. T. Matchev and R. j. Zhang, Nucl. Phys. B **491**, 3 (1997) [arXiv:hep-ph/9606211].

[39] J. M. Moreno, M. Quiros and M. Seco, Nucl. Phys. B **526**, 489 (1998) [arXiv:hep-ph/9801272].

[40] J. M. Moreno, M. Quiros and M. Seco, Nucl. Phys. B **526**, 489 (1998) [arXiv:hep-ph/9801272]. P. John and M. G. Schmidt, Nucl. Phys. B **598**, 291 (2001) [Erratum-ibid. B **648**, 449 (2003)] [arXiv:hep-ph/0002050]. G. D. Moore, JHEP **0003**, 006 (2000) [arXiv:hep-ph/0001274]. F. Csikor, Z. Fodor, P. Hegedus, A. Jakovac, S. D. Katz and A. Piroth, Phys. Rev. Lett. **85**, 932 (2000) [arXiv:hep-ph/0001087].

[41] N. Rius and V. Sanz, Nucl. Phys. B **570**, 155 (2000) [arXiv:hep-ph/9907460].

[42] G. D. Moore, Phys. Lett. B **412**, 359 (1997) [arXiv:hep-ph/9705248].

[43] H. A. Weldon, Phys. Rev. D **26**, 2789 (1982).

[44] D. Bodeker, G. D. Moore and K. Rummukainen, Phys. Rev. D **61**, 056003 (2000).

[45] Y. Li, S. Profumo and M. Ramsey-Musolf, arXiv:0811.1987 [hep-ph].

[46] M. Carena, G. Nardini, M. Quiros and C. E. M. Wagner, arXiv:0809.3760 [hep-ph].

[47] M. S. Carena, M. Quiros and C. E. M. Wagner, Phys. Lett. B **380**, 81 (1996) [arXiv:hep-ph/9603420].

[48] P. Elmfors, K. Enqvist, A. Riotto and I. Vilja, Phys. Lett. B **452**, 279 (1999) [arXiv:hep-ph/9809529].

[49] S. J. Huber and M. G. Schmidt, Nucl. Phys. B **606**, 183 (2001) [arXiv:hep-ph/0003122].

[50] A. Menon, D. E. Morrissey and C. E. M. Wagner, Phys. Rev. D **70**, 035005 (2004) [arXiv:hep-ph/0404184].

[51] S. J. Huber, T. Konstandin, T. Prokopec and M. G. Schmidt, Nucl. Phys. B **757**, 172 (2006) [arXiv:hep-ph/0606298].

[52] S. P. Martin, arXiv:hep-ph/9709356.

[53] K. Kajantie, M. Laine, K. Rummukainen and M. E. Shaposhnikov, Phys. Rev. Lett. **77**, 2887 (1996) [arXiv:hep-ph/9605288].

[54] J. Erler and M. J. Ramsey-Musolf, Prog. Part. Nucl. Phys. **54** (2005) 351 [arXiv:hep-ph/0404291].

[55] M. J. Ramsey-Musolf, AIP Conf. Proc. **842** (2006) 661 [arXiv:hep-ph/0603023].

[56] M. J. Ramsey-Musolf, arXiv:nucl-th/0608035.

[57] A. Kurylov and M. J. Ramsey-Musolf, Phys. Rev. Lett. **88**, 071804 (2002) [arXiv:hep-ph/0109222].

[58] S. Profumo, M. J. Ramsey-Musolf and S. Tulin, arXiv:hep-ph/0608064.

[59] A. Kurylov, M. J. Ramsey-Musolf and S. Su, Phys. Rev. D **68** (2003) 035008 [arXiv:hep-ph/0303026].

[60] J. Hisano, T. Moroi, K. Tobe and M. Yamaguchi, Phys. Rev. D **53** (1996) 2442 [arXiv:hep-ph/9510309].

[61] M. J. Ramsey-Musolf and S. Su, arXiv:hep-ph/0612057.

[62] D. A. Bryman, Comments Nucl. Part. Phys. **21**, 101 (1993).

[63] W. J. Marciano and A. Sirlin, Phys. Rev. Lett. **71**, 3629 (1993).

[64] R. Decker and M. Finkemeier, Nucl. Phys. B **438**, 17 (1995) [arXiv:hep-ph/9403385].

[65] V. Cirigliano and I. Rosell, JHEP **0710**, 005 (2007) [arXiv:0707.4464 [hep-ph]].

[66] V. Cirigliano and I. Rosell, Phys. Rev. Lett. **99**, 231801 (2007) [arXiv:0707.3439 [hep-ph]].

[67] D. I. Britton *et al.*, Phys. Rev. D **46**, 885 (1992).

[68] G. Czapek *et al.*, Phys. Rev. Lett. **70**, 17 (1993).

[69] T. Numao and D. A. Bryman [PIENU collaboration], future experiment, https://www.pienu.triumpf.ca.

[70] D. Počanić and A. van der Shaaf [PEN collaboration], future experiment, http://pen.phys.virginia.edu/.

[71] B. A. Campbell and D. W. Maybury, Nucl. Phys. B **709**, 419 (2005) [arXiv:hep-ph/0303046].

[72] A. Masiero, P. Paradisi and R. Petronzio, Phys. Rev. D **74**, 011701 (2006) [arXiv:hep-ph/0511289].

[73] P. Herczeg, Phys. Rev. D **52**, 3949 (1995).

[74] M. J. Ramsey-Musolf, S. Su and S. Tulin, Phys. Rev. D **76**, 095017 (2007) [arXiv:0705.0028 [hep-ph]].

[75] E. Katz, L. Randall and S. f. Su, Nucl. Phys. B **536**, 3 (1998) [arXiv:hep-ph/9801416].

[76] M. E. Peskin and T. Takeuchi, Phys. Rev. Lett. **65**, 964 (1990).

[77] [CDF Collaboration], arXiv:hep-ex/0703034.

[78] S. Profumo, M. J. Ramsey-Musolf and G. Shaughnessy, arXiv:0705.2425 [hep-ph].

[79] G. W. Bennett *et al.* [Muon G-2 Collaboration], Phys. Rev. D **73**, 072003 (2006) [arXiv:hep-ex/0602035].

[80] J. C. Hardy and I. S. Towner, Phys. Rev. C **71**, 055501 (2005) [arXiv:nucl-th/0412056].

[81] M. J. Ramsey-Musolf, Phys. Rev. D **62**, 056009 (2000) [arXiv:hep-ph/0004062].

[82] V. D. Barger and K. m. Cheung, Phys. Lett. B **480**, 149 (2000) [arXiv:hep-ph/0002259].

[83] S.C. Bennett and C.E. Wieman, Phys. Rev. Lett. **82**, 2484 (1999); C.S. Wood *et al.*, Science **275**, 1759 (1997).

[84] W. J. Marciano, Phys. Rev. D **60**, 093006 (1999).

[85] SLAC E158 Collaboration (P.L. Anthony et al.), Phys.Rev.Lett. **95**, 081601 (2005).

[86] JLab Experiment E-02-020, R. Carlini, J.M. Finn, S. Kowalski, and S. Page, spokespersons.

[87] G. P. Zeller *et al.* [NuTeV Collaboration], Phys. Rev. Lett. **88**, 091802 (2002) [Erratum-ibid. **90**, 239902 (2003)] [arXiv:hep-ex/0110059].

[88] J. Schechter and J. W. F. Valle, Phys. Rev. D **22**, 2227 (1980).

[89] J. Rosiek, Phys. Rev. D **41**, 3464 (1990).

[90] J. Rosiek, arXiv:hep-ph/9511250.

[91] G. Passarino and M. J. G. Veltman, Nucl. Phys. B **160**, 151 (1979).

[92] A. Czarnecki and W. J. Marciano, Phys. Rev. D **64**, 013014 (2001) [arXiv:hep-ph/0102122].

[93] M. J. Ramsey-Musolf, Eur. Phys. J. A **24S2**, 197 (2005) [arXiv:nucl-th/0501023].

[94] A. Gaponenko *et al.* [TWIST Collaboration], Phys. Rev. D **71**, 071101 (2005) [arXiv:hep-ex/0410045].

[95] B. Jamieson *et al.* [TWIST Collaboration], arXiv:hep-ex/0605100.

[96] N. Danneberg *et al.*, Phys. Rev. Lett. **94**, 021802 (2005).

[97] P.S.I.-Experiment R99.06.1, Precision Measurement of the $\mu^+$ Lifetime ($G_F$) with the FAST Detector, J. Kirkby and M. Pohl, co-spokespersons.

[98] P.S.I.-Experiment R99.06.1, A Measurement of the Positive Muon Lifetime utilizing the $\mu$Lan (MUON Lifetime Analysis) Detector, D. Hertzog, contact person.

[99] J. C. Hardy, I. S. Towner and G. Savard, arXiv:nucl-ex/0511051.

[100] PIENU Collaboration, TRIUMF experiment 1072, D. Bryman and T. Numao, spokespersons.

[101] PIE Collaboration, PSI proposal (R05-01), D. Pocanic and A. VanderSchaaf, spokespersons.

[102] V. D. Barger, G. F. Giudice and T. Han, Phys. Rev. D **40**, 2987 (1989).

[103] W. J. Marciano and A. Sirlin, Phys. Rev. Lett. **96**, 032002 (2006) [arXiv:hep-ph/0510099].

[104] T. M. Ito and G. Prezeau, Phys. Rev. Lett. **94**, 161802 (2005) [arXiv:hep-ph/0410254].

[105] G. Prezeau and A. Kurylov, Phys. Rev. Lett. **95**, 101802 (2005) [arXiv:hep-ph/0409193].

[106] R. J. Erwin, J. Kile, M. J. Ramsey-Musolf and P. Wang, arXiv:hep-ph/0602240.

[107] P. Herczeg, Prog. Part. Nucl. Phys. **46**, 413 (2001).

[108] J. Deutsch and P. Quin in *Precision Tests of the Standard Electroweak Model*, P. Langacker, ed., World Scientific (Singapore) 1995, p. 706.

[109] N. Severijns, M. Beck and O. Naviliat-Cuncic, arXiv:nucl-ex/0605029.

[110] F. Scheck, *Electroweak and Strong Interactions: An Introduction to Theoretical Particle Physics*, Springer Verlag, 1996, p.282.

[111] L. Michel, Proc. Phys. Soc. A **63**, 514 (1950).

[112] C. Bouchiat, L. Michel, Phys. Rev. **106**, 170 (1957).

[113] J. D Jackson, S. B. Treiman, and H. W. Wyld, Jr., Phys. Rev. **106**, 517 (1957); Nucle. Phys. **4**, 206 (1957).

[114] N. Kaiser, Phys. Rev. C **64**, 028201 (2001) [arXiv:nucl-th/0105043].

[115] R. E. Behrends and A. Sirlin, Phys. Rev. Lett. **4**, 186 (1960).

[116] M. L. Brooks *et al.* [MEGA Collaboration], Phys. Rev. Lett. **83**, 1521 (1999) [arXiv:hep-ex/9905013].

[117] D. J. H. Chung, L. L. Everett, G. L. Kane, S. F. King, J. D. Lykken and L. T. Wang, Phys. Rept. **407** (2005) 1 [arXiv:hep-ph/0312378].

[118] S. Profumo and C. E. Yaguna, Phys. Rev. D **70** (2004) 095004 [arXiv:hep-ph/0407036].

[119] S. P. Martin and J. D. Wells, Phys. Rev. D **64** (2001) 035003 [arXiv:hep-ph/0103067].

[120] A. Hocker, arXiv:hep-ph/0410081, Published in "*Beijing 2004, ICHEP 2004, vol. 2*" 710-715.

[121] M. Ramsey-Musolf and M. B. Wise, Phys. Rev. Lett. **89** (2002) 041601 [arXiv:hep-ph/0201297].

[122] A. Strumia, Nucl. Phys. B **482** (1996) 24 [arXiv:hep-ph/9604417].

[123] H. Baer, A. Mustafayev, S. Profumo, A. Belyaev and X. Tata, JHEP **0507**, 065 (2005) [arXiv:hep-ph/0504001].

[124] C. A. Gagliardi, R. E. Tribble and N. J. Williams, Phys. Rev. D **72**, 073002 (2005) [arXiv:hep-ph/0509069].

[125] W. J. Marciano, Phys. Rev. D **60**, 093006 (1999) [arXiv:hep-ph/9903451].

[126] J. C. Hardy and I. S. Towner, Phys. Rev. Lett. **94**, 092502 (2005) [arXiv:nucl-th/0412050].

[127] A. Serebrov *et al.*, Phys. Lett. B **605**, 72 (2005) [arXiv:nucl-ex/0408009].

[128] B. Filippone, private communication.

[129] G. Savard and J. Hardy, private communication.

[130] S. L. Adler, E. W. . Colglazier, J. B. Healy, I. Karliner, J. Lieberman, Y. J. Ng and H. S. Tsao, Phys. Rev. D **11**, 3309 (1975).

[131] S. Gardner and C. Zhang, Phys. Rev. Lett. **86**, 5666 (2001) [arXiv:hep-ph/0012098].